Supplementary Material

Gold(I) and Silver(I) Complexes Containing Hybrid Sulfonamide/Thiourea Ligands as Potential Leishmanicidal Agents

Alice P. Borges [1], Malu M. S. Obata [2], Silvia H. Libardi [3], Rafael O. Trevisan [2], Victor M. Deflon [3], Ulrich Abram [4], Francis B. Ferreira [5], Luiz Antônio S. Costa [6], Antonio O. T. Patrocínio [7], Marcos V. da Silva [2], Júlio C. Borges [3] and Pedro I. S. Maia [1,*]

[1] Bioactive Compounds Development Research Group, Federal University of Triângulo Mineiro, Av. Dr. Randolfo Borges 1400, Uberaba 38025-440, MG, Brazil; aliceborges98@hotmail.com
[2] Department of Microbiology, Immunology and Parasitology, Federal University of Triângulo Mineiro, Av. Getúlio Guarita, Uberaba 38025-440, MG, Brazil; malu.mateus_21@hotmail.com (M.M.S.O.); rafaelotrevisan@gmail.com (R.O.T.); marcos.silva@uftm.edu.br (M.V.d.S.)
[3] São Carlos Institute of Chemistry, University of São Paulo, Av. Trabalhador São Carlense, 400, São Carlos 13566-590, SP, Brazil; libardish@gmail.com (S.H.L.); deflon@iqsc.usp.br (V.M.D.); borgesjc@iqsc.usp.br (J.C.B.)
[4] Institute of Chemistry and Biochemistry, Freie Universität Berlin, Fabeckstr. 34/36, 14195 Berlin, Germany; ulrich.abram@fu-berlin.de
[5] Associated Faculties of Uberaba, Av. do Tutuna 720, Uberaba 38061-500, MG, Brazil; francisbferreira@gmail.com
[6] Computational Chemistry Research Group, Institute of Exact Sciences, Federal University of Juiz de Fora, Campus Universitário s/n Martelos, Juiz de Fora 36036-900, MG, Brazil; luiz.costa@ufjf.br
[7] Laboratory of Photochemistry and Material Science, Institute of Chemistry, Federal University of Uberlândia, Av. João Naves de Ávila 2121, Uberlândia 38400-902, MG, Brazil; otaviopatrocinio@ufu.br
* Correspondence: pedro.maia@uftm.edu.br

Table of Contents

Part 1. IR spectroscopy . 1

Figure S1.1: IR (ATR) spectrum of HL**3**^{FPh};
Figure S1.1: IR (ATR) spectrum of HL**4**^{ClPh};
Figure S1.2: IR (ATR) spectrum of HL**5**^{NO2Ph};
Figure S1.3: IR (ATR) spectrum of HL**6**^{Al};
Figure S1.5: IR (ATR) spectrum of $[Ag(HL3^{FPh})_2]NO_3$ (**Ag3**);
Figure S1.6: IR (ATR) spectrum of $[Ag(HL4^{ClPh})_2]NO_3$ (**Ag4**);
Figure S1.7: IR (ATR) spectrum of $[Ag(HL5^{NO2Ph})_2]NO_3$ (**Ag5**);
Figure S1.8: IR (ATR) spectrum of $[Ag(HL6^{Al})_2]NO_3$ (**Ag6**);
Figure S1.9: IR (ATR) spectrum of $[Au(HL1^{Ch})_2]Cl$ (**Au1**);
Figure S1.10: IR (ATR) spectrum of $[Au(HL2^{Ph})_2]Cl$ (**Au2**);
Figure S1.11: IR (ATR) spectrum of $[Au(HL3^{FPh})_2]Cl$ (**Au3**);
Figure S1.12: IR (ATR) spectrum of $[Au(HL4^{ClPh})_2]Cl$ (**Au4**);
Figure S1.13: IR (ATR) spectrum of $[Au(HL5^{NO2Ph})_2]Cl$ (**Au5**);
Figure S1.14: IR (ATR) spectrum of $[Au(HL6^{Al})_2]Cl$ (**Au6**);
Table S1: Selected absorption bands in the infrared region for free ligands and complexes;

Part 2. NMR spectroscopy . 9

Figure S2.1: ^{1}H NMR spectrum of HL**3**^{FPh} in DMSO-d_6;
Figure S2.2: ^{1}H NMR spectrum of HL**4**^{ClPh} in DMSO-d_6;
Figure S2.3: ^{1}H NMR spectrum of HL**5**^{NO2Ph} in DMSO-d_6;
Figure S2.4: ^{1}H NMR spectrum of HL**6**^{Al} in DMSO-d_6;
Figure S2.5: ^{19}F NMR spectrum (377 MHz) of H**L3**^{FPh} in DMSO-d_6;
Figure S2.6: ^{1}H NMR spectrum of $[Ag(HL3^{FPh})_2]NO_3$ (**Ag3**) in DMSO-d_6;
Figure S2.7: ^{1}H NMR spectrum of $[Ag(HL4^{ClPh})_2]NO_3$ (**Ag4**) in DMSO-d_6;
Figure S2.8: ^{1}H NMR spectrum of $[Ag(HL5^{NO2Ph})_2]NO_3$ (**Ag5**) in DMSO-d_6;
Figure S2.9: ^{1}H NMR spectrum of $[Ag(HL6^{Al})_2]NO_3$ (**Ag6**) in DMSO-d_6;
Figure S2.10: ^{1}H NMR spectrum of $[Au(HL1^{Ch})_2]Cl$ (**Au1**) in DMSO-d_6;
Figure S2.11: ^{1}H NMR spectrum of $[Au(HL2^{Ph})_2]Cl$ (**Au2**) in DMSO-d_6;
Figure S2.12: ^{1}H NMR spectrum of $[Au(HL3^{FPh})_2]Cl$ (**Au3**) in DMSO-d_6;
Figure S2.13: ^{1}H NMR spectrum of $[Au(HL4^{ClPh})_2]Cl$ (**Au4**) in DMSO-d_6
Figure S2.14: ^{1}H NMR spectrum of $[Au(HL5^{NO2Ph})_2]Cl$(**Au5**) in DMSO-d_6;
Figure S2.15: ^{1}H NMR spectrum of $[Au(HL6^{Al})_2]Cl$ (**Au6**) in DMSO-d_6;
Figure S2.16: ^{19}F NMR spectrum (377 MHz) of $[Ag(HL3^{FPh})_2]NO_3$ (**Ag3**) in DMSO-d_6;
Figure S2.17: ^{19}F NMR spectrum (377 MHz) of $[Au(HL3^{FPh})_2]Cl$ (**Au3**) in DMSO-d_6;

Part 3. ESI+ MS spectra . 18

Figure S3.1: ESI(+) MS spectrum of $[Ag(HL3^{FPh})_2]NO_3$ (**Ag3**);
Figure S3.2: ESI(+) MS spectrum of $[Au(HL1^{Ch})_2]Cl$ (**Au1**);
Figure S3.4: ESI(+) MS spectrum of $[Au(HL2^{Ph})_2]Cl$ (**Au2**);
Figure S3.5: ESI(+) MS spectrum of $[Au(HL3^{FPh})_2]Cl$ (**Au3**);
Figure S3.6: ESI(+) MS spectrum of $[Au(HL4^{ClPh})_2]Cl$ (**Au4**);
Figure S3.7: ESI(+) MS spectrum of $[Au(HL6^{Al})_2]Cl$ (**Au6**);

Part 4. Crystallographic data. 24

Figure S4.1: Hydrogen bonds involved in the crystalline structure of the **HL3**^{FPh} ligand. Intermolecular hydrogen bonds: [N(1)···O(1) = 2.910(3) Å, N(1)-H(1)···O(1)= 115.4°], [N(2)···S(1) = 3.311(2) Å, N(2)-H(2)···S(1) = 160.8°], [N(1)···O(2) = 3.420(3) Å, N(1)-H(1)···O(2) =

98.1°], [N(3)···O(2) = 2.959(2) Å, N(3)-H(3)···O(2) = 147.7°]. Intramolecular hydrogen bonding: [N(3)···N(1) = 2.659(3) Å, N(3)-H(3)···N(1)= 110.3 °]. Used symmetry operations (') x-1, y, z, ('') -x, -y+1, -z+1 and (''') -x, -y+2, -z+1. Red dotted lines (between donor and acceptor atoms) represent hydrogen bonds;

Figure S4.2: Hydrogen bonds involved in the crystalline structure of the **HL5^{NO2Ph}** ligand. Intermolecular hydrogen bonds: [N(1)···O(1') = 2.887(4) Å, N(1)-H(1)···O(1')= 117.4°], [N(2)···S(1'') = 3.347(3) Å, N(2)-H(2)···S(1'') = 165.2°], [N(3) ···O(2''') = 3.040(4) Å, N(3)-H(3)···O(2''') = 151.8 °]. Used symmetry operations (') x-1, y, z, ('') -x, -y+1, -z+1 and (''') -x, -y, -z+1. Blue dotted lines (between donor and acceptor atoms) represent;

Figure S4.8: Hydrogen bonds involved in the crystalline structure of the **HL6^{Al}** ligand. Intermolecular hydrogen bonds: [N(3)···O(2) = 3.024(3) Å, N(3)-H(3)···O(2)= 129.0°], [N(2)···S(1) = 3.3475(18) Å, N(2)-H(2)···S(1) = 159.0 °], [N(1)···S(1) = 3.356(2) Å, N(1)-H(1)···S(1)= 118.4 °]. Used symmetry operations (') -x, -y, -z+1, ('') -x+1, -y+1, -z+1 and (''') x-1, y, z. Blue dotted lines (between donor and acceptor atoms) represent hydrogen bonds;

Figure S4.4 Ellipsoid representation of [Au(HL1^{Ch})$_2$]Cl·CH_3OH (**Au1**·CH_3OH). The hydrogen atoms have been omitted for clarity. A solvent mask was calculated and 108 electrons were found in a volume of 518 Å^3 in 1 void per unit cell. This is consistent with the presence of 0.5[CH2Cl2;2H2O] per Asymmetric Unit which account for 120 electrons per unit cell.

Figure S4.5 Ellipsoid representation of [Au(HL2^{Ph})$_2$]Cl·CH_3OH (**Au2**·CH_3OH). The hydrogen atoms have been omitted for clarity.

Figure S4.6: Hydrogen bonds involved in the crystalline structure of the **Au2** complex. Intermolecular hydrogen bonds: [N(1)···Cl(1) = 3.173(4) Å, N(1)-H(1)···Cl(1)= 113.8 °], [O(1S)···Cl(1) = 3.135(5) Å, O(1S)-H(1S)···Cl(1) = 152.4°], [N(3A)···O(1) = 2.775(14) Å, N(3A)-H(3A)···O(1) = 146.1 °], [N(3B)···O(1) = 3.149(14) Å, N(3B)-H(3B)···O(1) = 136.9 °]. Intramolecular hydrogen bonding: [N(2)···O(1S) = 2.905(5) Å, N(2)-H(2)···O(1S)= 135.6 °]. Used symmetry operations (') -x, +y, -z. Blue dotted lines (between donor and acceptor atoms) represent hydrogen bonds;

Part 5. Photophysical studies 27

Figure S5.1: Electronic spectra of **Ag3** (green line), **Ag4** (orange line), **Ag5** (red line) and **Ag6** (purple line) in the 210 to 350 nm range (10^{-6} M CH_3CN solution);

Figure S5.2: Electronic spectra of **Au1** (blue line), **Au2** (pink line), **Au3** (green line), **Au4** (orange line), **Au5** (red line) and **Au6** (purple line) in the 210 to 350 nm range (10^{-6} M CH_3OH solution for **Au1**, **Au2**, **Au3**, **Au6** and 10^{-6} M solution CH_3CN for **Au4** and **Au5**);

Figure S5.9: Linear regression for **Ag3** (green line), **Ag4** (orange line), **Ag5** (red line) and **Ag6** (purple line);

Table S2: Electronic spectra data obtained for the **Ag3** and **Ag4** complexes;

Table S3: Electronic spectra data obtained for the **Ag5** and **Ag6** complexes;

Figure S5.10: Linear regression for **Au1** (blue line), **Au2** (pink line), **Au3** (green line), **Au4** (orange line), **Au5** (red line) and **Au6** (purple line);

Table S4: Electronic spectra data obtained for the **Au1** and **Au2** complexes;

Table S5: Electronic spectra data obtained for the **Au3** and **Au4** complexes;

Table S6: Electronic spectra data obtained for the **Au5** and **Au6** complexes;

Figure S5.5: (a) Emission spectra of **Au1** (blue line) and **Au2** (pink line) in CH_3OH at 298 K; λexc = 255 nm for **Au1** and 270 nm for **Au2**; (b) Emission spectra of CH_3OH at 298 K; λexc = 250 nm;

Figure S5.6: Emission spectra of **Au1** (blue dashed line) and **Au2** (pink dashed line) in MeOH at 77 K; λexc = 255 nm for **Au1** and 270 nm for **Au2**;

Part 6. DFT studies 32

Table S7. Basis set functions scheme used for the gold complexes.

Table S8: Vibrational modes and their theoretical assignments related to the C=S bond;
Figure S6.1: Optimized structures of the silver complexes;
Table S9: Main theoretical structural data of the silver complexes;
Figure S6.2: Optimized structures of the gold complexes;
Table S10: Main theoretical structural data of the gold complexes;
Figure S6.3: HOMO and LUMO orbitals in the silver complexes;
Figure S6.4 - HOMO and LUMO orbitals in the gold complexes;
Figure S6.5: Optimized structure of $[Au(HL3^{FPh})_2]^+$ (**Au3**) with the charges obtained for the AIM data;
Table S11: Electronic properties of the gold(I) complexes. The values are shown, respectively, for each bond in the order they appear;

Part 7. Biological studies 41

Figure S7.1: Graph of the viability versus concentrations (μM) of the compounds;
Figure S7.2: Leishmanicidal activity against to the *Leishmania infantum* parasite by concentrations of the compound. Blue curve represents the reference leishmanicidal drug, Glucantime. Black curve represents each compound;
Figure S7.3: Leishmanicidal activity against to the *Leishmania braziliensis* parasite by concentrations of the compound. Blue curve represents the reference leishmanicidal drug, Glucantime. Black curve represents each compound;
Figure S7.4: (a) percentage of the number of infected in 200 macrophages by *Leishmania infantum*; (b) percentage of leishmaniasis that infect 100 cells/macrophages; (c) average percentage of leishmaniasis that infect 200 cells/macrophages; of the selected compounds;
Figure S7.5: Image captured under a fluorescence microscope (EVOS) of Raw macrophages infected by *Leishmania infantum* after treatment with a Glucantime (leishmanicidal drug) (A) and the selected compounds;
Figure S7.6: (A) Fluorescence emission spectra (λ_{ex} = 295 nm) of LbOYE protein in the concentration of 1 μmol L^{-1} in the presence of increasing concentrations of the $HL1^{Ch}$ compound. (B) Variation of maximum fluorescence intensities (λ_{max} = 333 nm) and non-linear fit to the Hill equation (Equation 1). (C) Logarithmic relationship to obtain the number of bonding sites according to Equation 2. (D) Relationship of temperatures of 25 and 37 °C. The spectra were obtained in Tris-HCl buffer, pH 8.0; 100 mmol L^{-1} of NaCl and 2.5 % of DMSO;
Figure S7.7: (A) Fluorescence emission spectra (λ_{ex} = 295 nm) of LbOYE protein in the concentration of 1 μmol L^{-1} in the presence of increasing concentrations of the $HL3^{FPh}$ compound. (B) Variation of maximum fluorescence intensities (λ_{max} = 333 nm) and non-linear fit to the Hill equation (Equation 1). (C) Logarithmic relationship to obtain the number of bonding sites according to Equation 2. (D) Relationship of temperatures of 25 and 37 °C. The spectra were obtained in Tris-HCl buffer, pH 8.0; 100 mmol L^{-1} of NaCl and 2.5 % of DMSO.
Figure S7.8. Fluorescence emission spectra (λ_{ex} = 295 nm) of LbOYE protein in the concentration of 1 μmol L^{-1} in the presence of increasing concentrations of the $[Au(HL1^{Ch})_2]Cl$ (**Au1**) complex. (B) Variation of maximum fluorescence intensities (λ_{max} = 333 nm) and non-linear fit to the Hill equation (Equation 1). (C) Logarithmic relationship to obtain the number of bonding sites according to Equation 2. (D) Comparison between the temperatures of 25 °C and 37 °C. The spectra were obtained in Tris-HCl buffer, pH 8.0; 100 mmol L^{-1} of NaCl and 2.5 % of DMSO.

Part 8. Docking interactions 50

Figure S8.1: Representative figure of the $HL1^{Ch}$ ligand at the site of the LbOYE**;**
Figure S8.2: Representative figure of the $HL3^{FPh}$ ligand at the site of the LbOYE**;**

Figure S8.11: Representative figure of the $HL4^{ClPh}$ ligand at the site of the LbOYE**;**
Figure S8.12: Representative figure of the $HL5^{NO2Ph}$ ligand at the site of the LbOYE**;**
Figure S8.13: Representative figure of the $HL6^{Al}$ ligand at the site of the LbOYE**;**
Figure S8.14: Representative figure of the $[Ag(HL1^{Ch})_2]NO_3$ complex at the site of the LbOYE**;**
Figure S8.15: Representative figure of the $[Ag(HL2^{Ph})_2]NO_3$ complex at the site of LbOYE**;**
Figure S8.16: Representative figure of the $[Ag(HL3^{FPh})_2]NO_3$ complex at the site of the LbOYE**;**
Figure S8.17: Representative figure of the $[Ag(HL4^{ClPh})_2]NO_3$ complex at the site of the LbOYE**; Figure S8.18:** Representative figure of the $[Ag(HL5^{NO2Ph})_2]NO_3$ complex at the site of the LbOYE**;**
Figure S8.19: Representative figure of the $[Au(HL1^{Ch})_2]Cl$ complex at the site of the LbOYE;
Figure S8.20: Representative figure of the $[Au(HL2^{Ph})_2]Cl$ complex at the site of the LbOYE**;**
Figure S8.21: Representative figure of the $[Au(HL3^{FPh})_2]Cl$ complex at the site of the LbOYE**;**
Figure S8.22: Representative figure of the $[Au(HL4^{ClPh})_2]Cl$ complex at the site of the LbOYE**;**
Figure S8.23: Representative figure of the $[Au(HL5^{NO2Ph})2]Cl$ complex at the site of the LbOYE.

Figure S1.1 - IR (ATR) spectrum of HL**3**$^{\mathbf{FPh}}$.

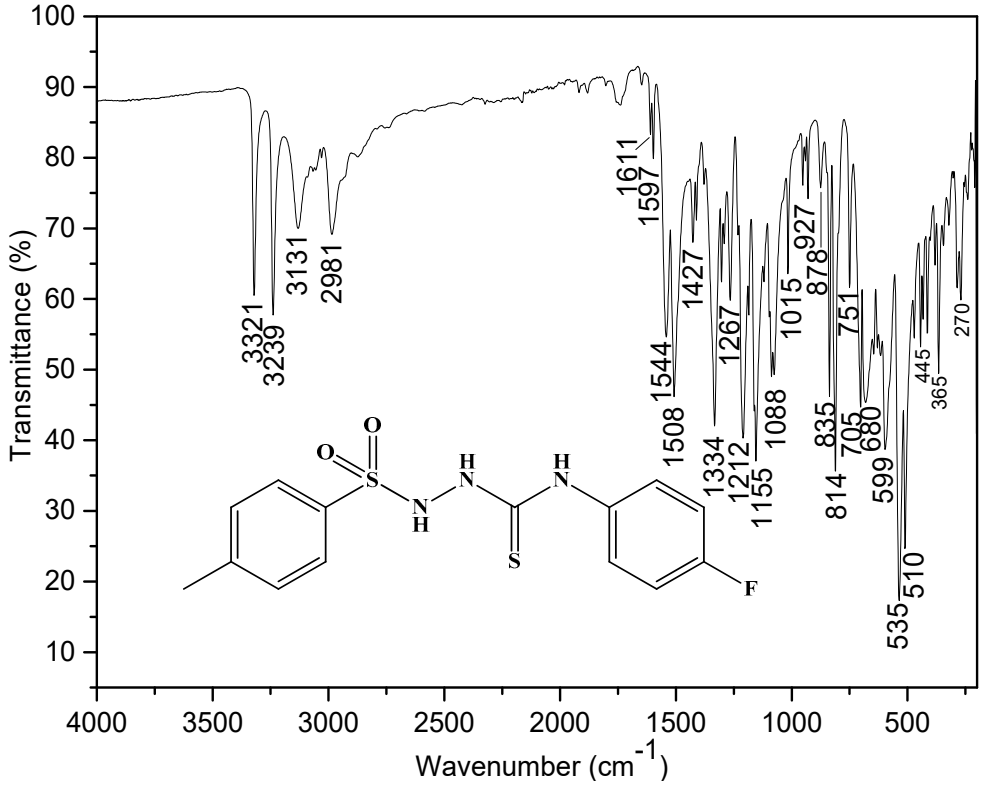

Figure S1.24 – IR (ATR) spectrum of HL**4**$^{\mathbf{ClPh}}$.

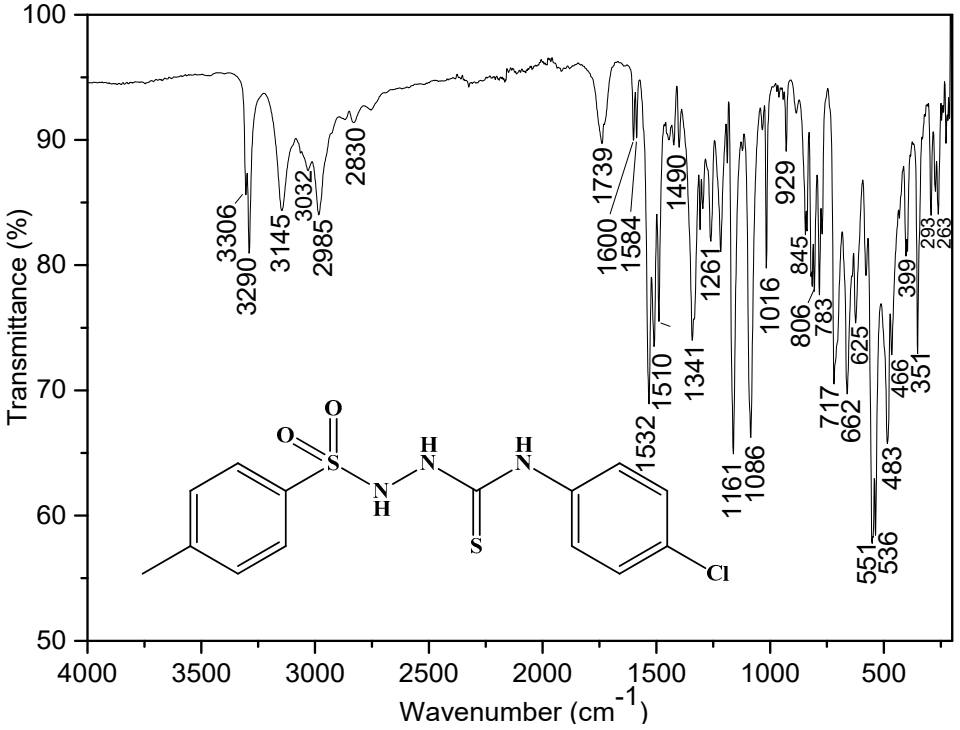

Figure S1.25 - IR (ATR) spectrum of HL**5**^{NO2Ph}.

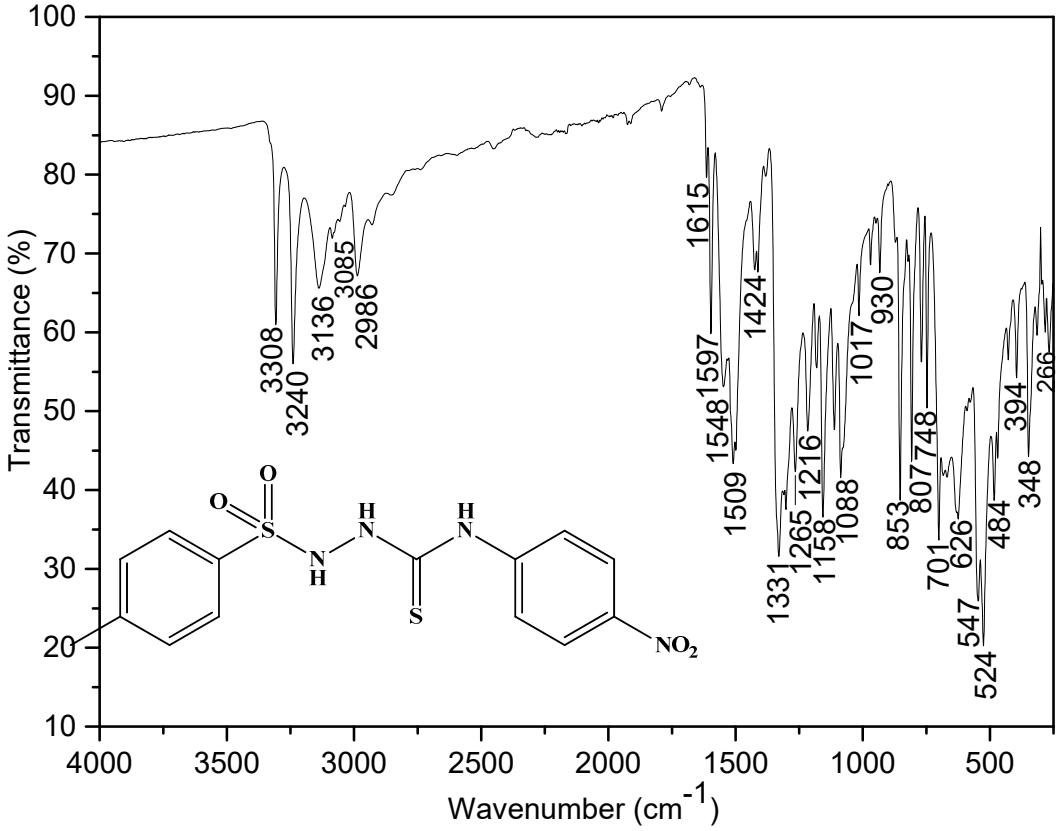

Figure S1.26 - IR (ATR) spectrum of HL**6**^{Al}.

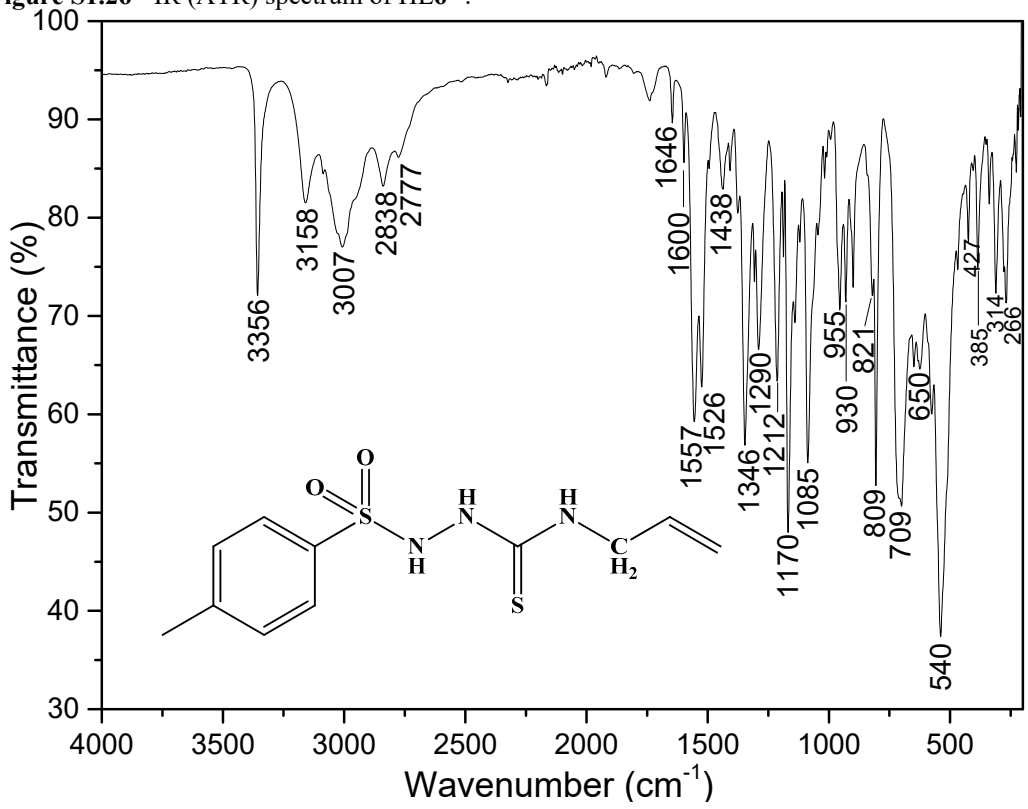

Figure S1.5 - IR (ATR) spectrum of $[Ag(HL3^{FPh})_2]NO_3$ (**Ag3**).

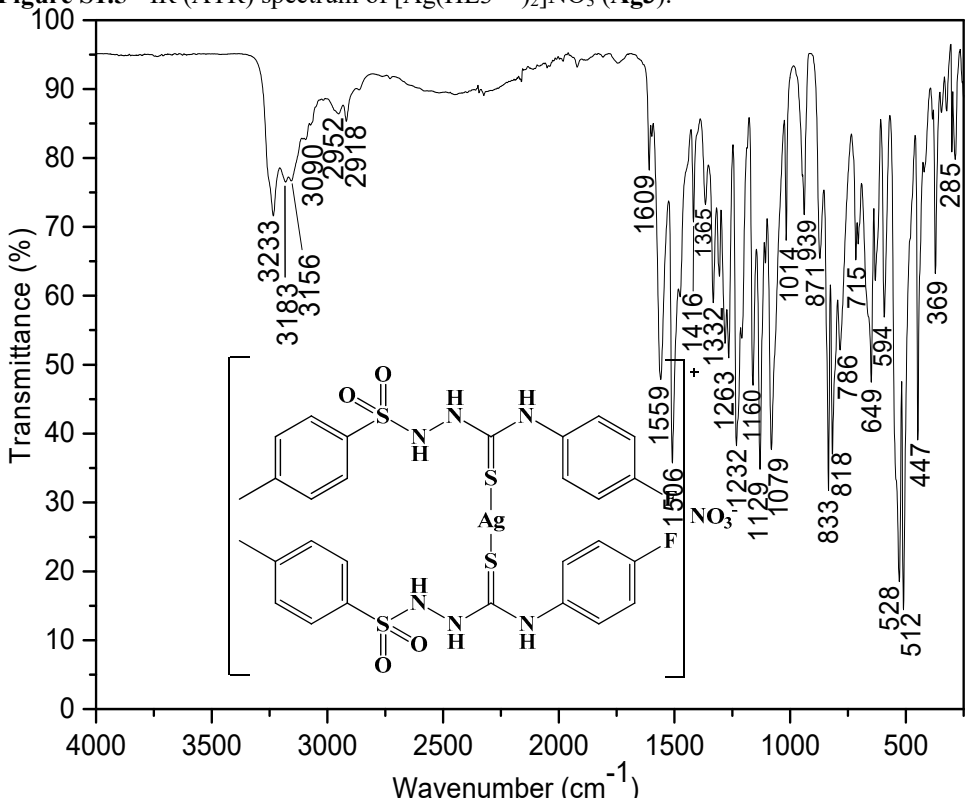

Figure S1.6 - IR (ATR) spectrum of $[Ag(HL4^{ClPh})_2]NO_3$ (**Ag4**).

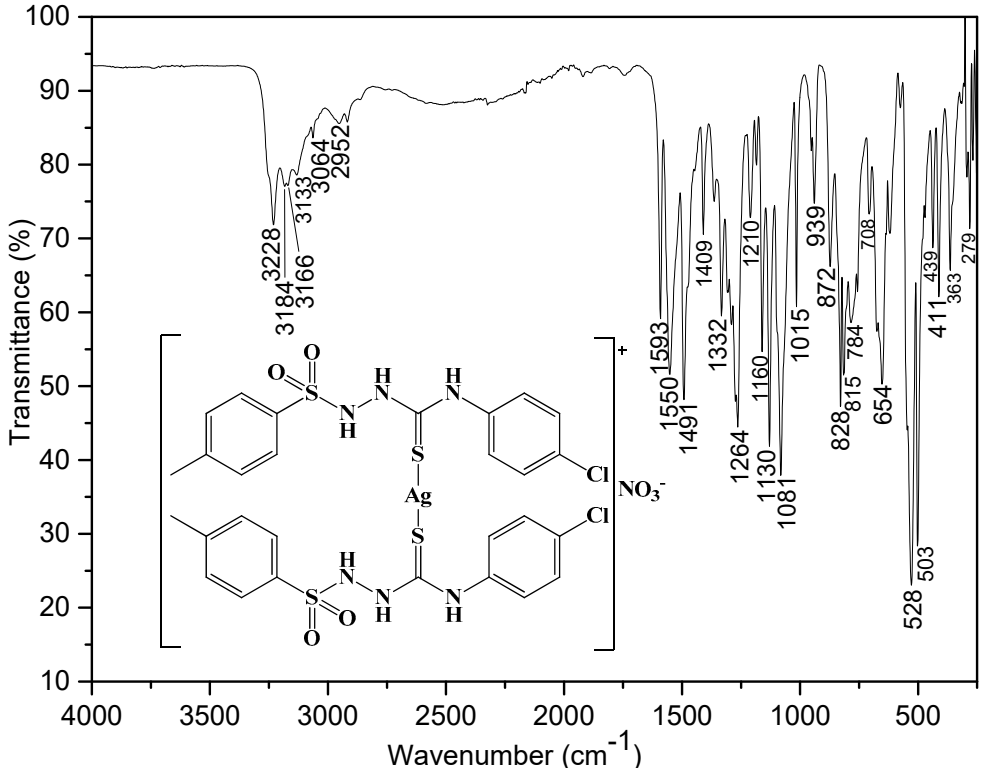

Figure S1.7 - IR (ATR) spectrum of $[Ag(HL5^{NO2Ph})_2]NO_3$ (**Ag5**).

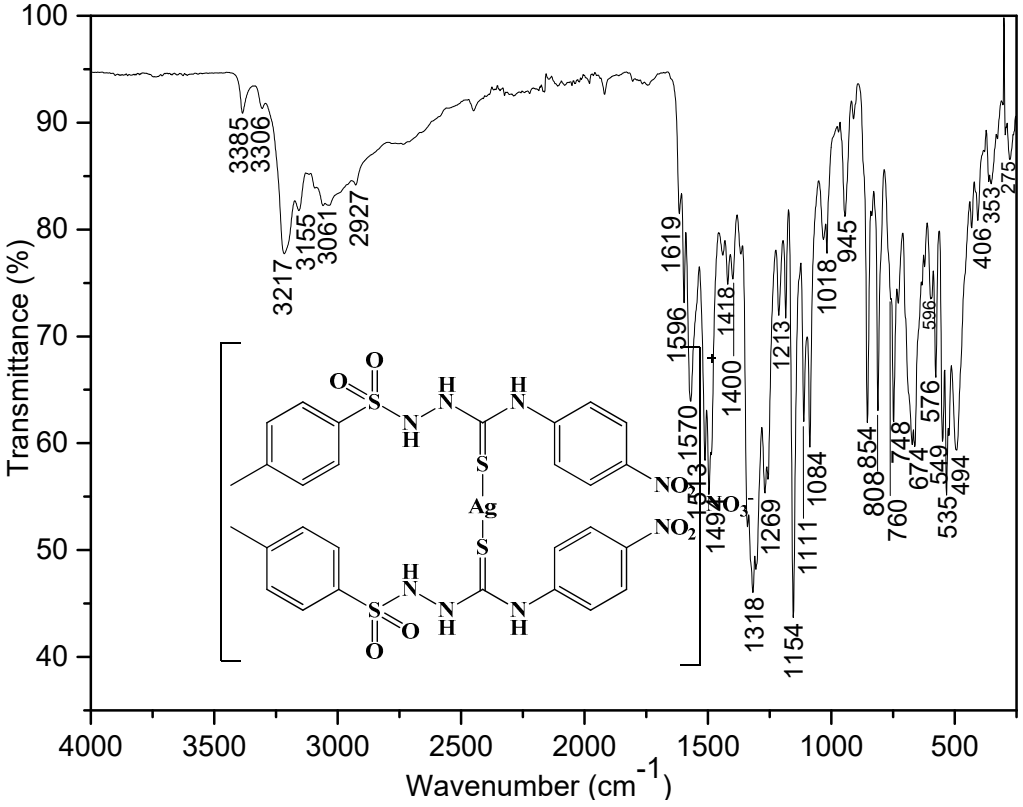

Figure S1.8 - IR (ATR) spectrum of $[Ag(HL6^{Al})_2]NO_3$ (**Ag6**).

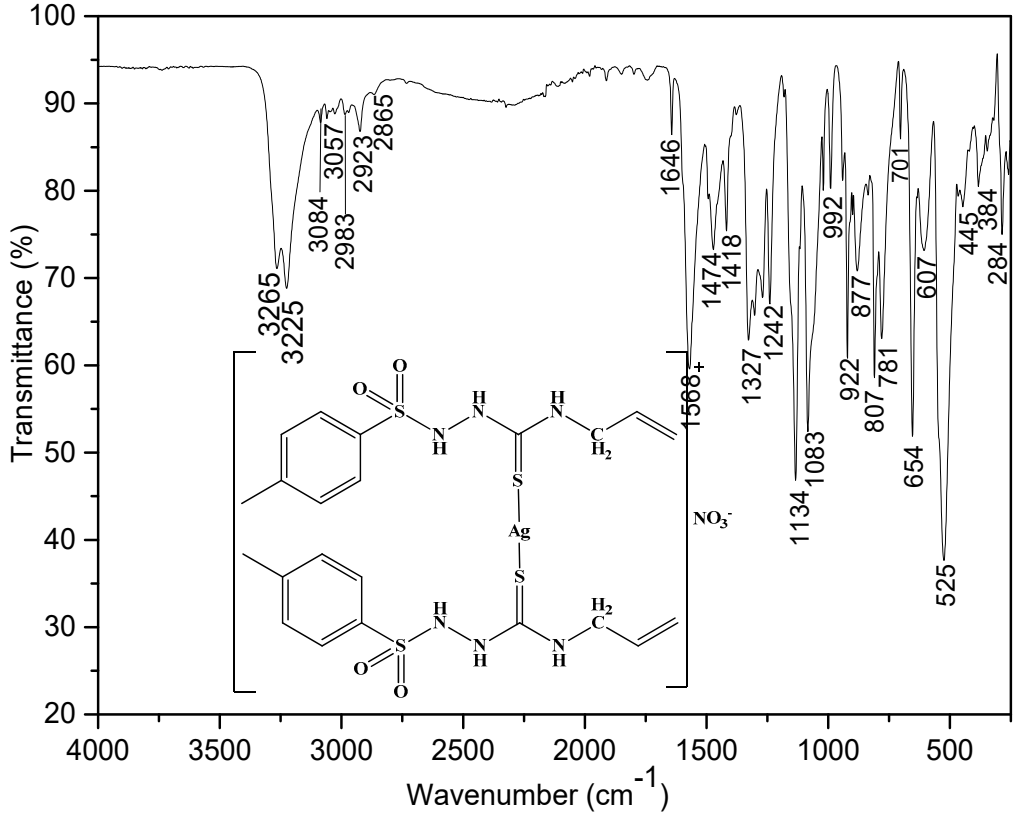

Figure S1.9 – IR (ATR) spectrum of $[Au(HL1^{Ch})_2]Cl$ (**Au1**).

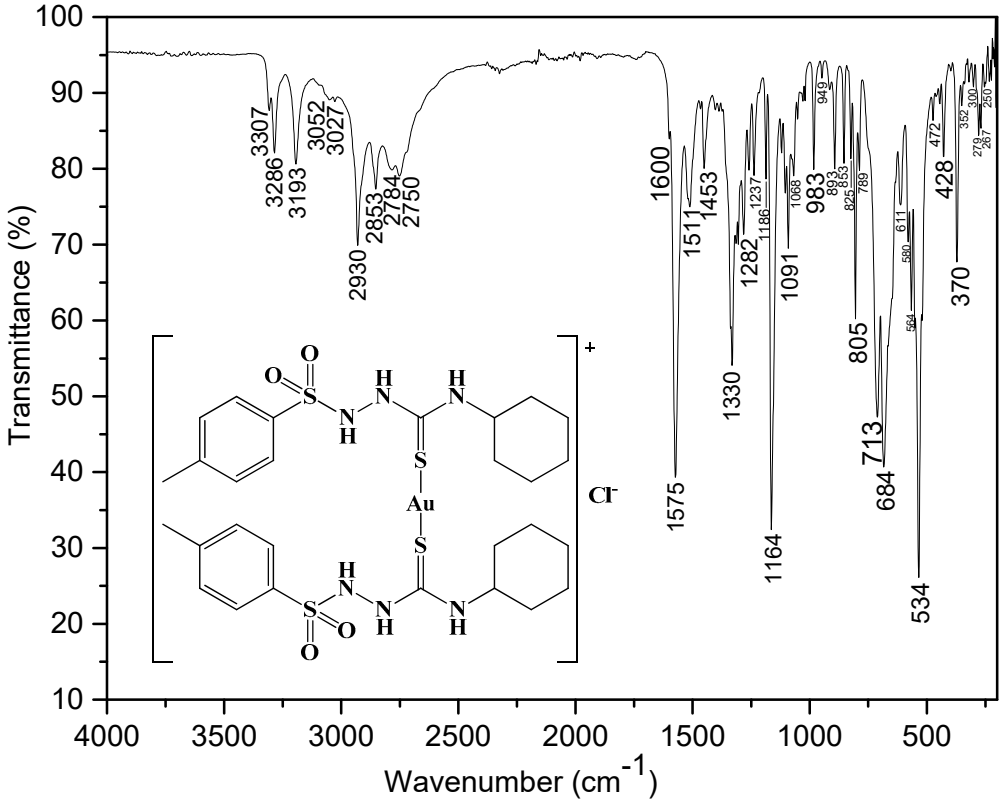

Figure S1.10 – IR (ATR) spectrum of $[Au(HL2^{Ph})_2]Cl$ (**Au2**).

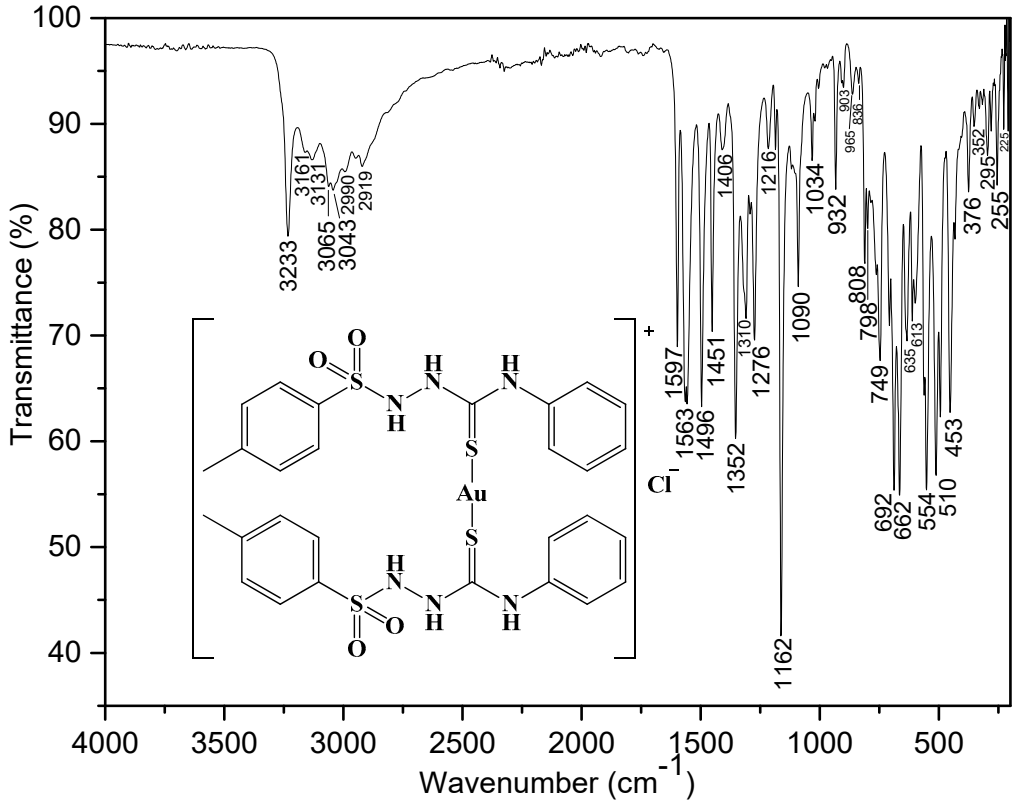

Figure S1.11 – IR (ATR) spectrum of $[Au(HL3^{FPh})_2]Cl$ (**Au3**).

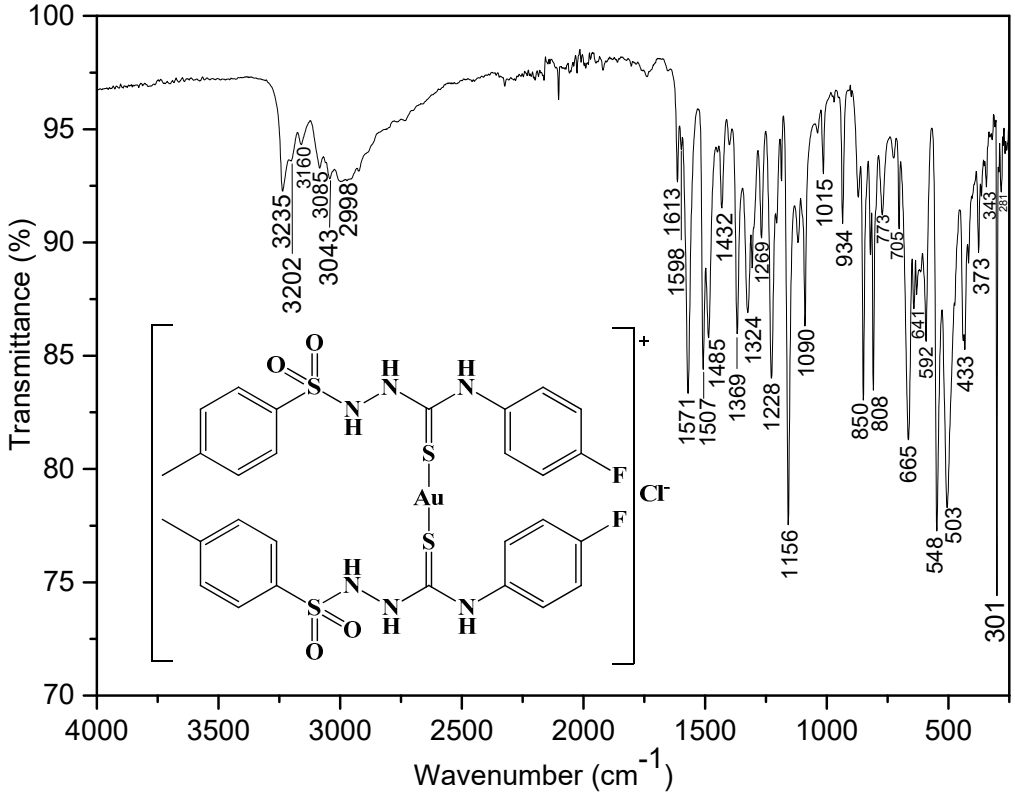

Figure S1.12 – IR (ATR) spectrum of $[Au(HL4^{ClPh})_2]Cl$ (**Au4**).

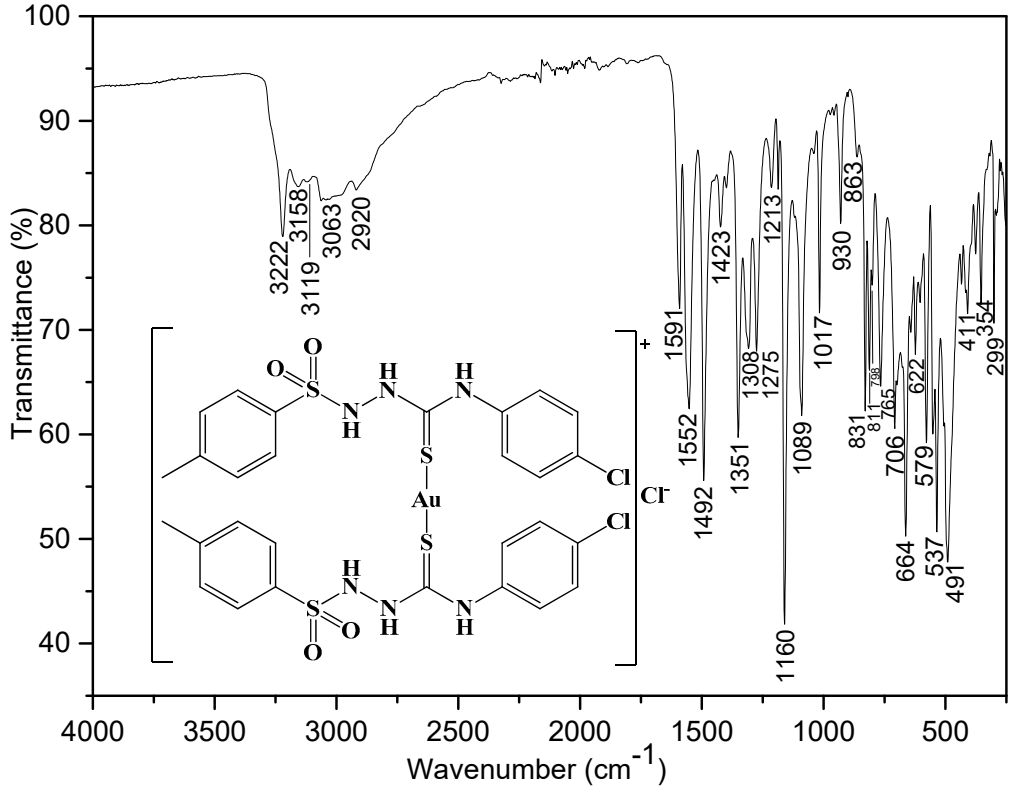

Figure S1.13 – IR (ATR) spectrum of $[Au(HL5^{NO2Ph})_2]Cl$ (**Au5**).

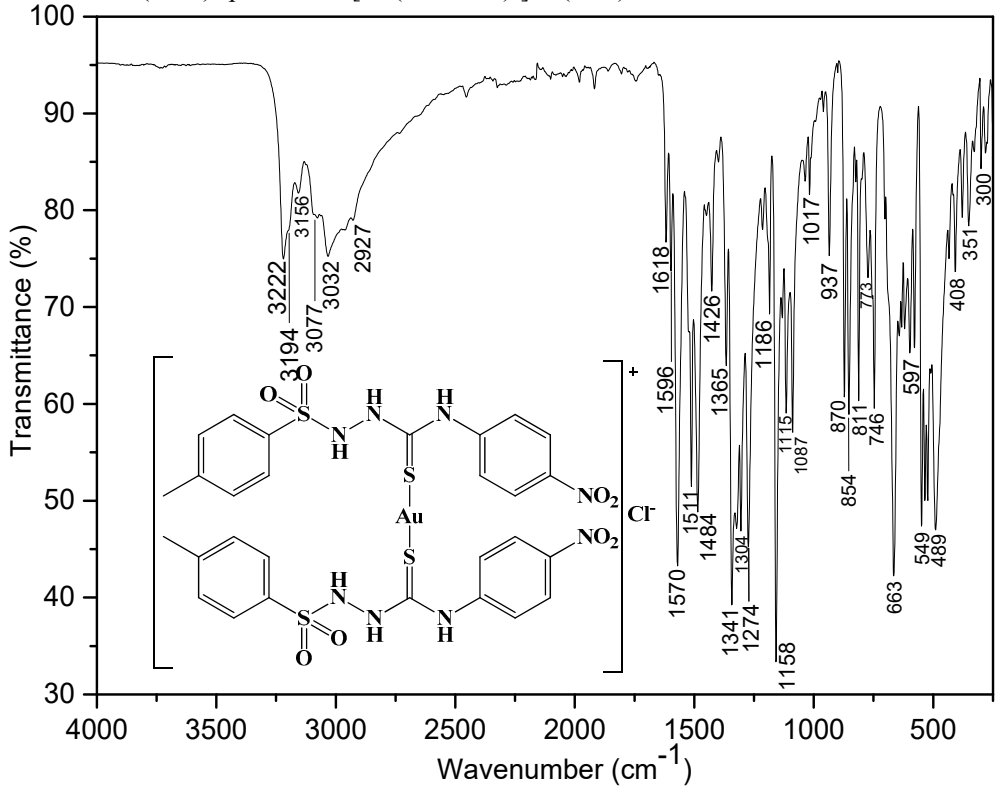

Figure S1.14 - IR (ATR) spectrum of $[Au(HL6^{Al})_2]Cl$ (**Au6**).

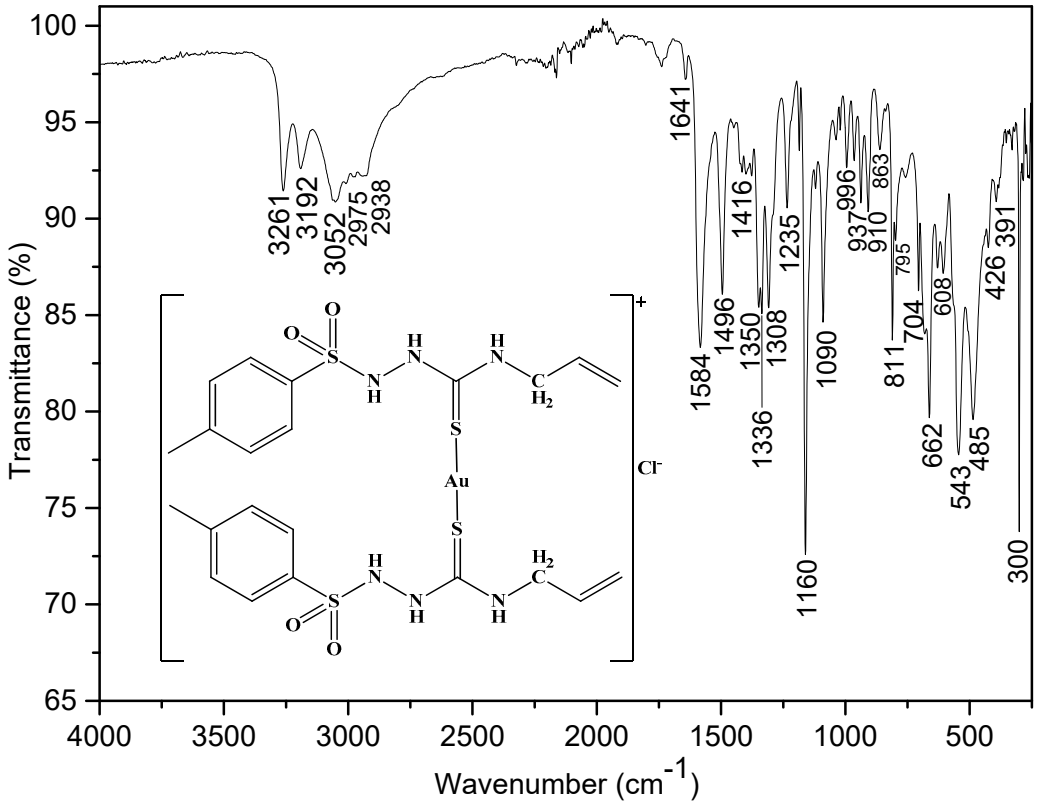

Table S1 - Selected absorption bands in the infrared region for free ligands and complexes.

	Selected bands/ cm^{-1}					
Compound	ν (N-H)	ν(-NH-CS-NH-)	ν(N-O)	ν_{ass}(S=O)	ν_s(S=O)	ν(C=S)
HL1^{Ch}	3371/3228/3167	1597	—	1352/1330	1166	808
HL2^{Ph}	3329/3228/3136	1597	—	1342/1328	1165	806
HL3^{FPh}	3320/3240/3133	1596	—	1333	1156	814
HL4^{ClPh}	3306/3290/3145	1600/1584	—	1341	1161	806
HL5^{NO2Ph}	3308/3240/3136	1615/1597	1424	1331	1158	807
HL6^{Al}	3358/3160	1600	—	1348	1170	809
Ag3	3233/3183/3156	1609	1416	1332	1160	786
Ag4	3228/3184/3166	1593	1409	1332	1160	784
Ag5	3385/3306/3217/3155	1619/1596	1418/1400	1318	1154	—
Ag6	3265/3225	1646	1418	1327	1134	781
Au1	3307/3286/3193	1600	—	1330	1164	789
Au2	3233/3161/3131	1597	—	1352	1162	798
Au3	3235/3202/3160	1613/1598	—	1324	1156	773
Au4	3222/3158/3119	1591	—	1351	1160	798
Au5	3222/3194/3156	1641	1426	1350	1160	795
Au6	3261/3192	1618/1596	—	1341	1158	773

Figure S2.1 – ^{1}H NMR spectrum of HL**3**$^{\mathbf{FPh}}$ in DMSO-d_6.

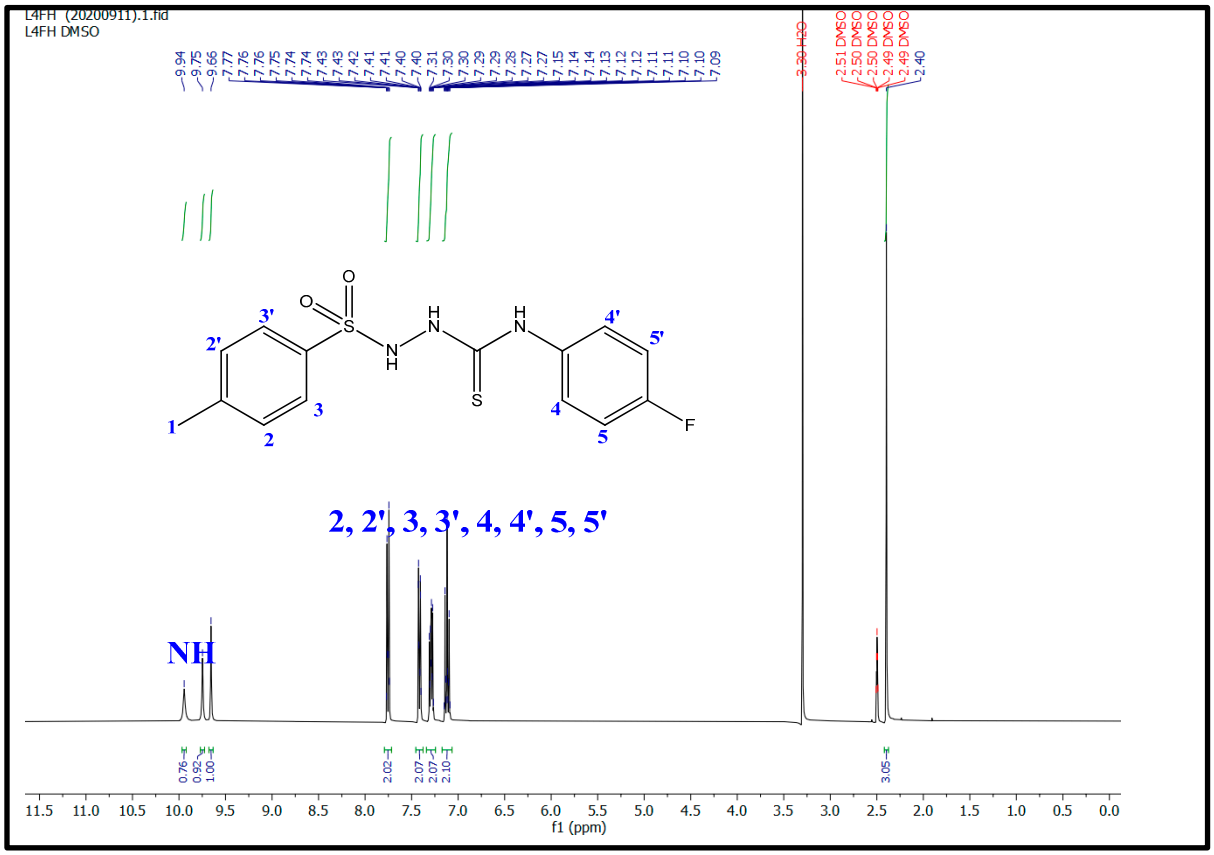

Figure S2.2 – ^{1}H NMR spectrum of HL**4**$^{\mathbf{ClPh}}$ in DMSO-d_6.

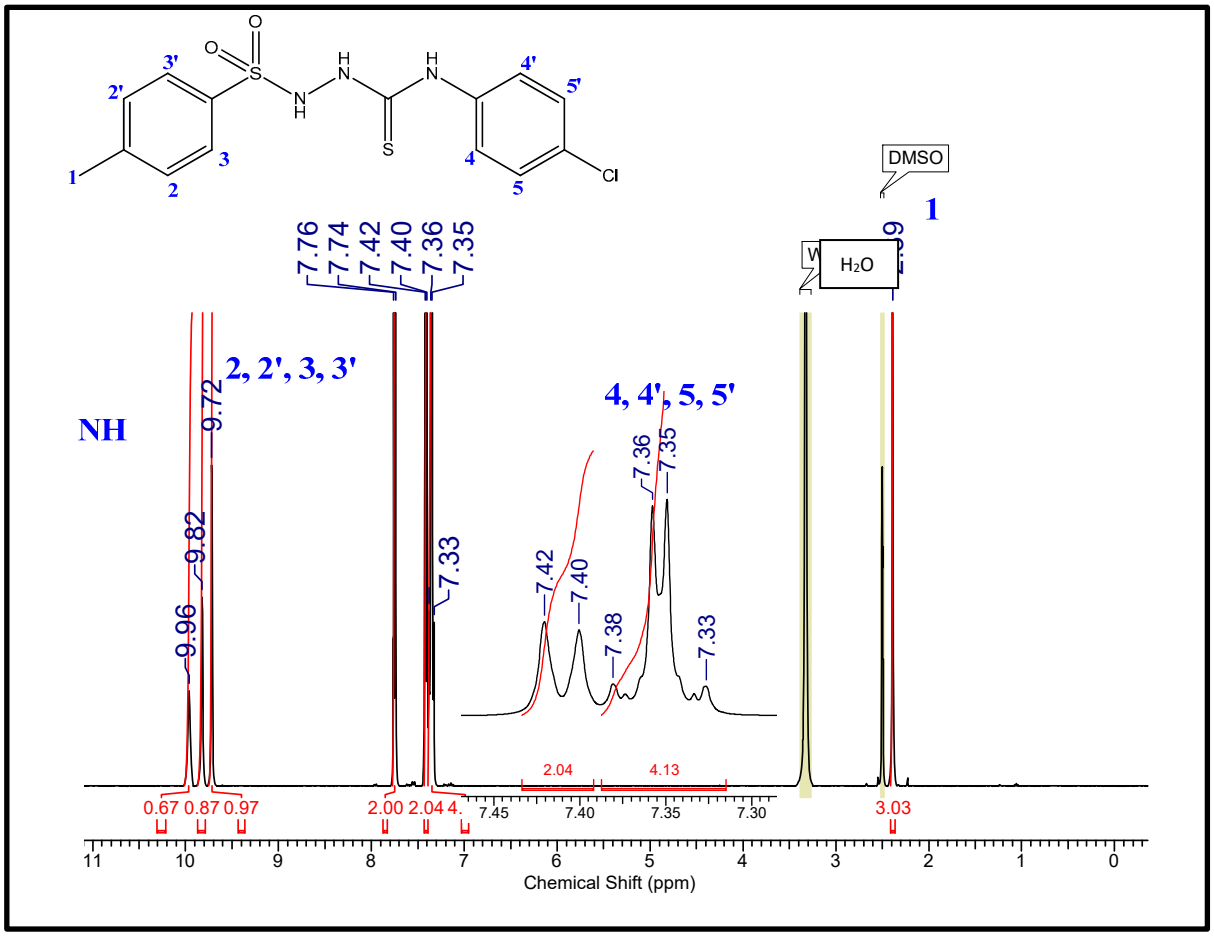

Figure S2.3 – ^{1}H NMR spectrum of HL5^{NO2Ph} in DMSO-d_6.

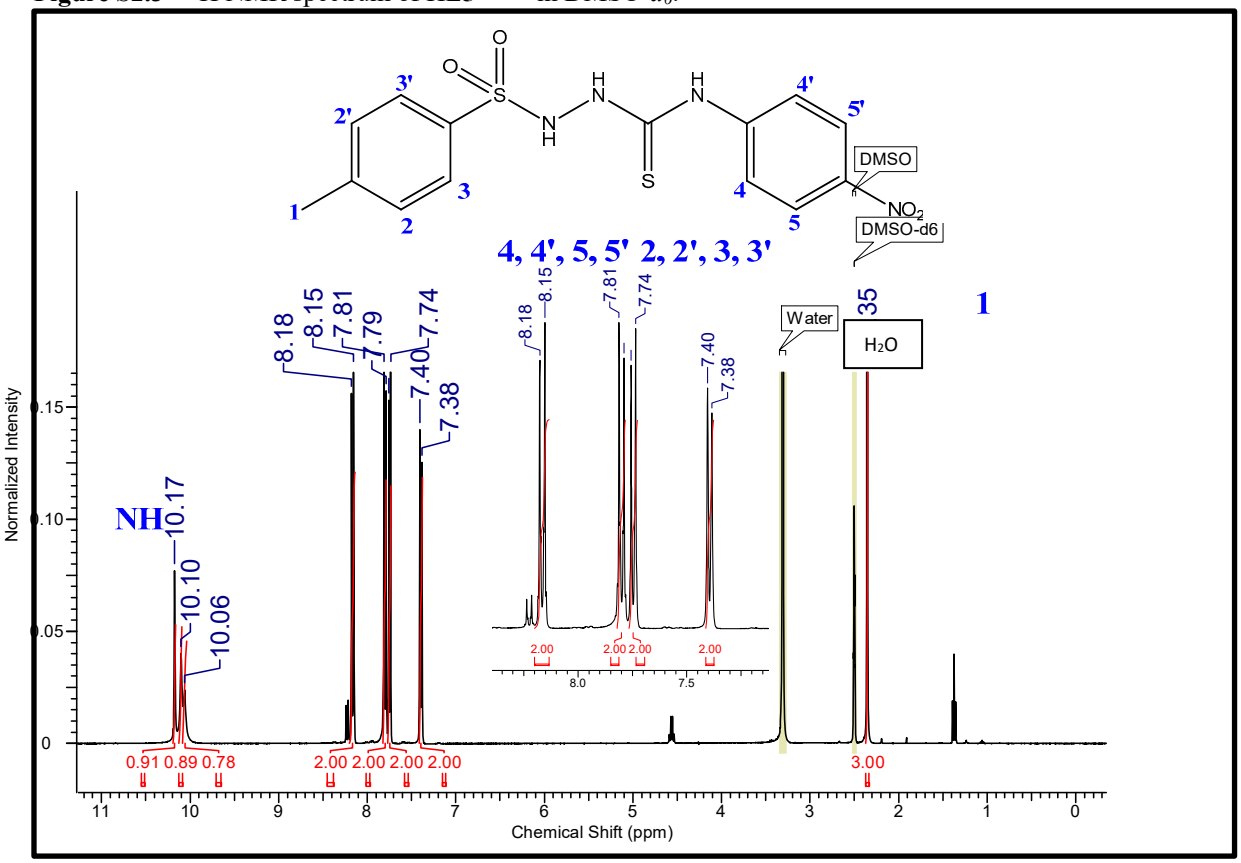

Figure S2.4 – ^{1}H NMR spectrum of HL6^{Al} in DMSO-d_6.

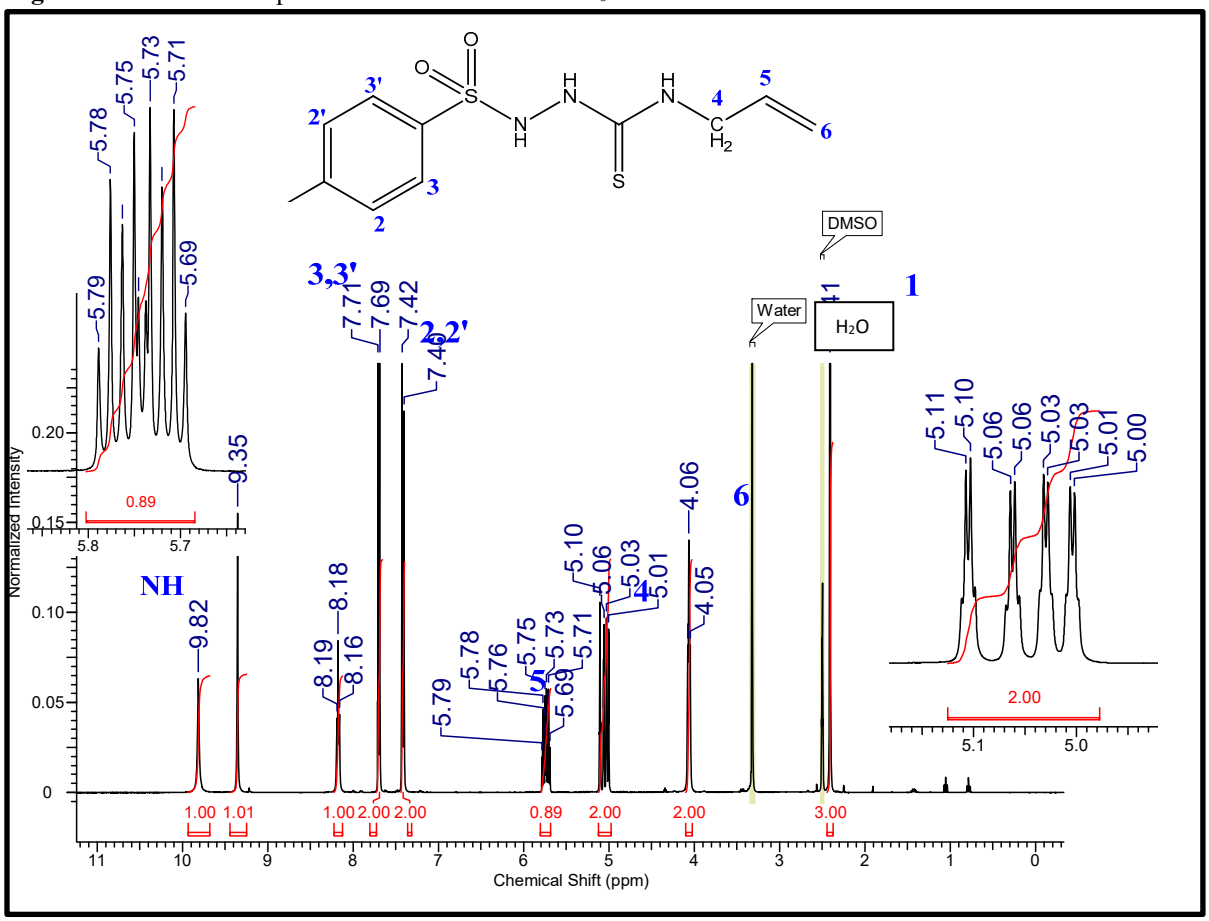

Figure S2.5 – ^{19}F NMR spectrum (377 MHz) of H**L3**$^{\mathbf{FPh}}$ in DMSO-d_6.

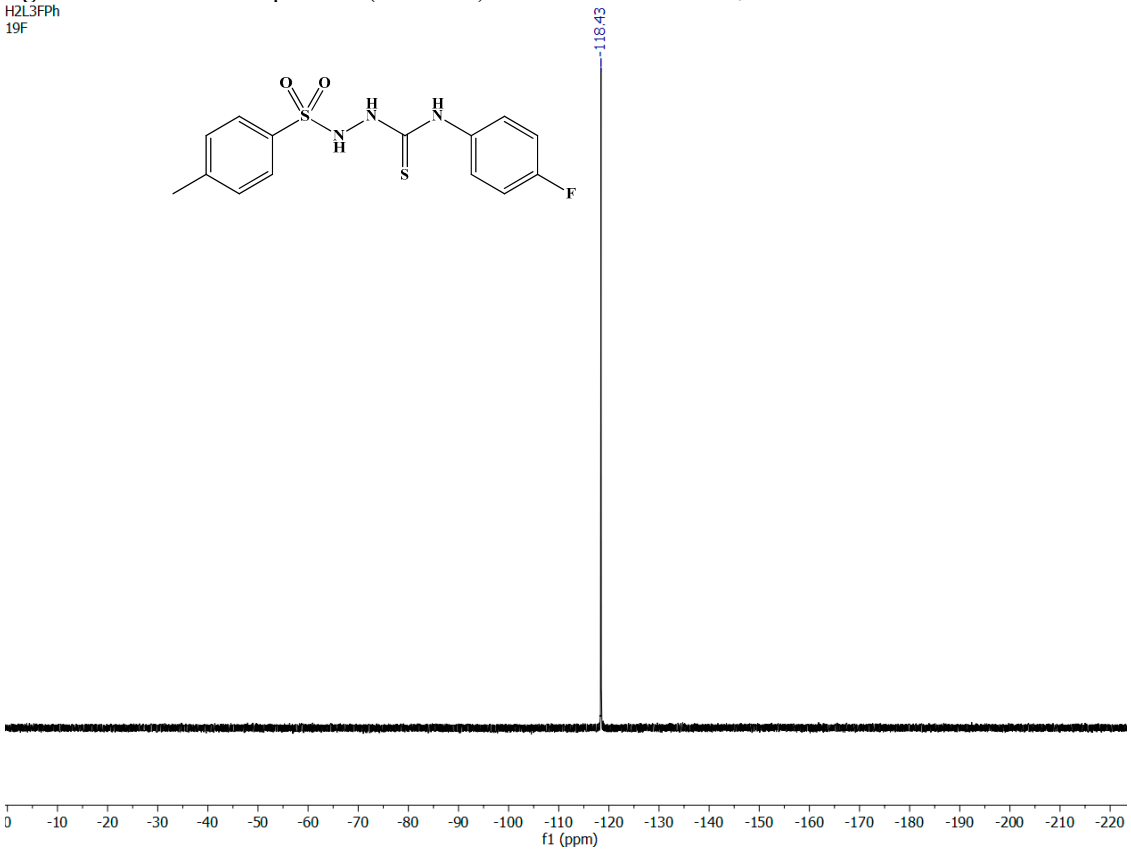

Figure S2.6 – ^{1}H NMR spectrum of [Ag(HL3^{FPh})$_2$]NO$_3$ (**Ag3**) in DMSO-d_6.

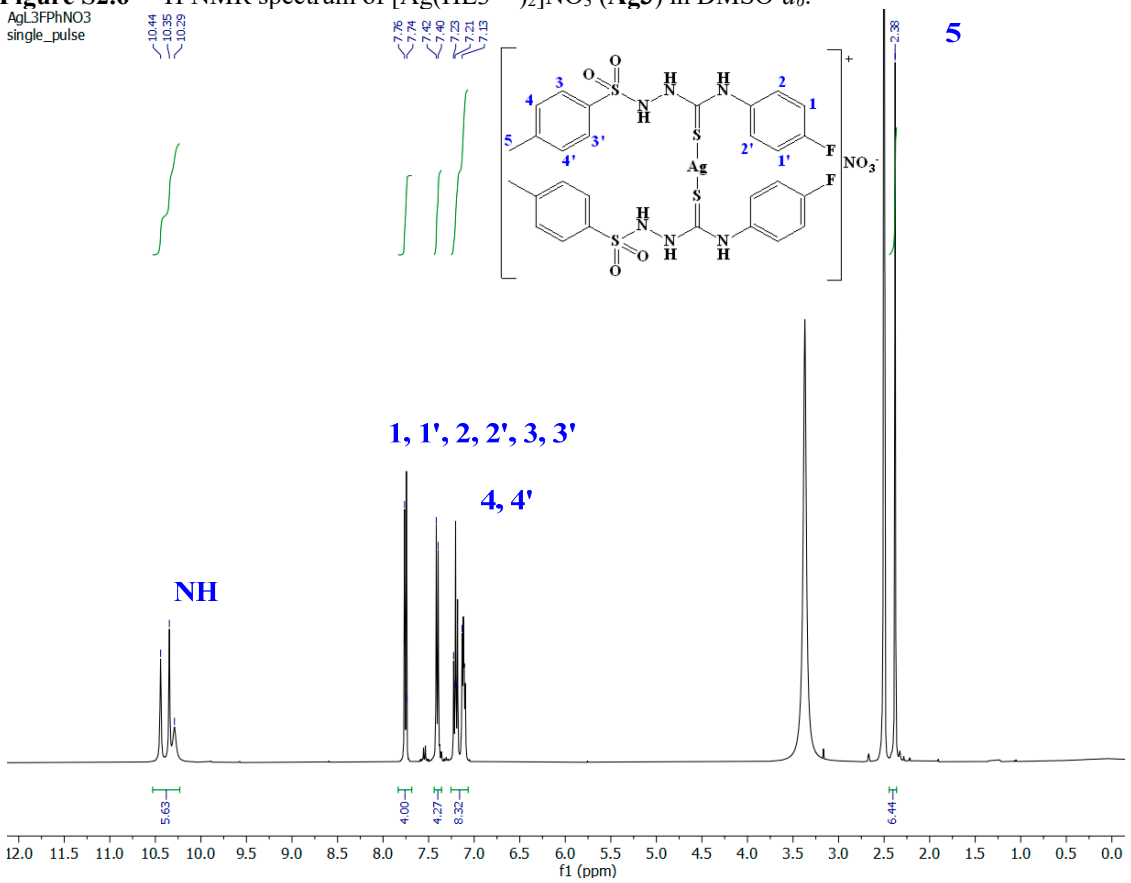

Figure S2.7 – ^{1}H NMR spectrum of $[Ag(HL4^{ClPh})_2]NO_3$ (**Ag4**) in DMSO-d_6.

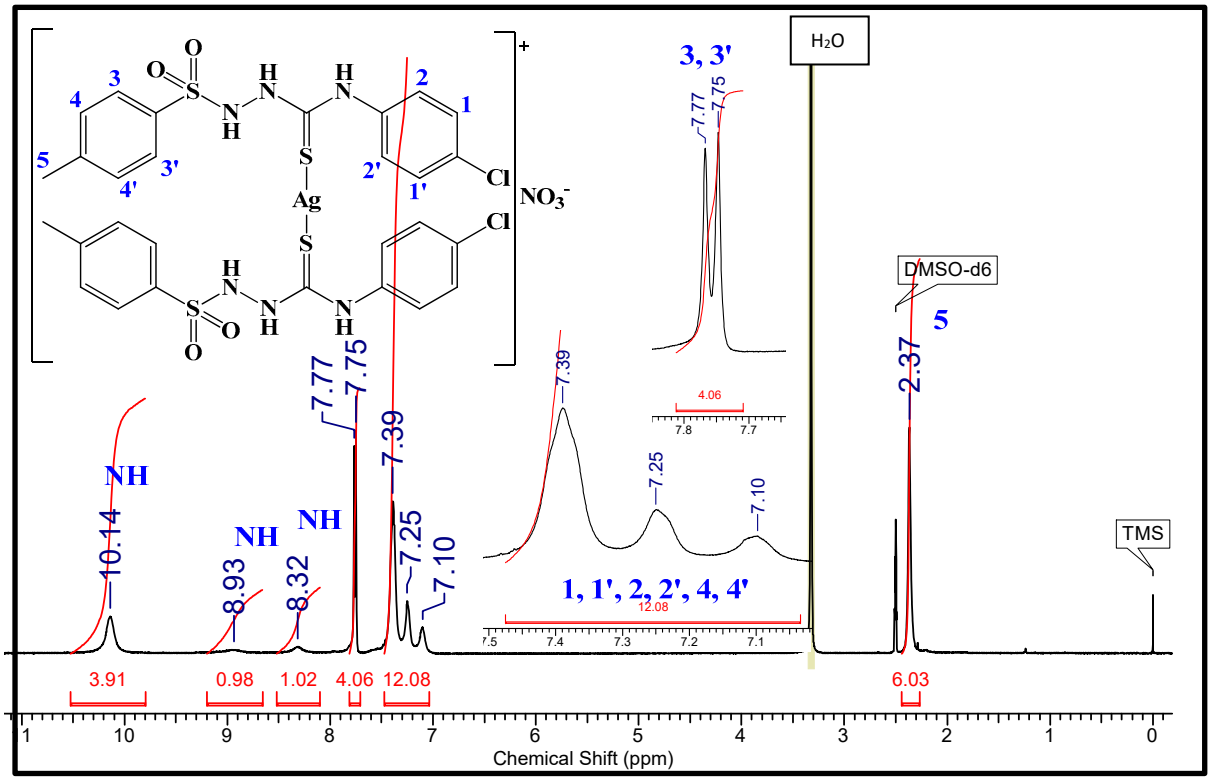

Figure S2.8 – ^{1}H NMR spectrum of $[Ag(HL5^{NO2Ph})_2]NO_3$ (**Ag5**) in DMSO-d_6.

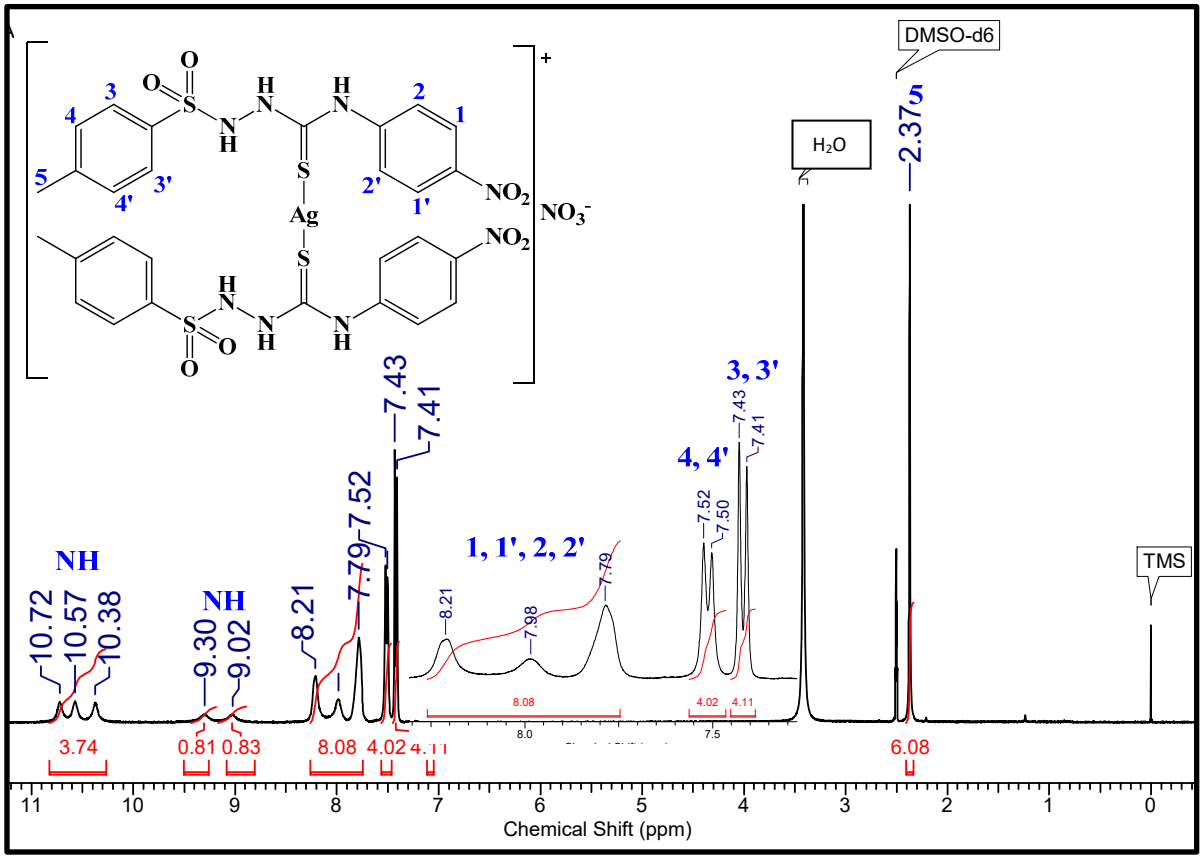

Figure S2.9 – ^{1}H NMR spectrum of [Ag(HL6^{Al})$_2$]NO$_3$ (**Ag6**) in DMSO-*d*$_6$.

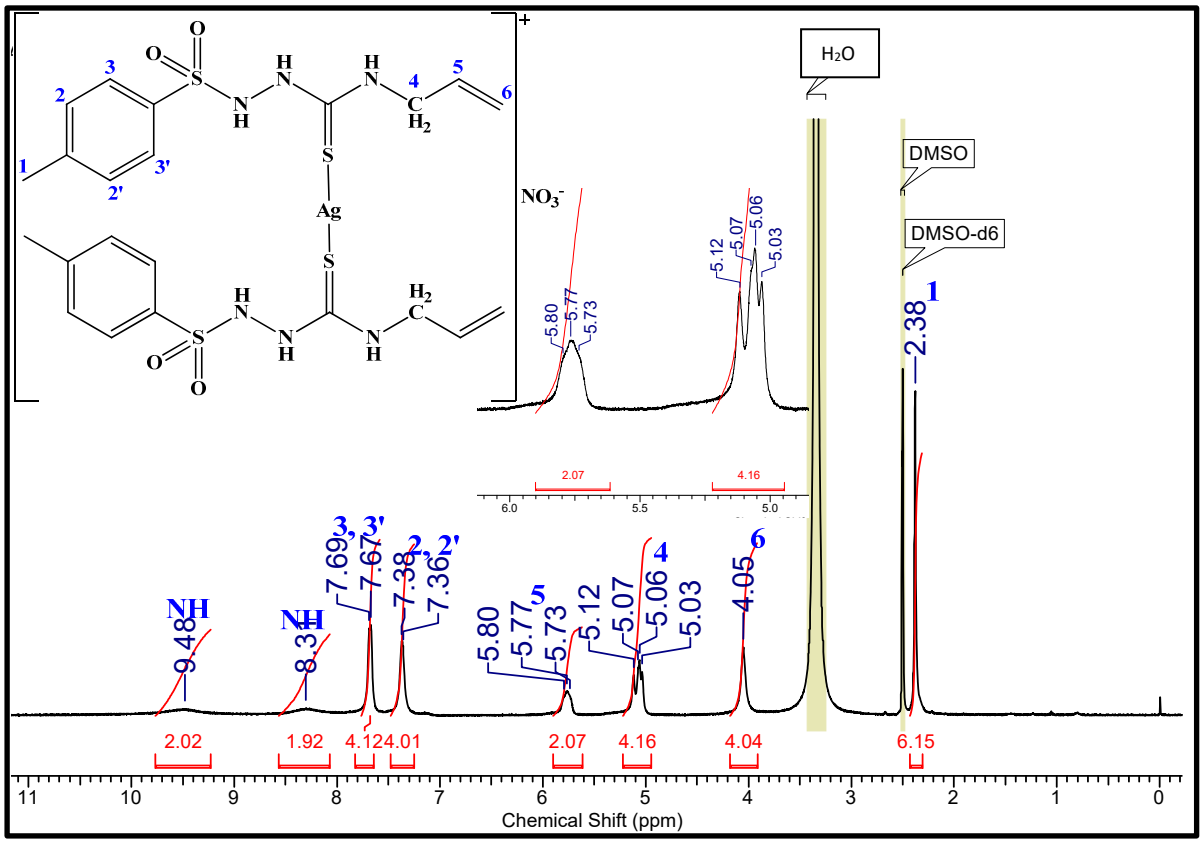

Figure S2.10 – ^{1}H NMR spectrum of [Au(HL1^{Ch})$_2$]Cl (**Au1**) in DMSO-*d*$_6$.

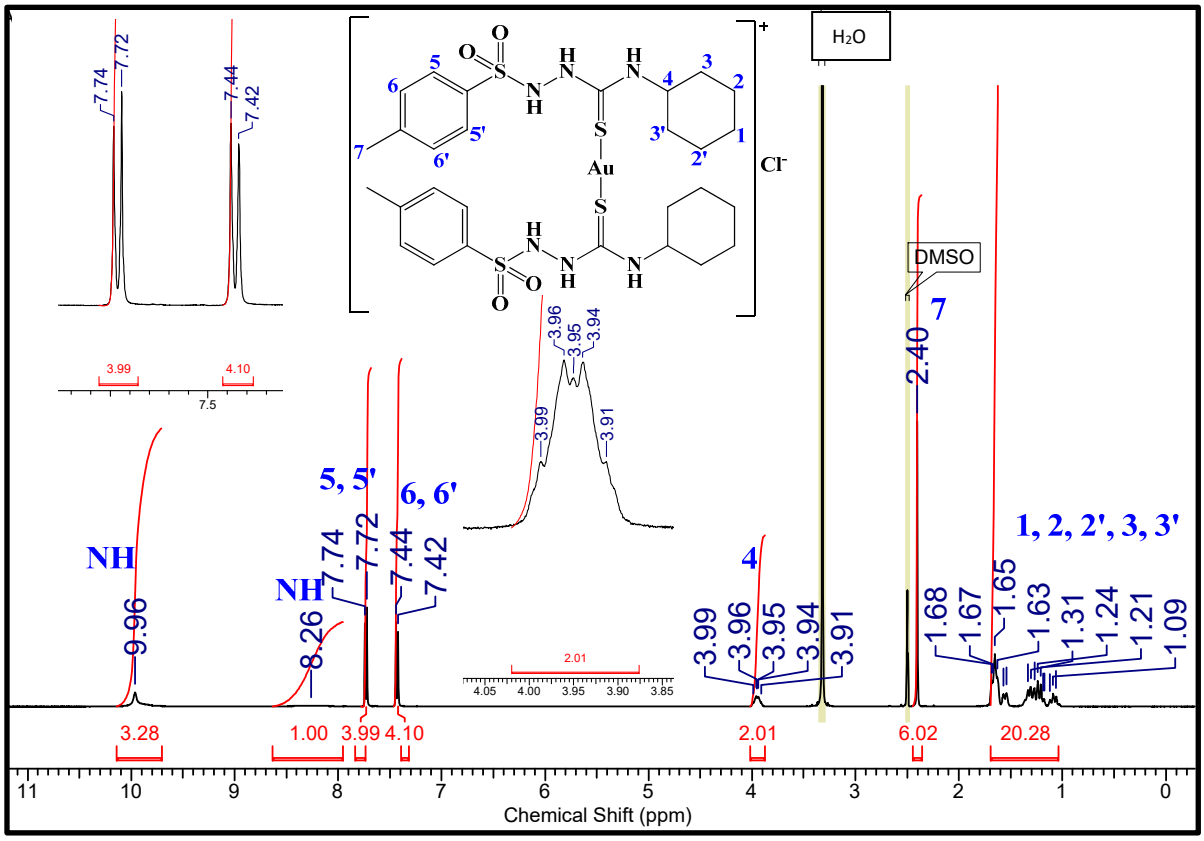

Figure S2.11 – ^{1}H NMR spectrum of [Au(HL2^{Ph})$_2$]Cl (**Au2**) in DMSO-d_6.

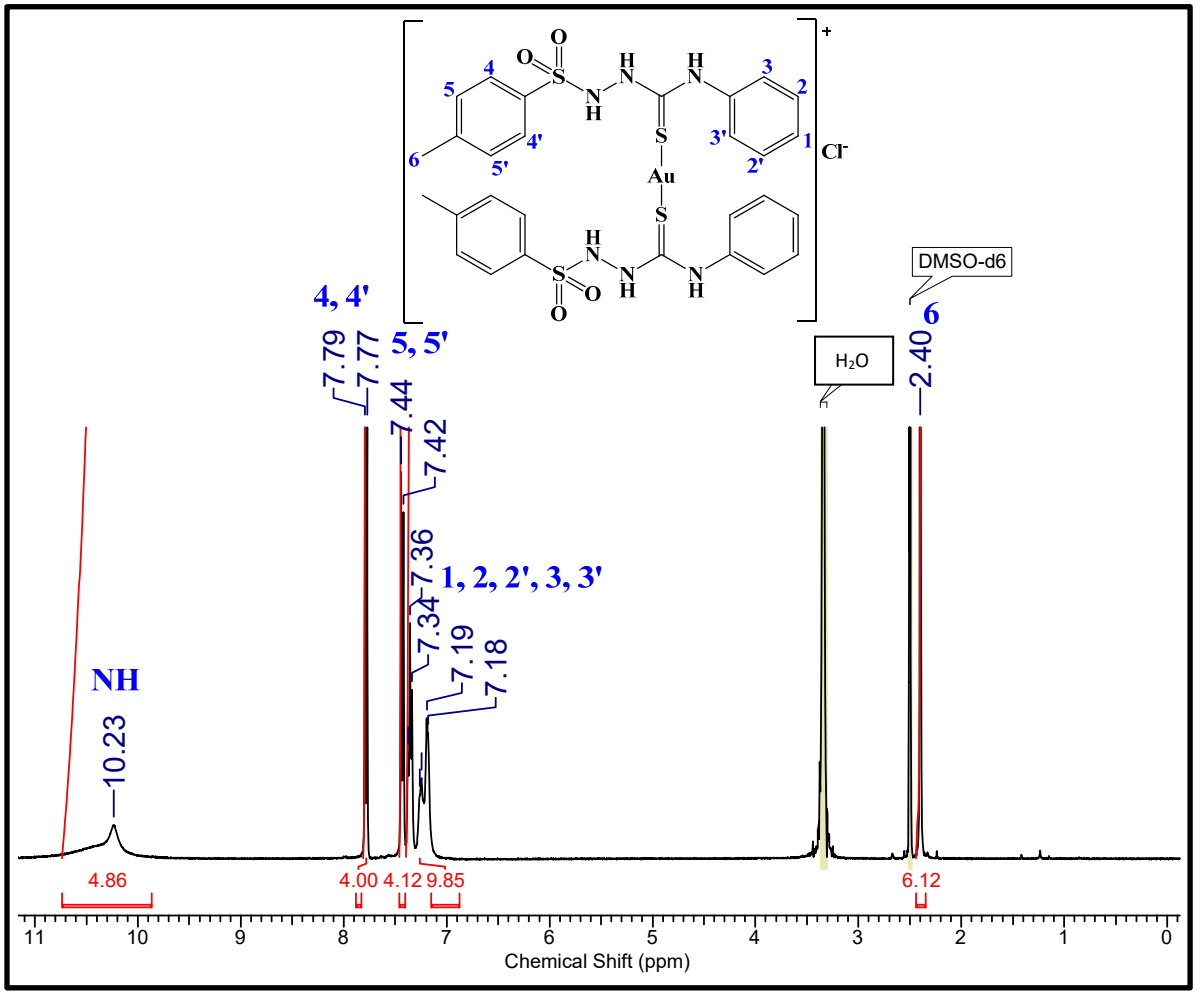

Figure S2.12 – ^{1}H NMR spectrum of [Au(HL3^{FPh})$_2$]Cl (**Au3**) in DMSO-d_6.

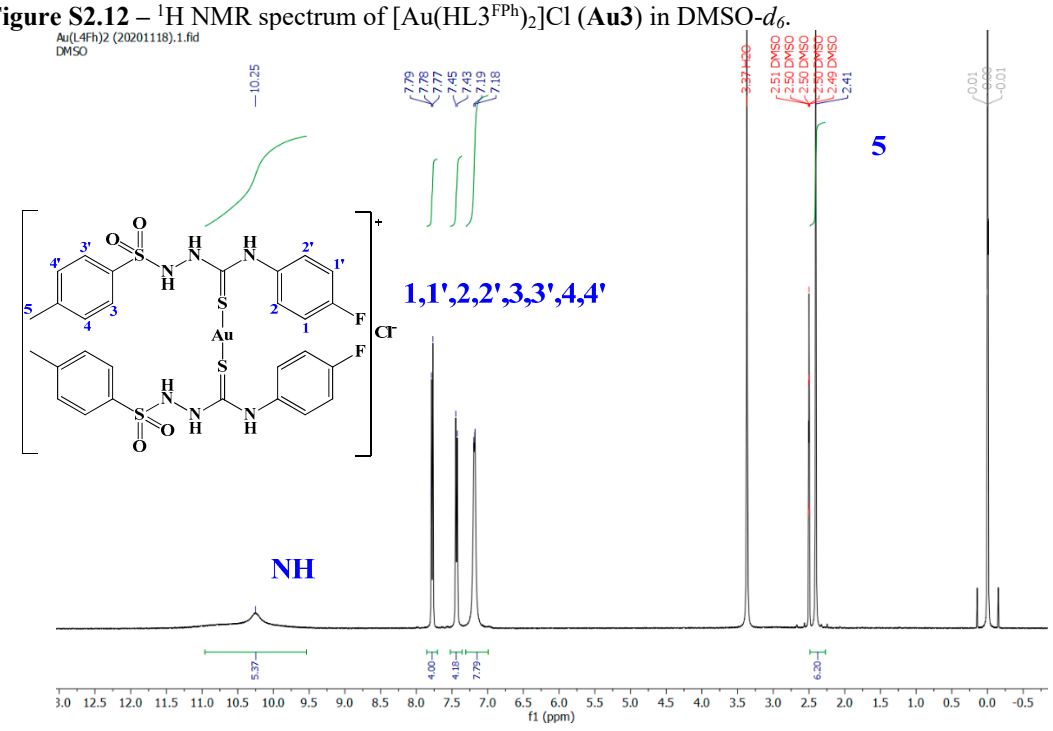

Figure S2.13 – ^{1}H NMR spectrum of [Au(HL4^{ClPh})$_2$]Cl (**Au4**) in DMSO-d_6.

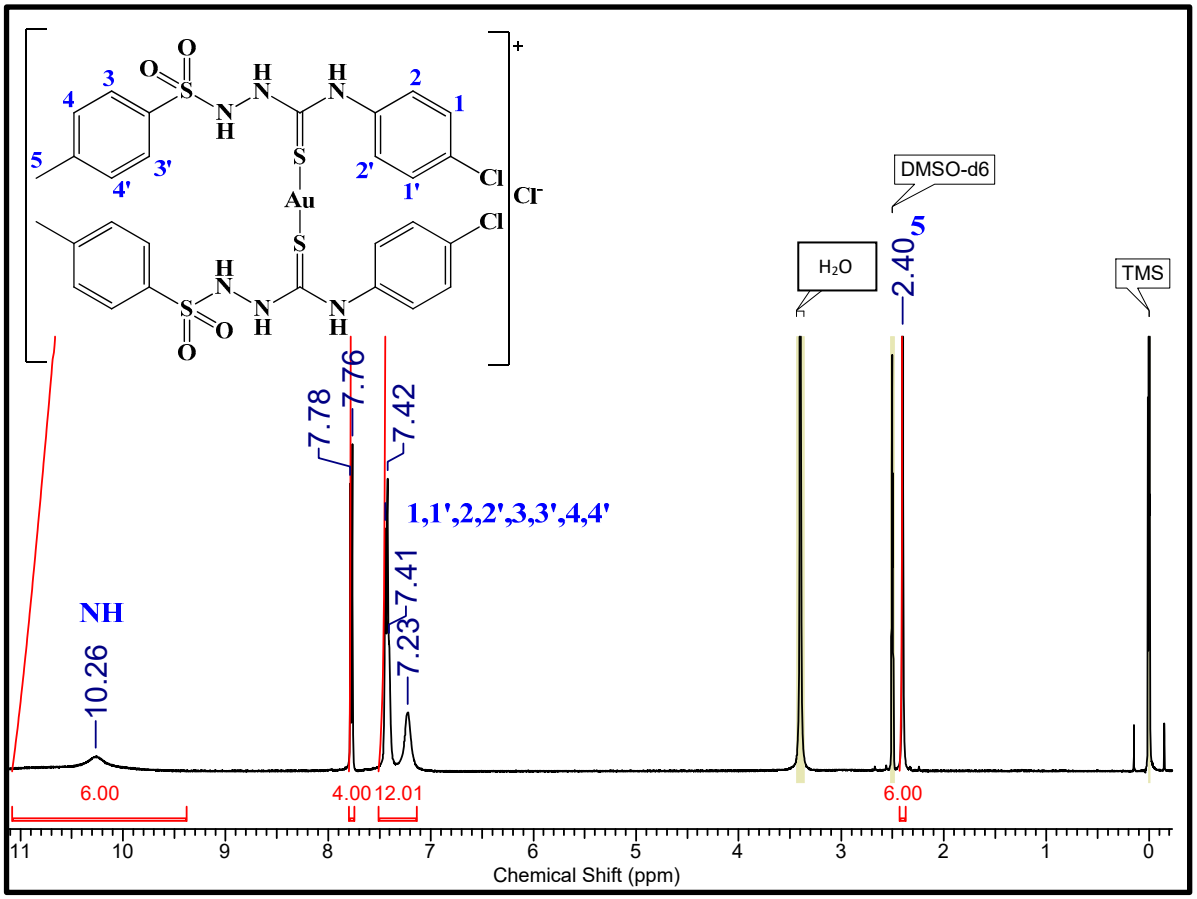

Figure S2.14 – ^{1}H NMR spectrum of [Au(HL5^{NO2Ph})$_2$]Cl(**Au5**) in DMSO-d_6.

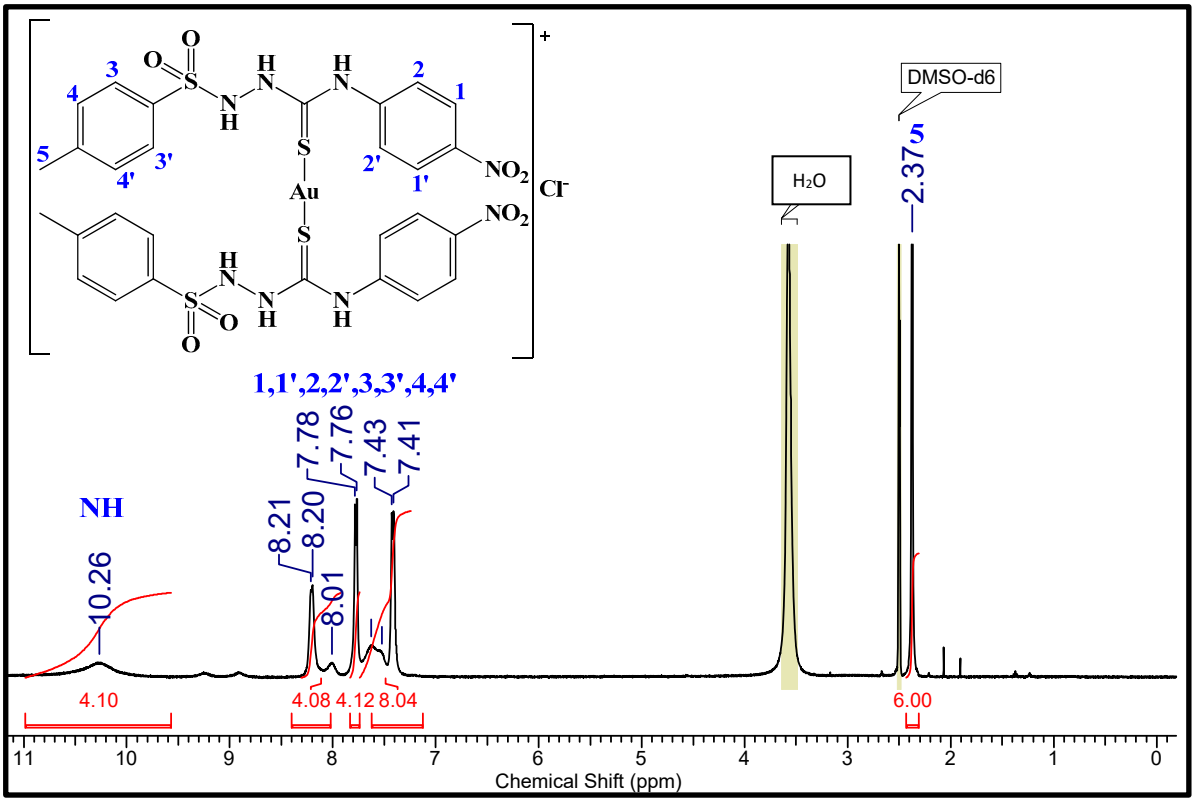

Figure S2.15 – ^{1}H NMR spectrum of [Au(HL6^{Al})$_2$]Cl (**Au6**) in DMSO-d_6.

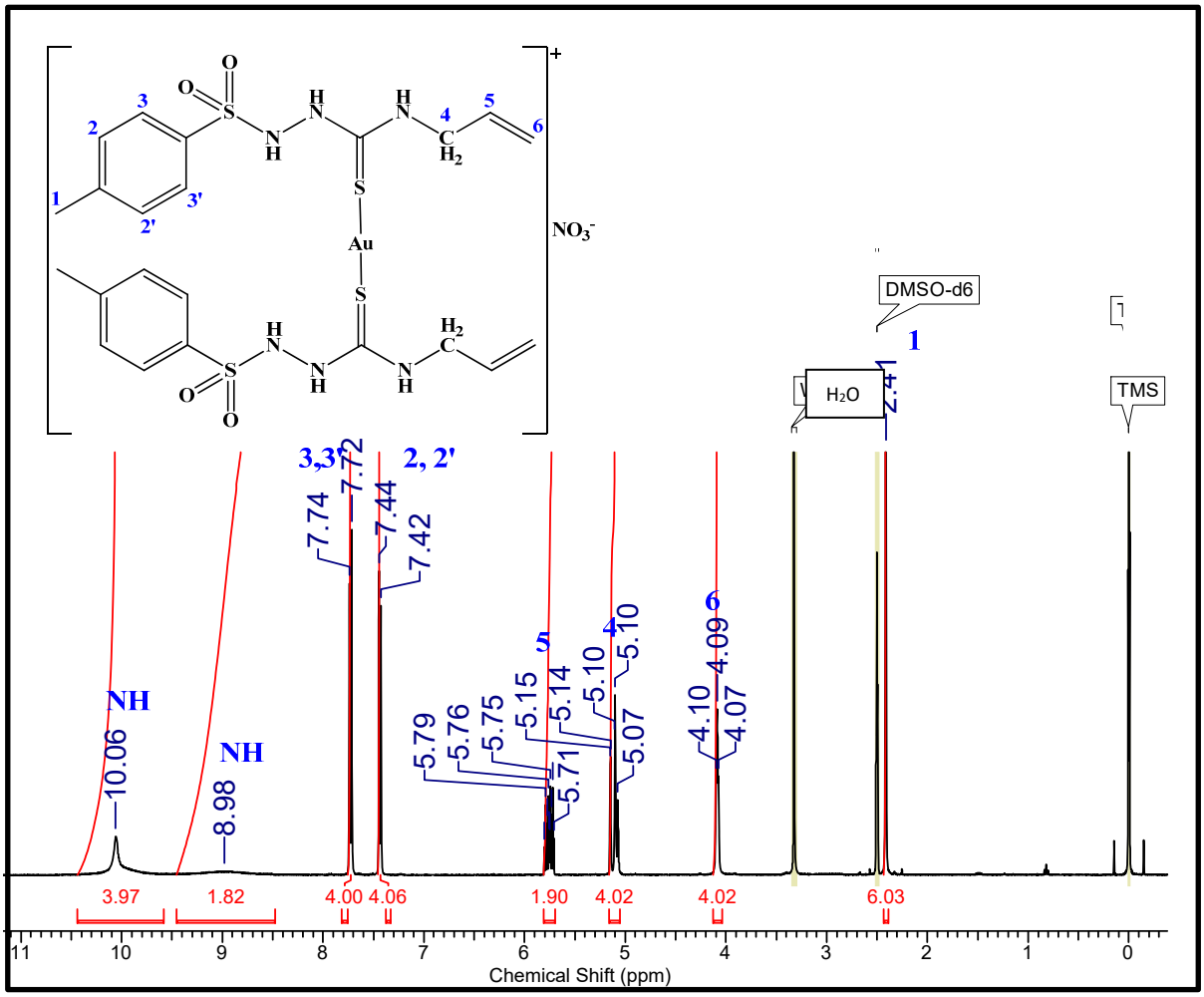

Figure S2.16 – ^{19}F NMR spectrum (377 MHz) of [Ag(HL3^{FPh})$_2$]NO$_3$ (**Ag3**) in DMSO-*d*$_6$.

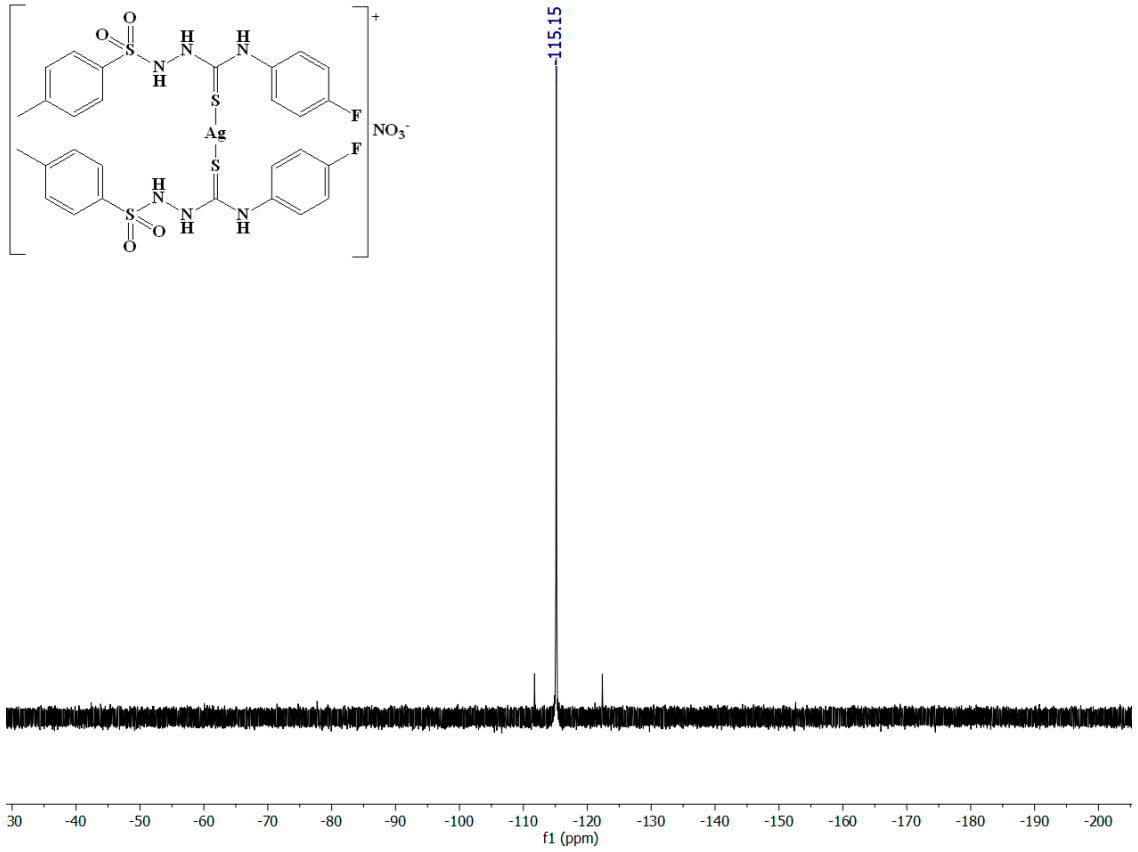

Figure S2.17 – ^{19}F NMR spectrum (377 MHz) of [Au(HL3^{FPh})$_2$]Cl (**Au3**) in DMSO-*d*$_6$.

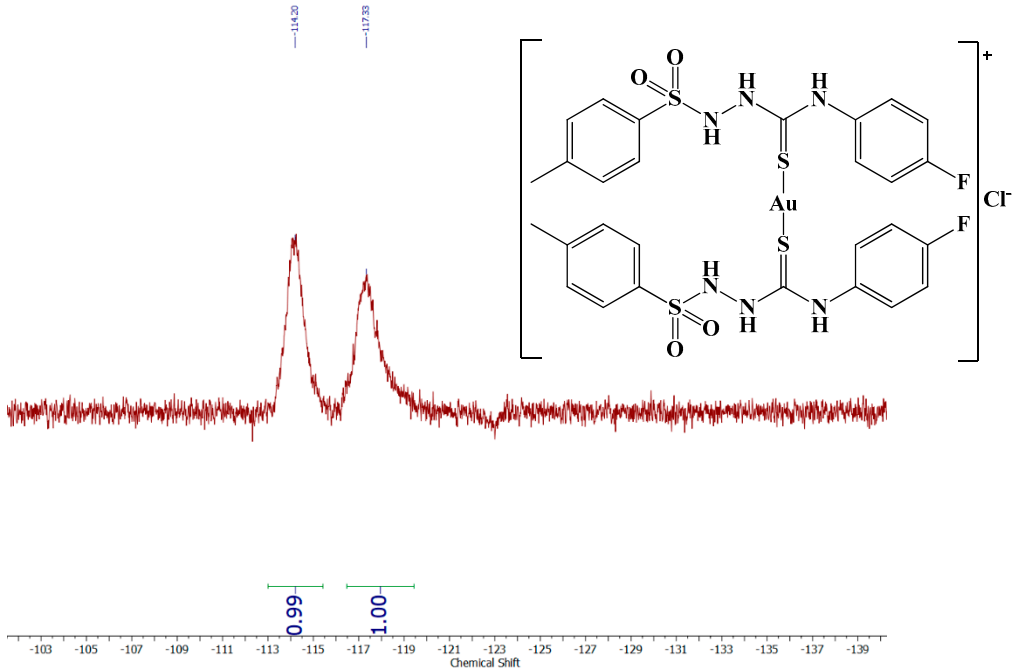

Figure S3.1 – ESI(+) MS spectrum of $[Ag(HL3^{FPh})_2]NO_3$ (**Ag3**).

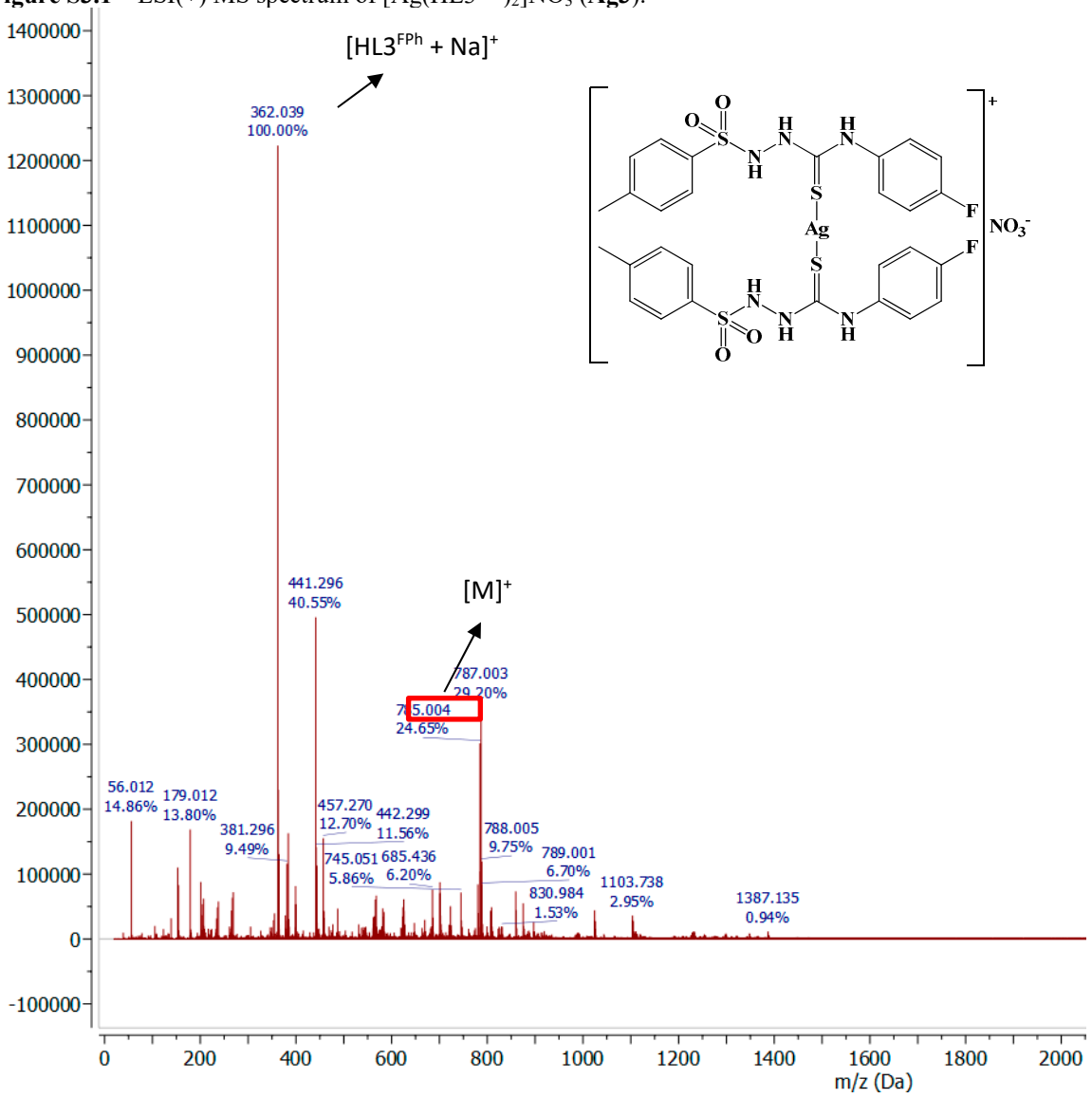

Figure S3.2 – ESI(+) MS spectrum of [Au(HL1^{Ch})$_2$]Cl (**Au1**).

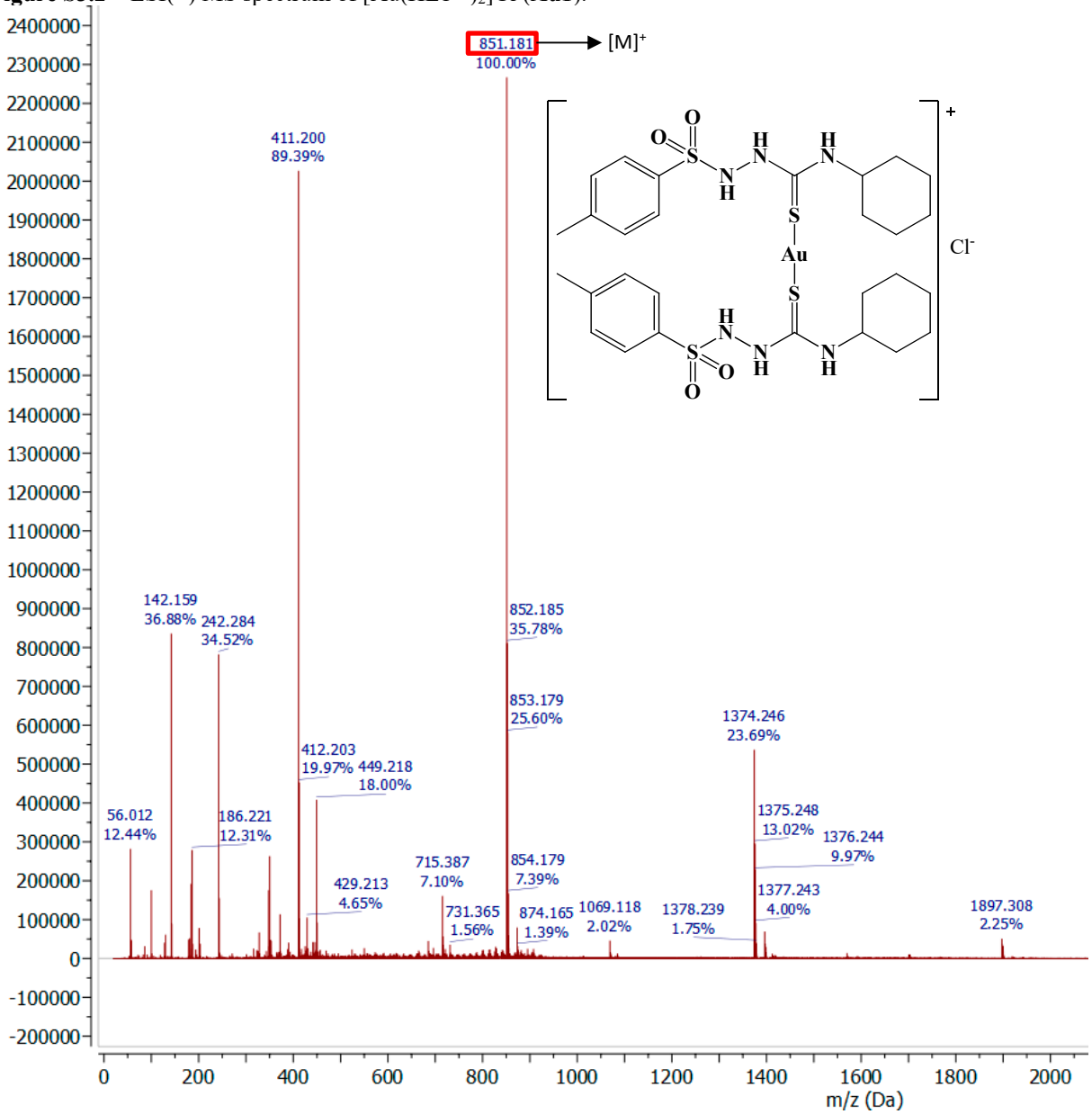

Figure S3.27 – ESI(+) MS spectrum of [Au(HL2^{Ph})$_2$]Cl (**Au2**).

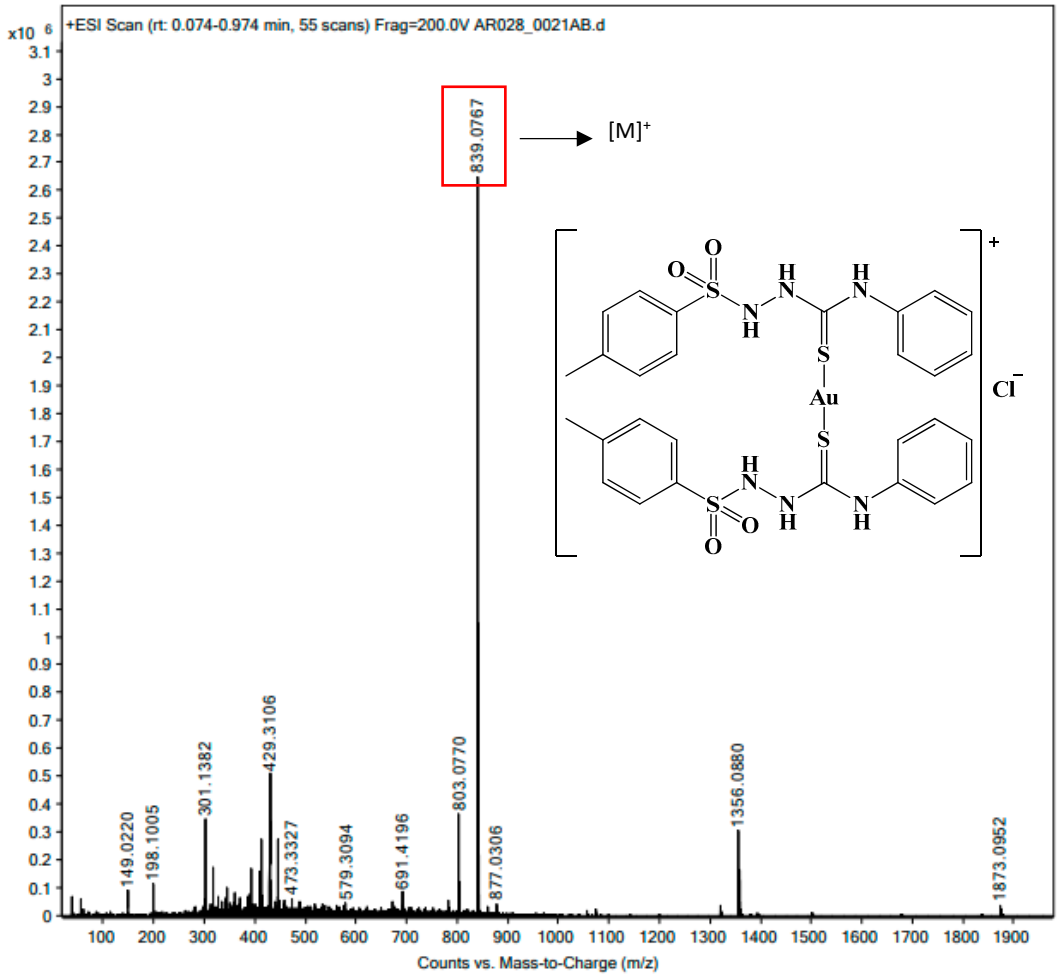

Figure S3.28 – ESI(+) MS spectrum of $[Au(HL3^{FPh})_2]Cl$ (**Au3**).

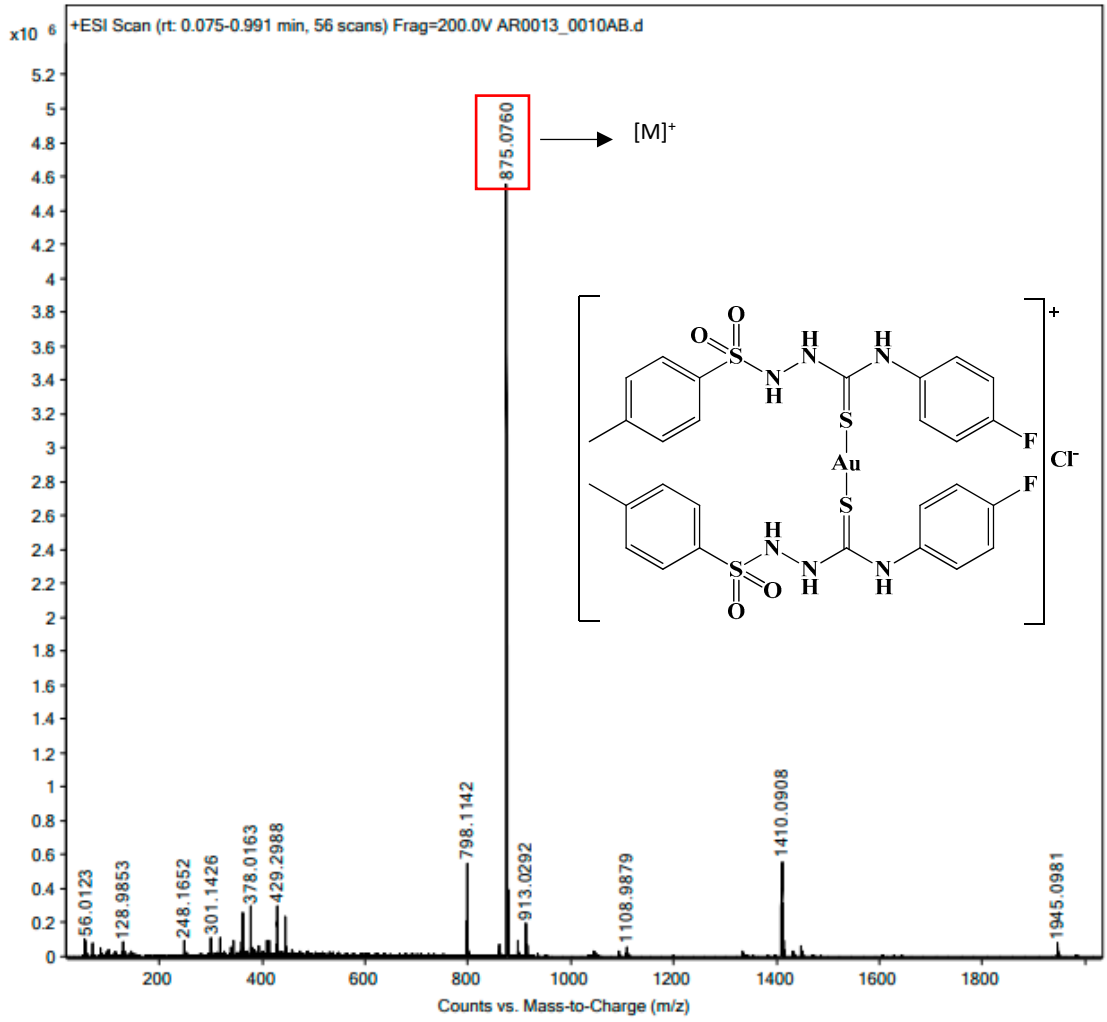

Figure S3.29 – ESI(+) MS spectrum of $[Au(HL4^{ClPh})_2]Cl$ (**Au4**).

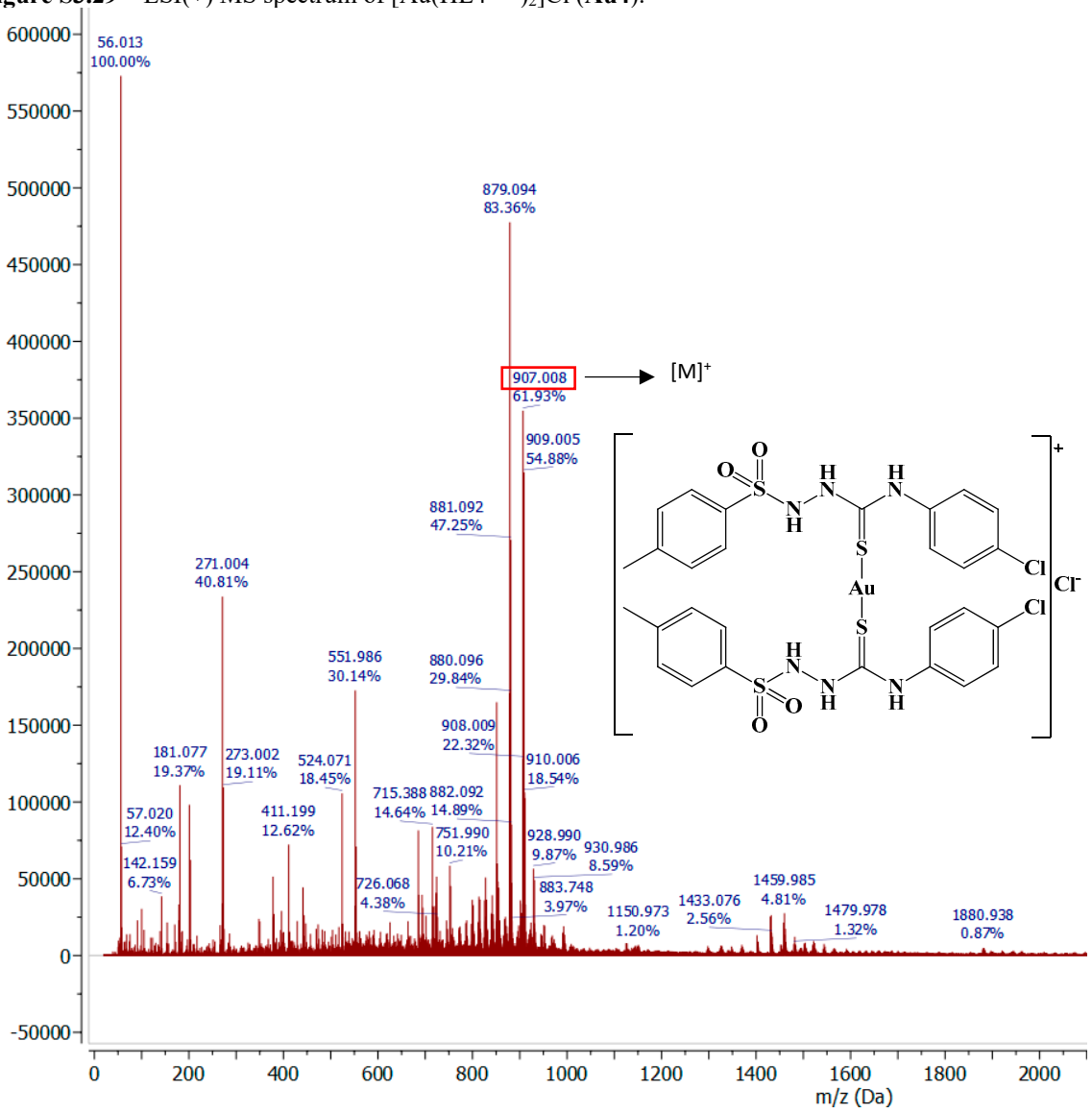

Figure S3.30 – ESI(+) MS spectrum of $[Au(HL6^{Al})_2]Cl$ (**Au6**).

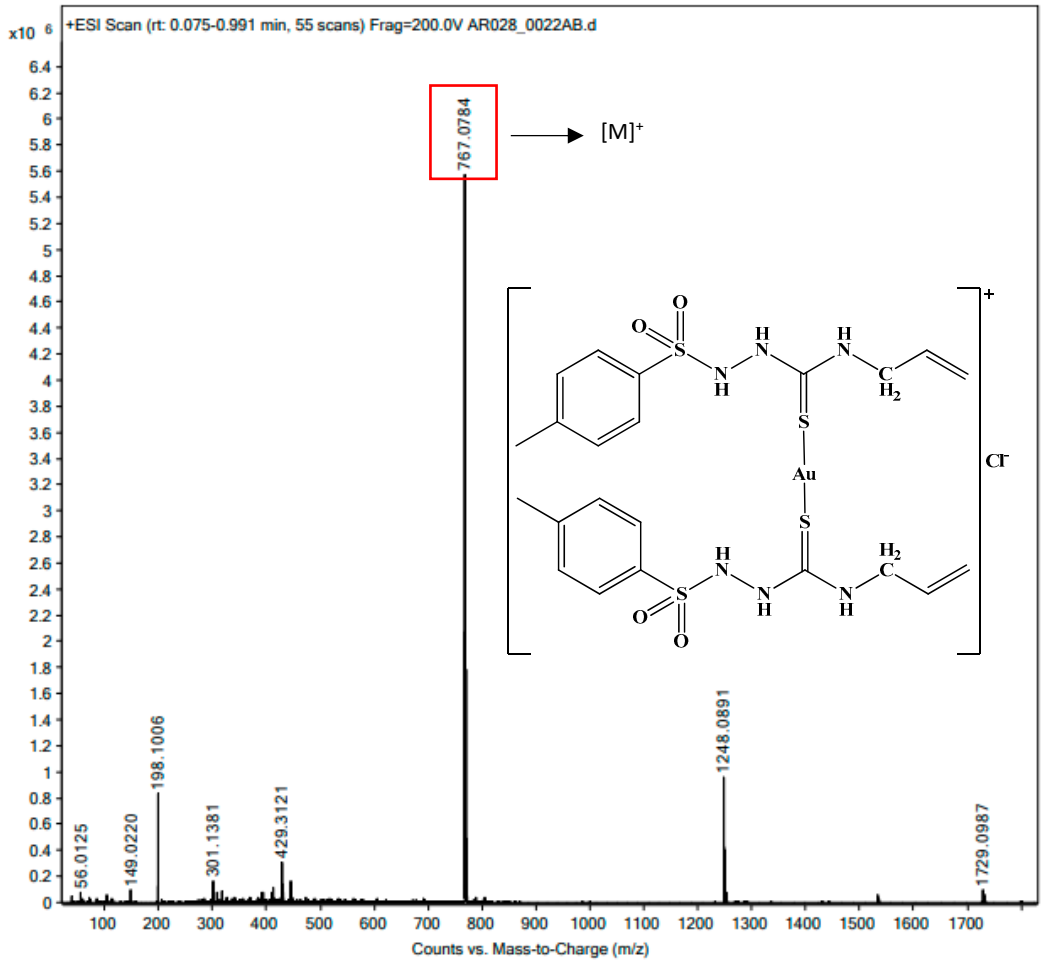

Figure S4.1 – Hydrogen bonds involved in the crystalline structure of the **HL3^{FPh}** ligand. Intermolecular hydrogen bonds: [N(1)···O(1) = 2.910(3) Å, N(1)-H(1)···O(1)= 115.4º], [N(2)···S(1) = 3.311(2) Å, N(2)-H(2)···S(1) = 160.8º], [N(1)···O(2) = 3.420(3) Å, N(1)-H(1)···O(2) = 98.1º], [N(3)···O(2) = 2.959(2) Å, N(3)-H(3)···O(2) = 147.7º]. Intramolecular hydrogen bonding: [N(3)···N(1) = 2.659(3) Å, N(3)-H(3)···N(1)= 110.3 º]. Symmetry operations used (') x-1, y, z, ('') -x, -y+1, -z+1 and (''') -x, -y+2, -z+1. Red dotted lines (between donor and acceptor atoms) represent hydrogen bonds.

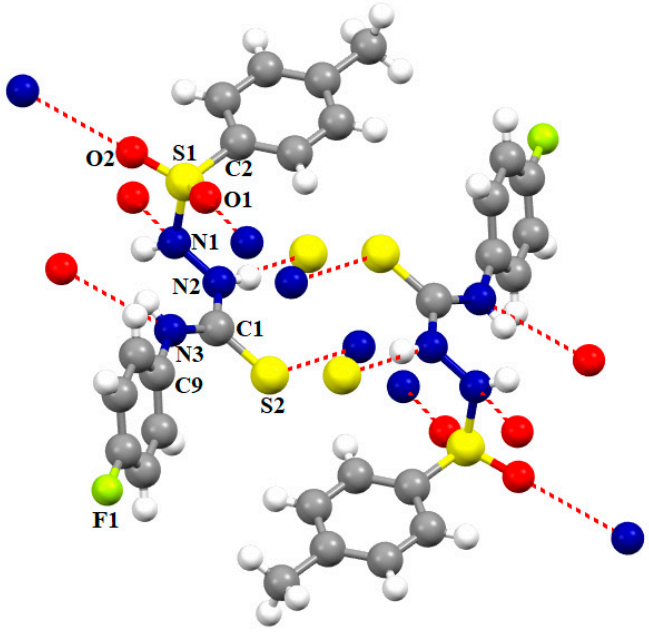

Figure S4.2 - Hydrogen bonds involved in the crystalline structure of the **HL5^{NO2Ph}** ligand. Intermolecular hydrogen bonds: [N(1)···O(1') = 2.887(4) Å, N(1)-H(1)···O(1')= 117.4º], [N(2)···S(1'') = 3.347(3) Å, N(2)-H(2)···S(1'') = 165.2º], [N(3) ···O(2''') = 3.040(4) Å, N(3)-H(3)···O(2''') = 151.8º]. Symmetry operations used (') x-1,y,z, ('') -x, -y+1, -z+1 and (''') -x,-y,-z+1. Blue dotted lines (between donor and acceptor atoms) represent hydrogen bonds.

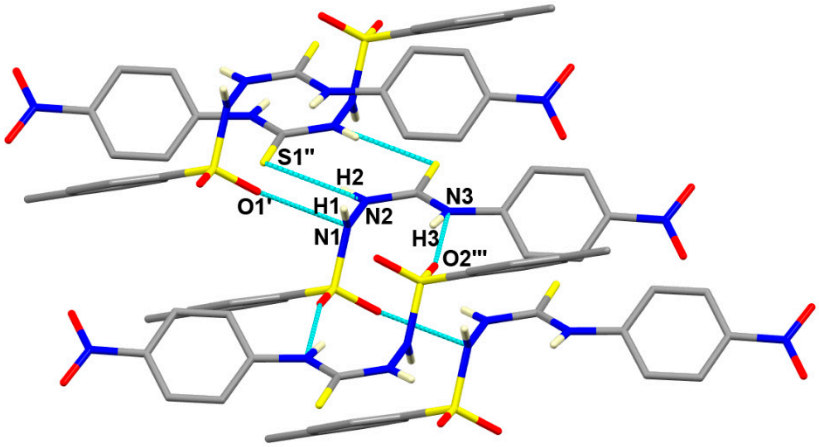

Figure S4.31 - Hydrogen bonds involved in the crystalline structure of the **HL6^{Al}** ligand. Intermolecular hydrogen bonds: [N(3)···O(2) = 3.024(3) Å, N(3)-H(3)···O(2)= 129.0º], [N(2)···S(1) = 3.3475(18) Å, N(2)-H(2)···S(1) = 159.0º], [N(1)···S(1) = 3.356(2) Å, N(1)-H(1)···S(1)= 118.4º]. Symmetry operations used (') -x, -y, -z+1, ('') -x+1, -y+1, -z+1 and (''') x-1, y, z. Blue dotted lines (between donor and acceptor atoms) represent hydrogen bonds.

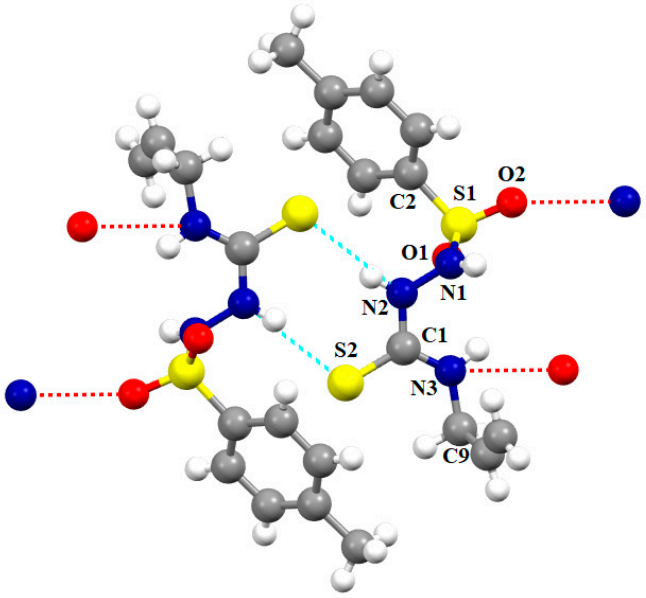

Figure S4.4 Ellipsoid representation of $[Au(HL1^{Ch})_2]Cl{\cdot}CH_3OH$ (**Au1**$\cdot CH_3OH$). The hydrogen atoms have been omitted for clarity. A solvent mask was calculated and 108 electrons were found in a volume of 518 Å^3 in 1 void per unit cell. This is consistent with the presence of 0.5[CH_2Cl_2; $2H_2O$] per Asymmetric Unit which account for 120 electrons per unit cell.

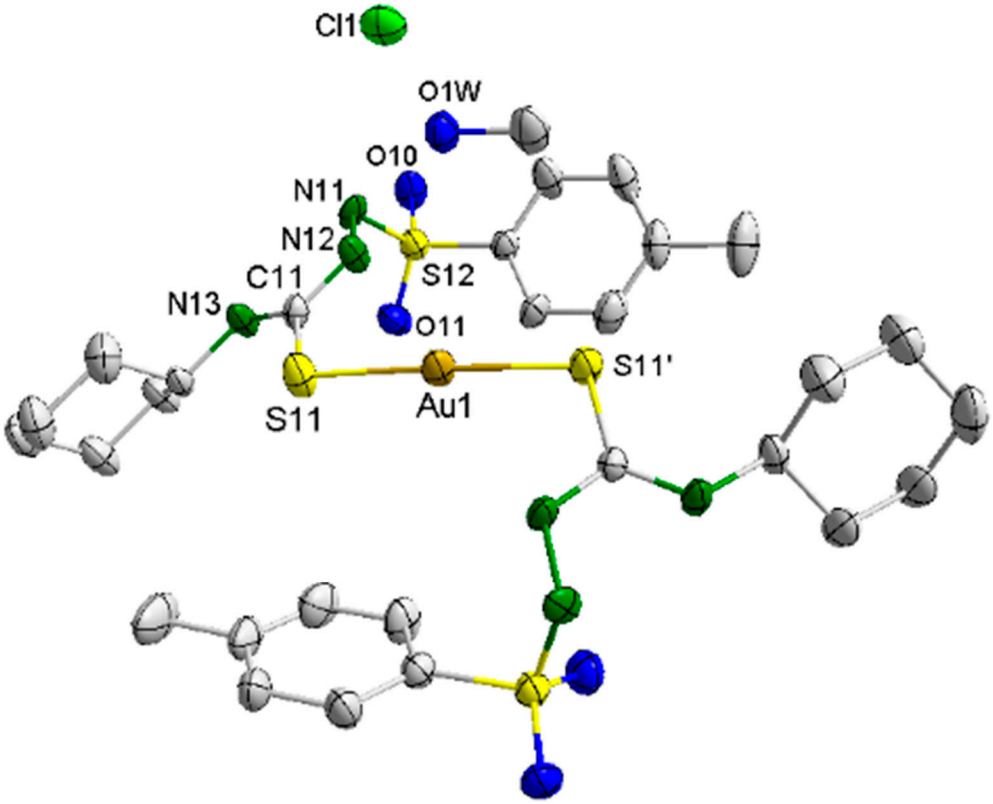

Figure S4.5 Ellipsoid representation of $[Au(HL2^{Ph})_2]Cl{\cdot}CH_3OH$ (**Au2**·CH_3OH). The hydrogen atoms have been omitted for clarity.

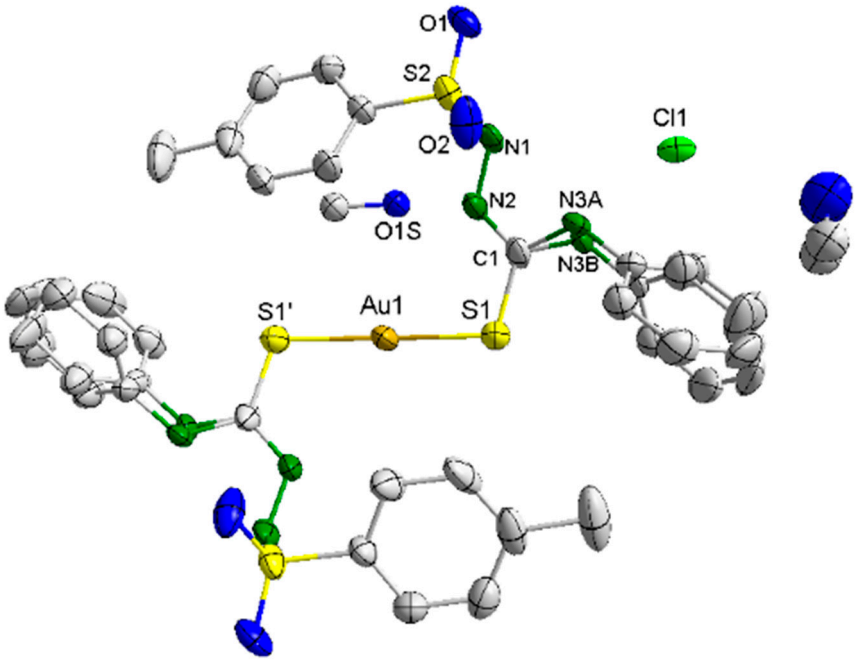

Figure S4.6 - - Hydrogen bonds involved in the crystalline structure of the **Au2** complex. Intermolecular hydrogen bonds: [N(1)···Cl(1) = 3.173(4) Å, N(1)-H(1)···Cl(1)= 113.8º], [O(1S)···Cl(1) = 3.135(5) Å, O(1S)-H(1S)···Cl(1) = 152.4º], [N(3A)···O(1) = 2.775(14) Å, N(3A)-H(3A)···O(1) = 146.1º], [N(3B)···O(1) = 3.149(14) Å, N(3B)-H(3B)···O(1) = 136.9º]. Intramolecular hydrogen bonding: [N(2)···O(1S) = 2.905(5) Å, N(2)-H(2)···O(1S)= 135.6 º]. Symmetry operations used (') -x, +y, -z. Blue dotted lines (between donor and acceptor atoms) represent hydrogen bonds.

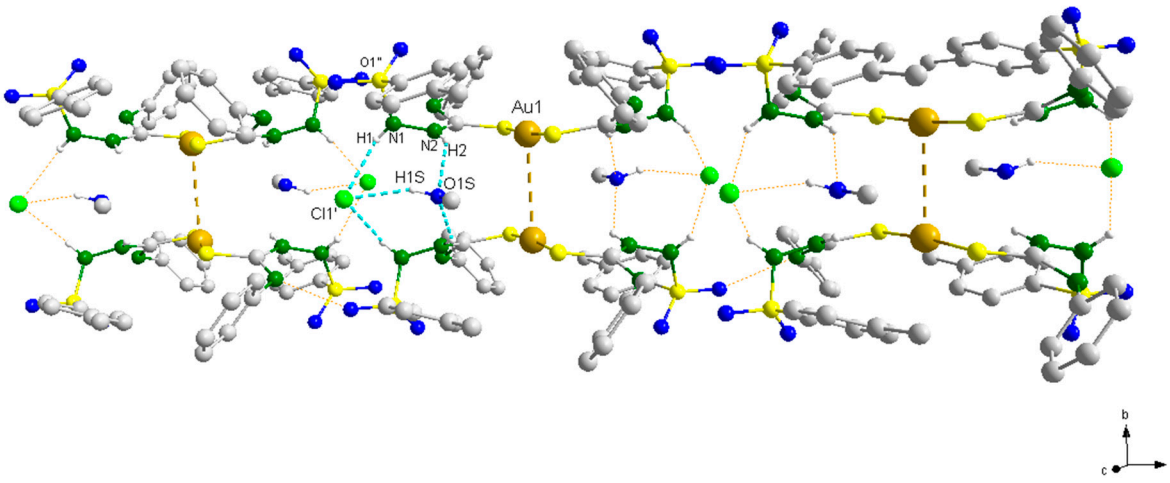

Figure S5.1 - Electronic spectra of **Ag3** (green line), **Ag4** (orange line), **Ag5** (red line) and **Ag6** (purple line) in the 210 to 350 nm range (10^{-6} M CH_3CN solution).

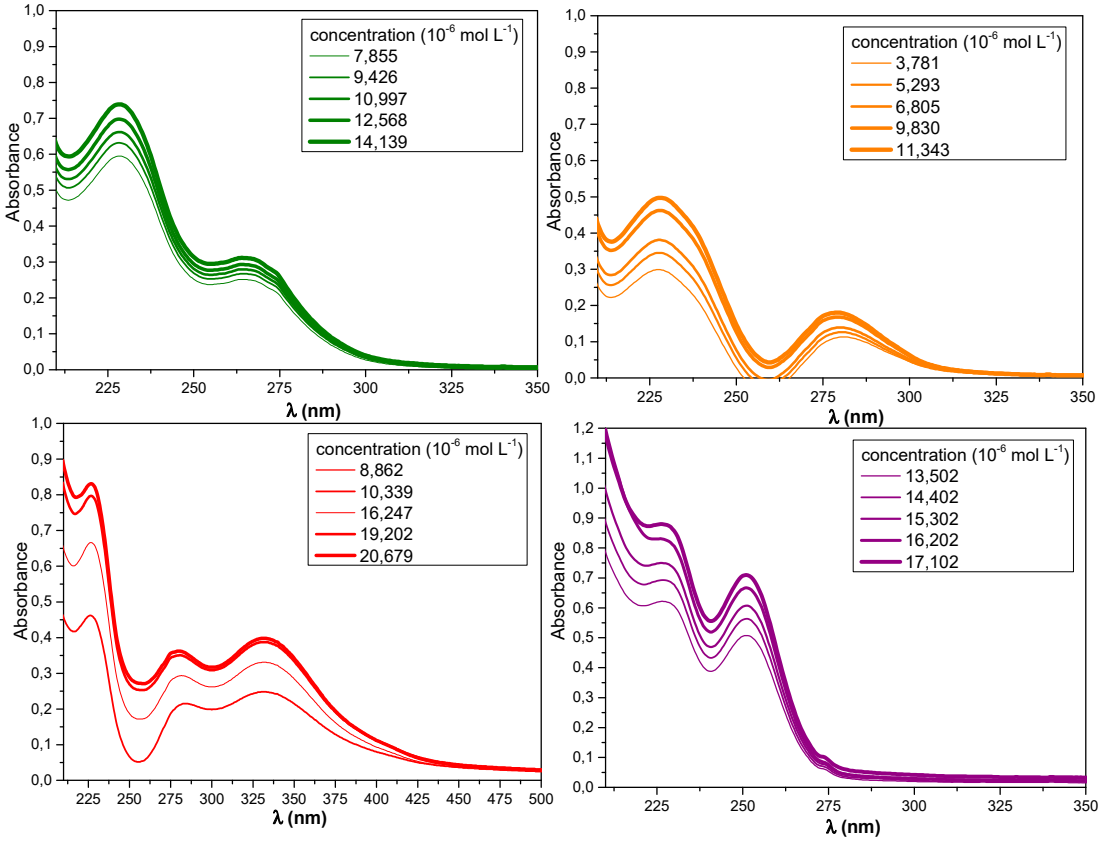

Figure S5.2 – Electronic spectra of **Au1** (blue line), **Au2** (pink line), **Au3** (green line), **Au4** (orange line), **Au5** (red line) and **Au6** (purple line) in the 210 to 350 nm range (10^{-6} M CH_3OH solution for **Au1**, **Au2**, **Au3**, **Au6** and 10^{-6} M solution CH_3CN for **Au4** and **Au5**).

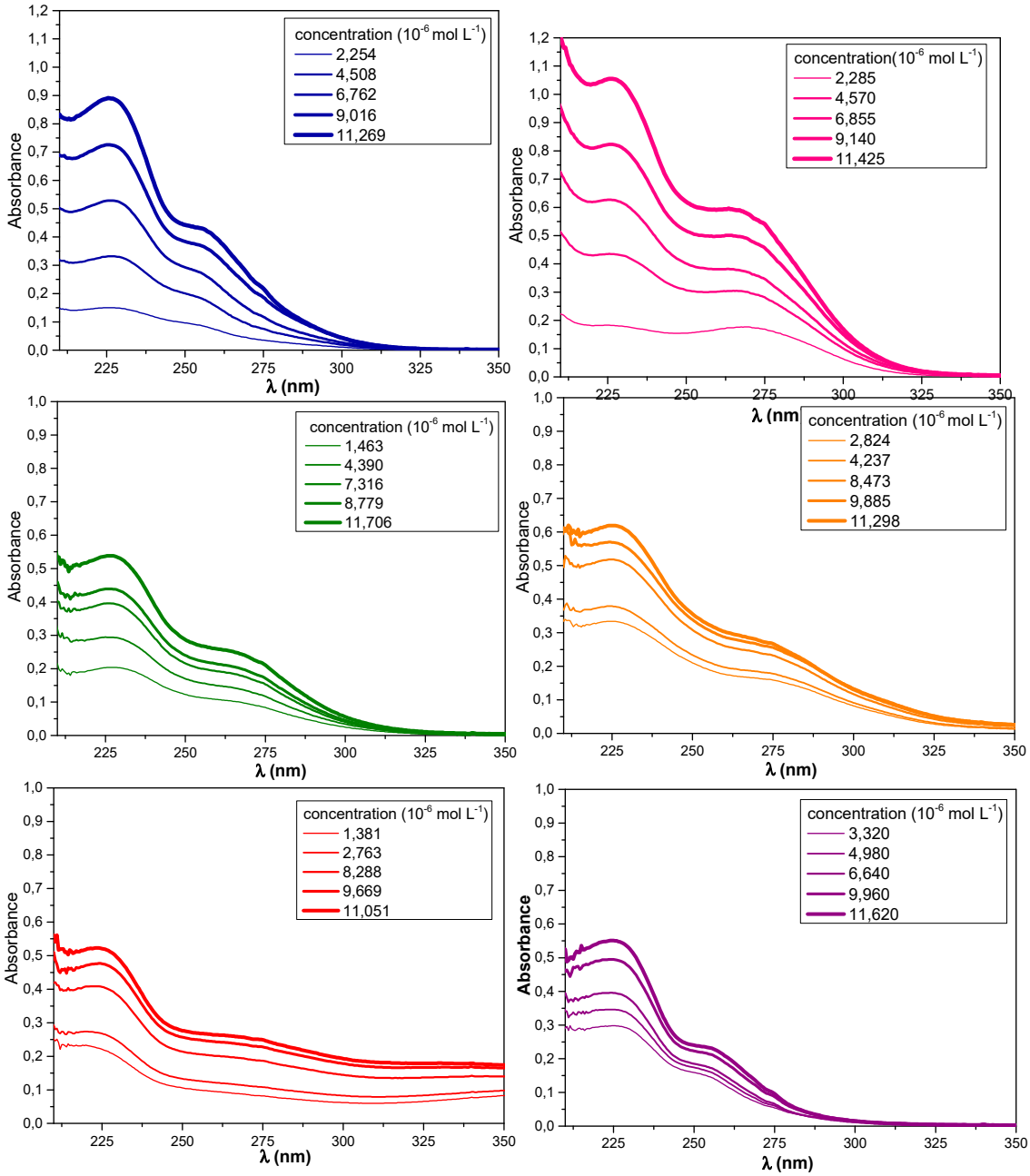

Figure S5.32 – Linear regression for **Ag3** (green line), **Ag4** (orange line), **Ag5** (red line) and **Ag6** (purple line).

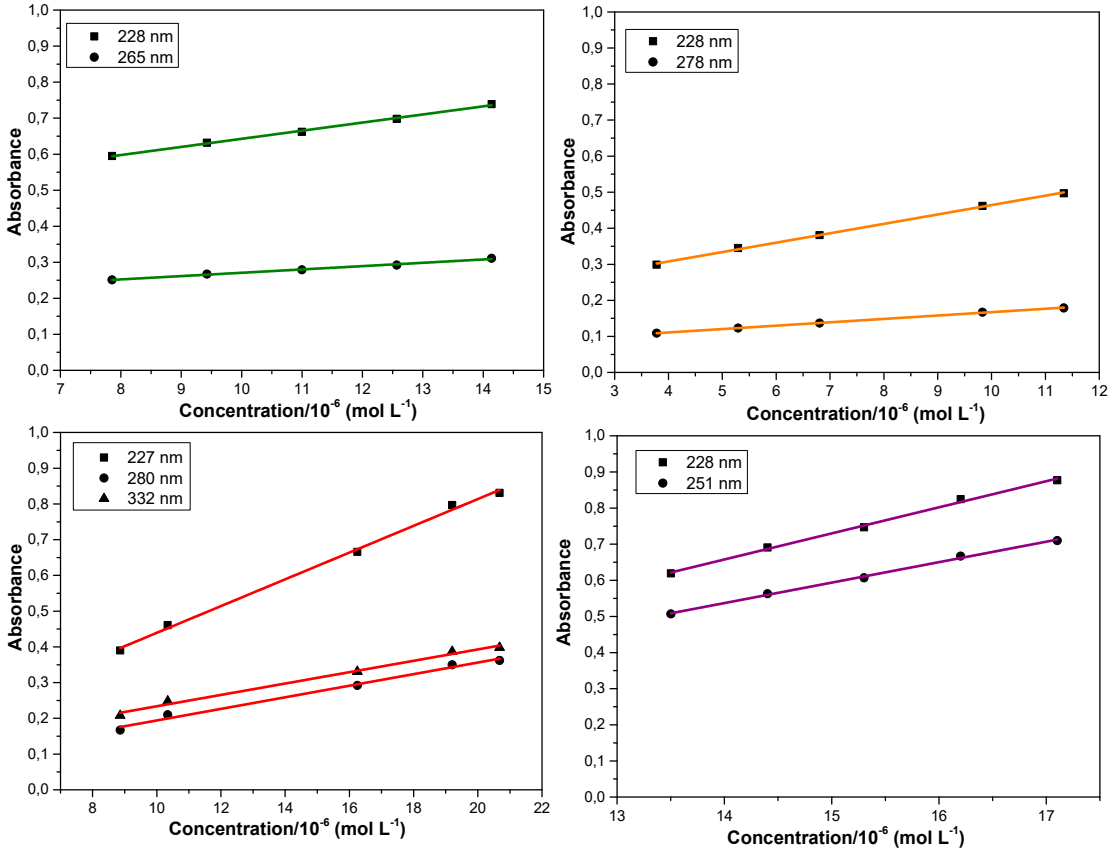

Table S2 – Electronic spectra data obtained for the **Ag3** and **Ag4** complexes.

Ag3 complex			**Ag4 complex**		
Concentration (10^{-6} mol L^{-1})	**A_{228}**	**A_{265}**	**Concentration (10^{-6} mol L^{-1})**	**A_{228}**	**A_{278}**
7.855	0.595	0.251	3.781	0.299	0.109
9.426	0.632	0.267	5.293	0.345	0.123
10.997	0.662	0.279	6.805	0.381	0.137
12.568	0.698	0.292	9.830	0.462	0.167
14.139	0.739	0.311	11.343	0.497	0.179

Table S3 - Electronic spectra data obtained for the **Ag5** and **Ag6** complexes.

Ag5 complex				**Ag6 complex**		
Concentration (10^{-6} mol L^{-1})	**A_{227}**	**A_{265}**	**A_{332}**	**Concentration (10^{-6} mol L^{-1})**	**A_{228}**	**A_{251}**
8.862	0.390	0.167	0.208	13.502	0.619	0.507
10.339	0.461	0.210	0.248	14.402	0.691	0.563
16.247	0.666	0.292	0.331	15.302	0.747	0.607
19.202	0.797	0.350	0.387	16.202	0.825	0.667
20.679	0.831	0.362	0.398	17.102	0.877	0.71

Figure S5.33– Linear regression for **Au1** (blue line), **Au2** (pink line), **Au3** (green line), **Au4** (orange line), **Au5** (red line) and **Au6** (purple line).

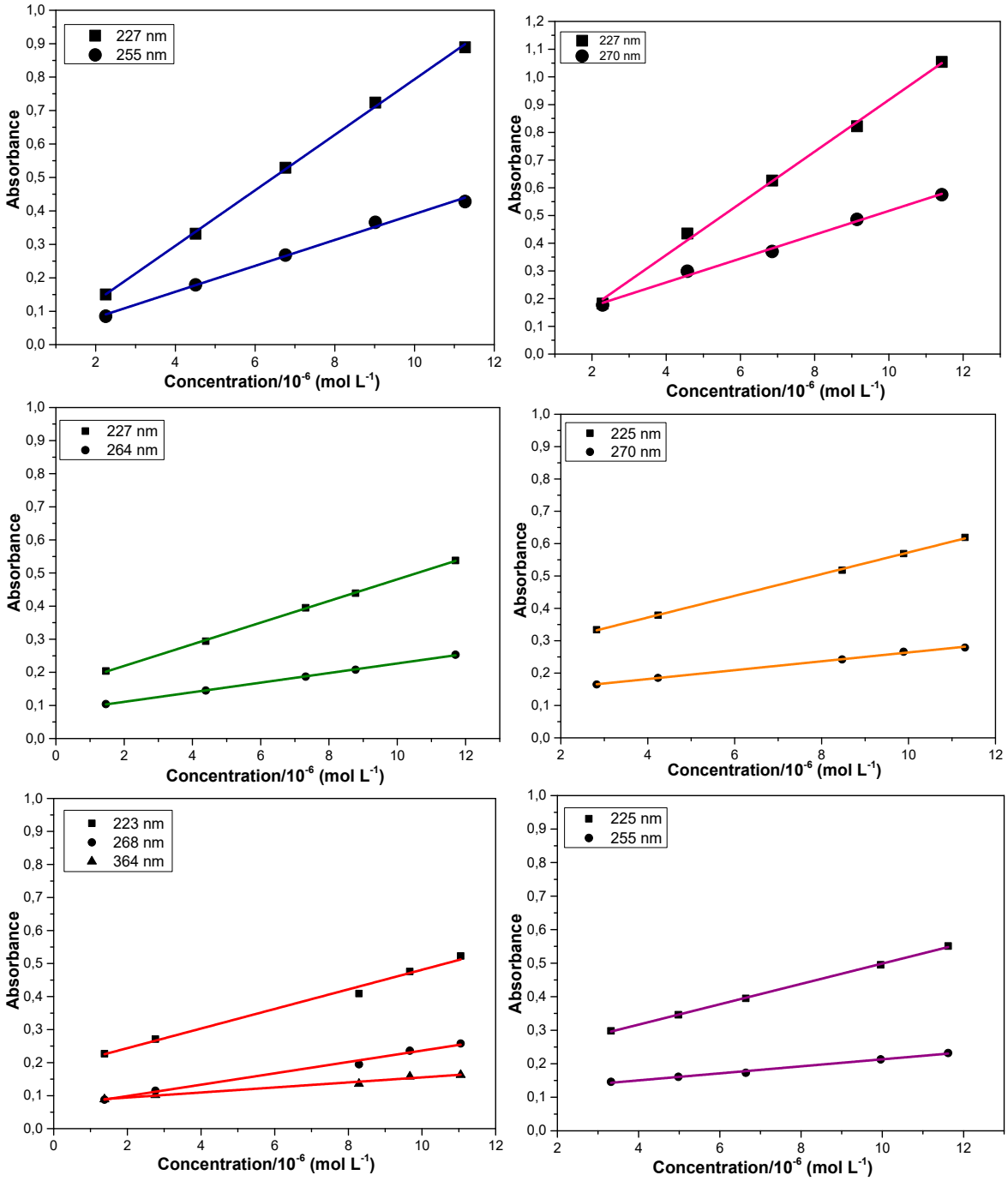

Table S4 - Electronic spectra data obtained for the **Au1** and **Au2** complexes.

Au1 complex			**Au2 complex**		
Concentration (10^{-6} mol L^{-1})	**A_{227}**	**A_{255}**	**Concentration (10^{-6} mol L^{-1})**	**A_{227}**	**A_{270}**
2.254	0.150	0.085	2.285	0.182	0.177
4.508	0.332	0.179	4.570	0.435	0.299
6.762	0.529	0.268	6.855	0.626	0.370
9.016	0.724	0.366	9.140	0.822	0.486
11.269	0.889	0.428	11.425	1.054	0.575

Table S5- Electronic spectra data obtained for the **Au3** and **Au4** complexes.

Au3 complex			Au4 complex		
Concentration (10^{-6} mol L^{-1})	**A_{227}**	**A_{264}**	**Concentration (10^{-6} mol L^{-1})**	**A_{225}**	**A_{270}**
1.463	0.204	0.104	2.824	0.334	0.165
4.390	0.294	0.145	4.237	0.379	0.185
7.316	0.395	0.187	8.473	0.518	0.242
8.779	0.439	0.208	9.885	0.569	0.266
11.706	0.538	0.253	11.298	0.619	0.279

Table S6- Electronic spectra data obtained for the **Au5** and **Au6** complexes.

Au5 complex				Au6 complex		
Concentration (10^{-6} mol L^{-1})	**A_{223}**	**A_{268}**	**A_{364}**	**Concentration (10^{-6} mol L^{-1})**	**A_{225}**	**A_{255}**
1.381	0.227	0.088	0.089	3.320	0.298	0.146
2.763	0.271	0.115	0.102	4.980	0.346	0.161
8.288	0.409	0.195	0.136	6.640	0.395	0.173
9.669	0.476	0.236	0.158	9.960	0.495	0.213
11.051	0.523	0.258	0.163	11.620	0.551	0.232

Figure S5.5 – (a) Emission spectra of **Au1** (blue line) and **Au2** (pink line) in CH_3OH at 298 K; λexc = 255 nm for **Au1** and 270 nm for **Au2**; (b) Emission spectra of CH_3OH at 298 K; λexc = 250 nm.

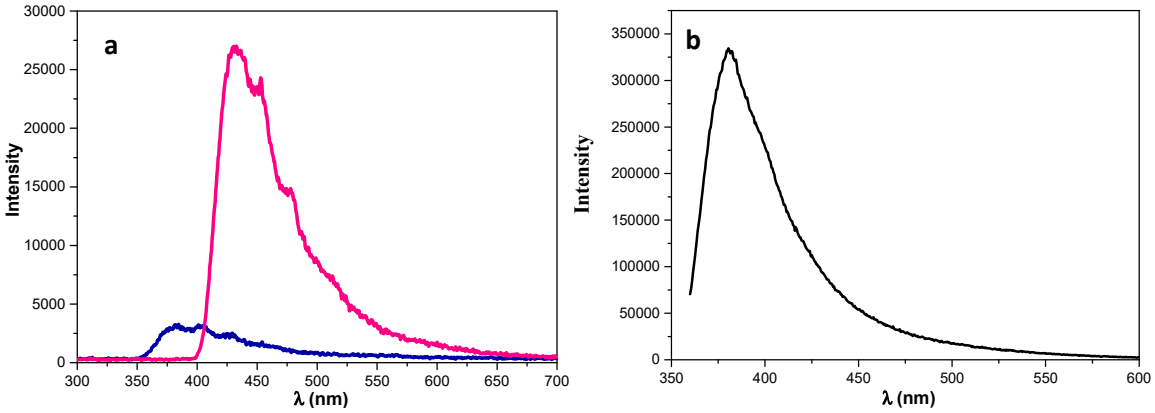

Figure S5.6 – Emission spectra of **Au1** (blue dashed line) and **Au2** (pink dashed line) in MeOH at 77 K; *λ*exc = 255 nm for **Au1** and 270 nm for **Au2**.

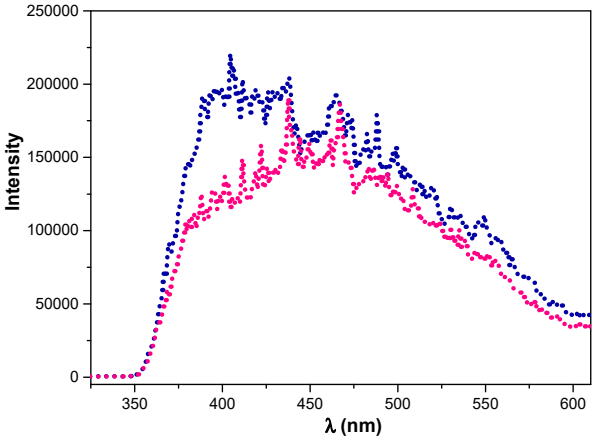

Table S7. Basis set functions used for gold complexes.

```
NewGTO H
S   3
1        12.98511484            0.0305015
2         1.95908134            0.2062392
3         0.44403649            0.7632592
S   1
1         0.11282695            1.0000000
P   1
1         0.80305095            1.0000000
end

NewGTO C
S   5
1      4949.46032594            0.0021254
2       758.82582124            0.0138797
3       172.62336223            0.0699682
4        47.77742113            0.2630053
5        15.15140603            0.6510212
S   2
1         5.39400345            0.7300080
2         2.11083628            0.2699919
S   1
1         0.52460137            1.0000000
S   1
1         0.15964728            1.0000000
P   4
1        18.97219923            0.0156205
2         4.18721595            0.0966388
3         1.21388239            0.3264242
4         0.38698643            0.5613164
P   1
1         0.12406489            1.0000000
D   1
1         0.61467289            1.0000000
end

NewGTO N
S   5
1      6711.76398035            0.0022301
2      1029.56088507            0.0140080
3       234.62552896            0.0699756
4        65.08616322            0.2624838
5        20.68134371            0.6513023
S   2
1         7.35948620            0.7394324
2         2.86133058            0.2605675
S   1
1         0.75772555            1.0000000
S   1
1         0.22278085            1.0000000
P   4
1        26.95312900            0.0161302
2         6.01777874            0.1007562
3         1.76062640            0.3305209
4         0.56064983            0.5525926
P   1
1         0.17525619            1.0000000
D   1
```

```
1        0.89591019            1.0000000
end

NewGTO O
S   5
1     8897.19445619            0.0023229
2     1365.26538810            0.0140091
3      311.21828724            0.0694697
4       86.33353862            0.2611441
5       27.42841118            0.6530540
S   2
1        9.74740298            0.7418317
2        3.77109950            0.2581682
S   1
1        1.04455407            1.0000000
S   1
1        0.30382295            1.0000000
P   4
1       34.75998468            0.0172481
2        7.80757529            0.1079455
3        2.29096903            0.3383584
4        0.71677956            0.5364479
P   1
1        0.21323853            1.0000000
D   1
1        1.25011953            1.0000000
end

NewGTO S
S   5
1    88298.52965731            0.0037231
2    13783.75049251            0.0144966
3     3273.99080251            0.0569731
4      933.93904998            0.2171714
5      294.47682844            0.7076356
S   2
1        5.19930244            0.5076446
2        2.03425969            0.4923553
S   1
1      101.30556573            1.0000000
S   1
1       37.95800089            1.0000000
S   1
1       15.05040359            1.0000000
S   1
1        0.38772280            1.0000000
S   1
1        0.15157298            1.0000000
P   6
1      759.75242296            0.0015116
2      180.00565026            0.0113965
3       56.73558346            0.0560869
4       20.36270362            0.1849910
5        7.76216777            0.3713178
6        3.02062956            0.3746960
P   1
1        1.11706212           -1.0000000
P   1
1        0.41415858            1.0000000
P   1
```

```
1        0.12911675            1.0000000
D   1
1        0.47158905            1.0000000
end

NewGTO Au
S   8
1  14703222.86676416            0.0037526
2   2262824.67803200            0.0100581
3    541256.94037958            0.0214627
4    164442.91034176            0.0419279
5     59155.59429110            0.0745368
6     24111.28878337            0.1319630
7     10152.24890131            0.2484028
8      4170.67168425            0.4678957
S   3
1       243.52806941           -0.4833215
2       117.22573806           -0.4189882
3        53.38778177           -0.0976901
S   2
1      1707.43394310            0.5704913
2       708.28135147            0.4295086
S   2
1        10.72476847            0.5023106
2         4.98291235            0.4976893
S   2
1         1.37574165           -0.7187708
2         0.66299967           -0.2812291
S   1
1        25.23167009            1.0000000
S   1
1         0.11066351            1.0000000
S   1
1         0.03911478            1.0000000
P   8
1     57867.45693148            0.0025583
2     14466.07282046            0.0069902
3      5096.80289128            0.0204152
4      2035.23445681            0.0610881
5       842.36068729            0.1629640
6       361.46395991            0.3385020
7       161.78689265            0.3128406
8        73.04451373            0.0946414
P   3
1        16.95126547            0.2800147
2         7.89562180            0.4069449
3         3.73415826            0.3130403
P   1
1        35.18821179           -1.0000000
P   1
1         1.40958119            1.0000000
P   1
1         0.52307734            1.0000000
P   1
1         0.12434867            1.0000000
P   1
1         0.03469933            1.0000000
D   5
1      1057.31409955            0.0149745
2       315.34985277            0.0904567
```

3 118.76210977 0.2923335
4 49.52241329 0.4170518
5 21.54470227 0.1851834
D 2
1 9.19880872 -0.7782852
2 3.88284809 -0.2217147
D 1
1 1.23471691 1.0000000
D 1
1 0.35702456 1.0000000
F 4
1 86.31773515 0.0583691
2 27.55700975 0.2444140
3 9.83940823 0.4153993
4 3.31580164 0.2818174
F 1
1 0.84103480 1.0000000

Table S8 - Vibrational modes and their theoretical assignments in related to the C=S bond.

Compound	Vibrational frequency / cm^{-1}	Vibrational mode assignment
$Au(HL1^{Ch})_2Cl$	790.64 / 794.59	$\nu C{=}S + \delta_{oop}CH_{2(ciclohexane)}$
$Au(HL2^{Ph})_2Cl$	744.73 / 746.69	$\nu C{=}S + \delta NCN + \delta_{oop}CH_{2(ph)}$
$Au(HL3^{FPh})_2Cl$	738.89 / 741.70	$\nu C{=}S + \delta NCN + \delta_{oop}CH_{2(ph)}$
$Au(HL4^{ClPh})_2Cl$	767.65 / 768.30	$\nu C{=}S + \delta NCN + \delta_{oop}CH_{2(ph)}$
$Au(HL5^{NO2Ph})_2Cl$	755.56 / 756.37	$\nu C{=}S + \delta NCN + \delta_{oop}CH_{2(ph)}$
$Au(HL6^{Al})_2Cl$	782.41 / 798.73	$\nu C{=}S + \delta NCN + \delta_{roc\text{-}as}NH$

Figure S6.1 - Optimized structures of the silver complexes.

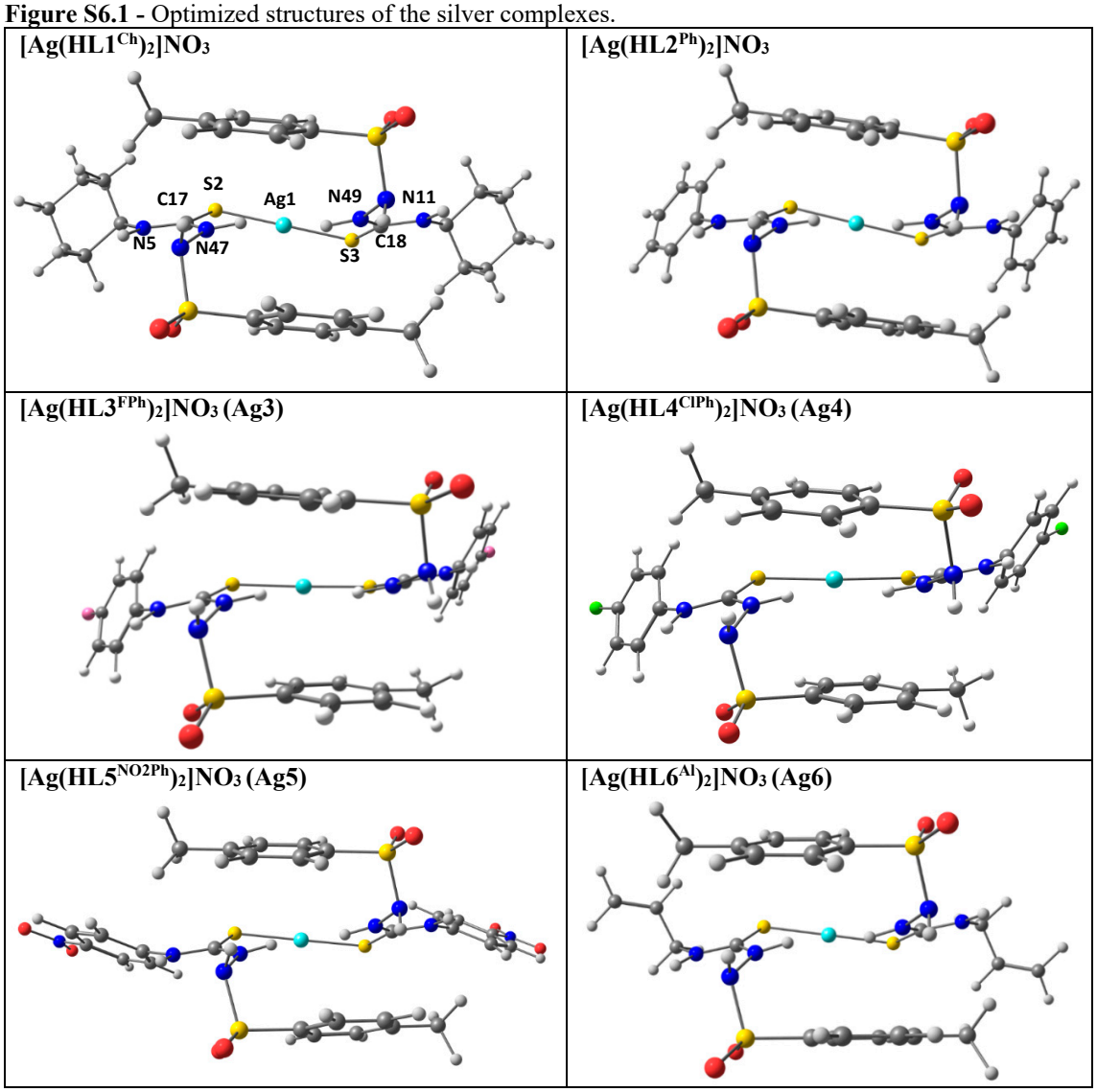

Table S9 - Main theoretical structural data of the silver complexes.

		Complexes					
	Atoms Selected	**Ag1**	**Ag2**	**Ag3**	**Ag4**	**Ag5**	**Ag6**
Distances/ Å	Ag1-S3	2.409	2.411	2.507	2.508	2.416	2.408
	Ag1-S2	2.409	2.408	2.507	2.508	2.415	2.411
Angles/°	S3-Ag1-S2	172.8	172.7	164.4	164.0	175.2	173.4
DIEDRAL /°	Ag1-S_2-C17-N_5	17.4	14.2	11.8	11.7	13.7	16.8
	Ag1-S3-C18-N_{49}	-162.8	-163.8	-168.6	-168.2	-169.5	-163.0
	Ag1-S2-C17-N47	-163.7	-165.9	-168.5	-168.5	-169.5	-164.3
	Ag1-S3-C18-N_{11}	18.3	16.5	11.8	12.1	13.7	18.1

Figure S6.2 - Optimized structures of the gold complexes.

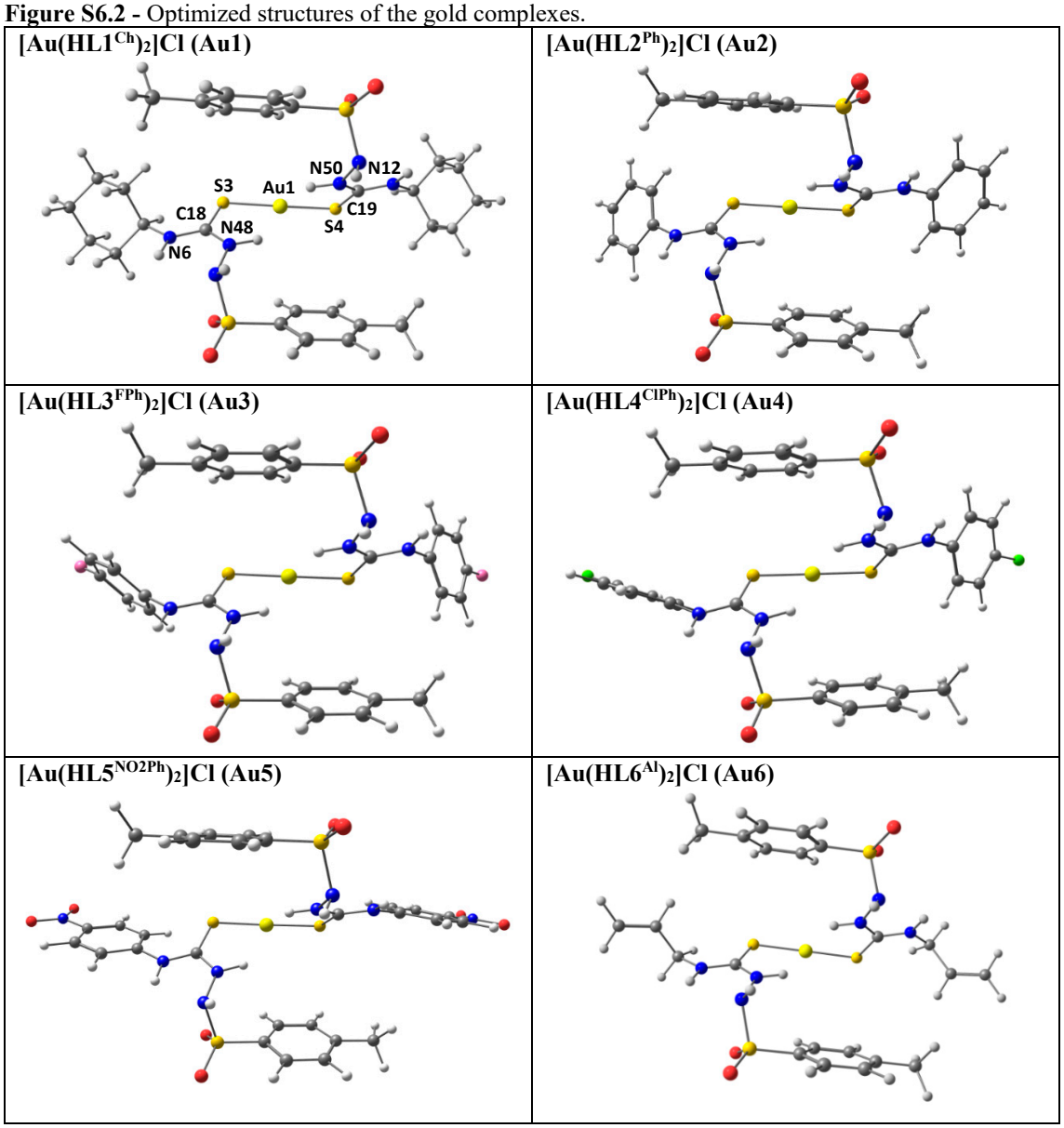

Table S10 – Main theoretical structural data of the gold complexes.

		Complexes					
	Atoms Selected	**Au1**	**Au2**	**Au3**	**Au4**	**Au5**	**Au6**
Distances/ Å	Au1-S4	2.284	2.289	2.287	2.287	2.286	2.284
	Au1-S3	2.284	2.289	2.287	2.287	2.286	2.284
Angles/°	S4-Au1-S3	174.0	175.0	174.3	175.0	175.1	174.8
DIEDRAL/°	Au1-S4-C19-N12	11.1	15.3	9.2	6.9	6.2	8.4
	Au1-S4-C19-N50	-171.8	-167.3	-173.2	-174.7	-177.5	-173.8
	Au1-S3-C18-N48	-173.4	-176.0	-176.0	-178.1	-178.2	-174.3
	Au1-S3-C18-N6	9.2	5.3	6.8	4.8	5.3	7.8

Figure S6.3 - HOMO and LUMO orbitals in the silver complexes.

[Ag(HL1^{Ch})$_2$]NO$_3$ (Ag1)	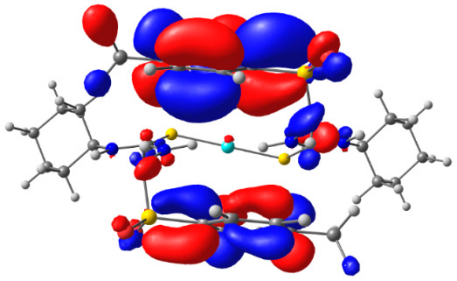
[Ag(HL2^{Ph})$_2$]NO$_3$ (Ag2)	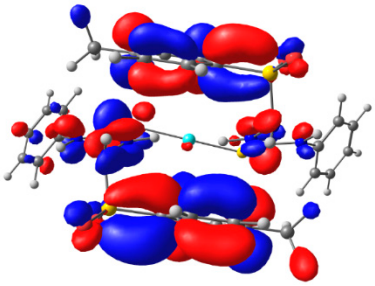
[Ag(HL3^{FPh})$_2$]NO$_3$ (Ag3)	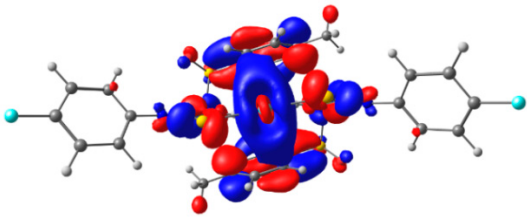
[Ag(HL4^{ClPh})$_2$]NO$_3$ (Ag4)	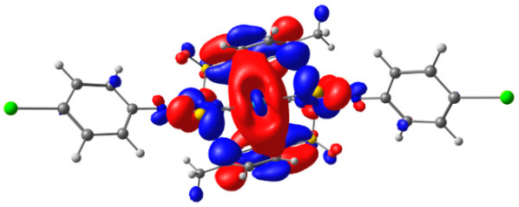
[Ag(HL5^{NO2Ph})$_2$]NO$_3$ (Ag5)	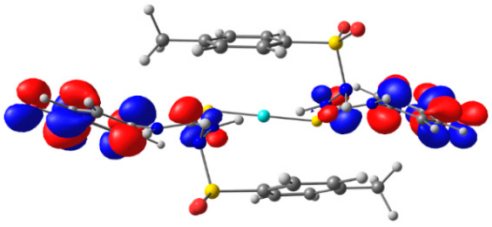
[Ag(HL6^{Al})$_2$]NO$_3$ (Ag6)	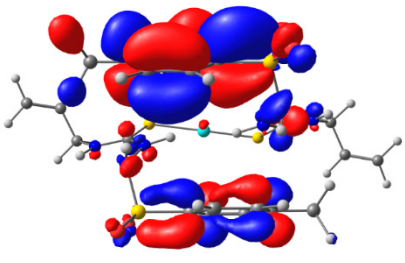

Figure S6.4 - HOMO and LUMO orbitals in the gold complexes.

[Au(HL1^{Ch})$_2$]Cl (Au1)	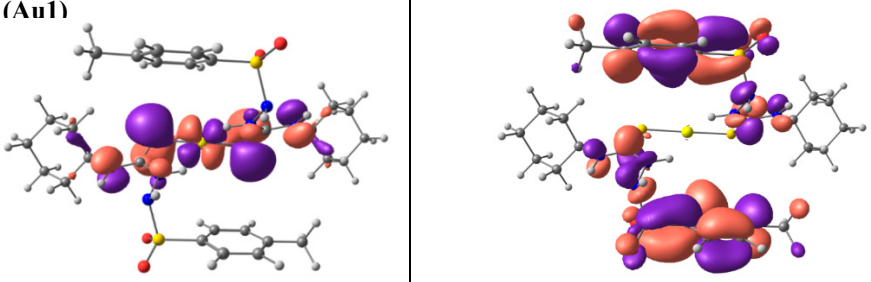
[Au(HL2^{Ph})$_2$]Cl (Au2)	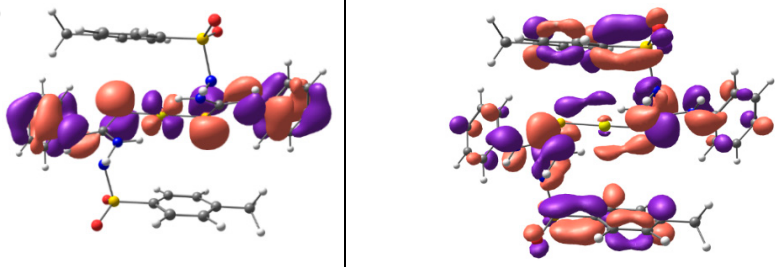
[Au(HL3^{FPh})$_2$]Cl (Au3)	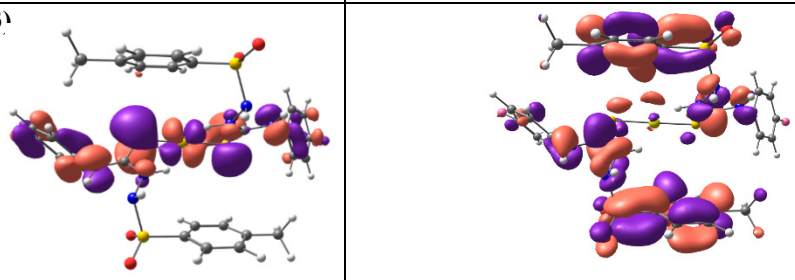
[Au(HL4^{ClPh})$_2$]Cl (Au4)	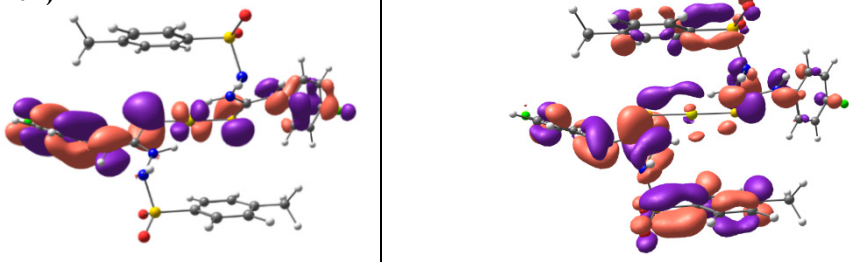
[Au(HL5^{NO2Ph})$_2$]Cl (Au5)	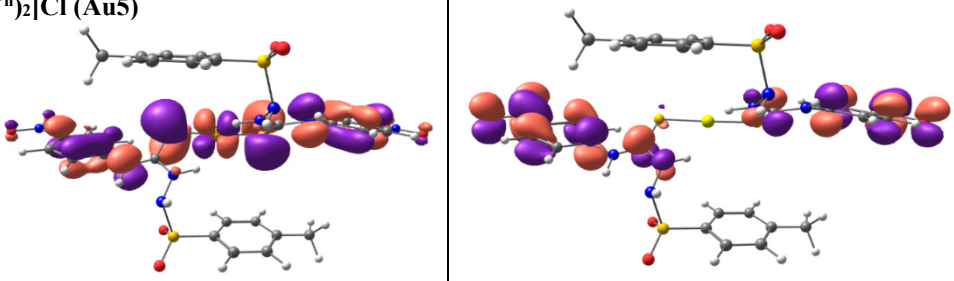
[Au(HL6^{Al})$_2$]Cl (Au6)	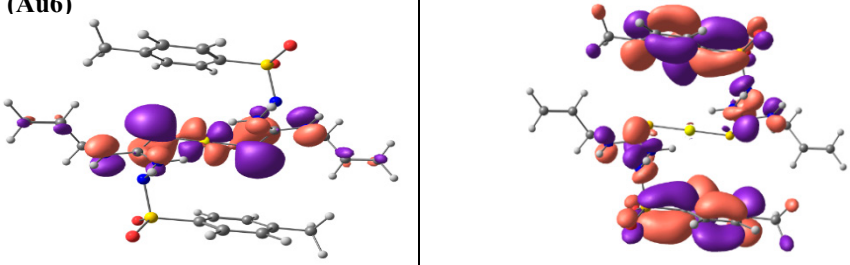

Figure S6.5 – Optimized structure of $[Au(HL3^{FPh})_2]^+$ (**Au3**) with the charges obtained for the AIM data.

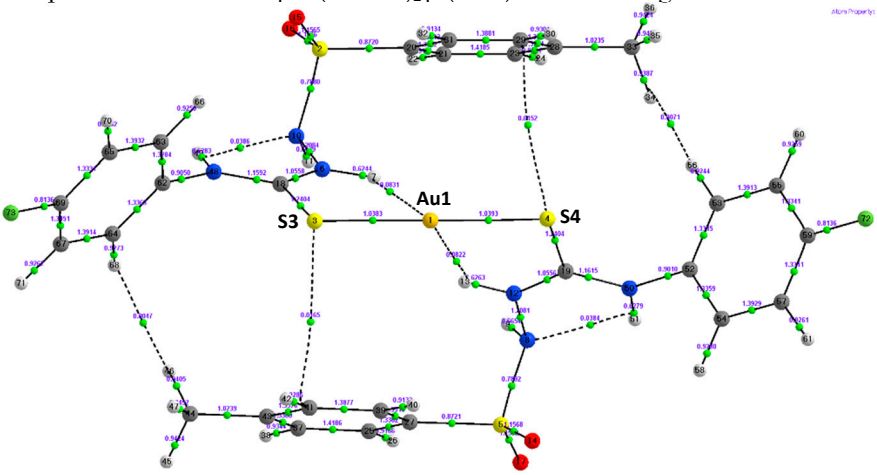

Table S11 – Electronic properties of the gold(I) complexes. The values are shown, respectively, for each bond in the order they appear.

$[Au(HL1^{Ch})_2]Cl$ (**Au1**)	q	DI	ρ	$\nabla^2\rho$
Au	+0.1028			
S3	+0.0588			
S4	+0.0589			
S3-Au-S4		1.0459/1.0463	+0.1114/+0.1115	+0.1698/+0.1695
S3-C18		1.2225	+0.1910	-0.2597
S4-C19		1.2226	+0.1910	-0.2593
$[Au(HL2^{Ph})_2]Cl$ (**Au2**)	q	DI	ρ	$\nabla^2\rho$
Au	+0.1229			
S3	+0.0710			
S4	+0.0661			
S3-Au-S4		1.0344/1.0396	+0.1104/+0.1104	+0.1704/+0.1705
S3-C18		1.2346	+0.1909	-0.2383
S4-C19		1.2355	+0.1911	-0.2403
$[Au(HL3^{FPh})_2]Cl$ (**Au3**)	q	DI	ρ	$\nabla^2\rho$
Au	+0.1078			
S3	+0.0912			
S4	+0.0880			
S3-Au-S4		1.0383/1.0393	+0.1111/+0.1111	+0.1691/+0.1686
S3-C18		1.2404	+0.1917	-0.2292
S4-C19		1.2404	+0.1917	-0.2312
$[Au(HL4^{ClPh})_2]Cl$ (**Au4**)	q	DI	ρ	$\nabla^2\rho$
Au	+0.1110			
S3	+0.0994			
S4	+0.0946			
S3-Au-S4		1.0350/1.0367	+0.1110/+0.1110	+0.1690/+0.1686
S3-C18		1.2446	+0.1915	-0.2251
S4-C19		1.2439	+0.1916	-0.2269
$[Au(HL5^{NO2Ph})_2]Cl$ (**Au5**)	q	DI	ρ	$\nabla^2\rho$
Au	+0.1255			
S3	+0.1277			
S4	+0.1269			
S3-Au-S4		1.0285/1.0291	+0.1112/+0.1112	+0.1700/+0.1701
S3-C18		1.2611	+0.1925	-0.2081
S4-C19		1.2605	+0.1925	-0.2093
$[Au(HL6^{Al})_2]Cl$ (**Au6**)	q	DI	ρ	$\nabla^2\rho$
Au	+0.1078			
S3	+0.0610			
S4	+0.0606			
S3-Au-S4		1.0432/1.0441	+0.1113/+0.1114	+0.1702/+0.1702
S3-C18		1.2238	+0.1906	-0.2545
S4-C19		1.2236	+0.1907	-0.2553

Figure S7.1 – Graph of the viability versus concentrations (μM) of the compounds.

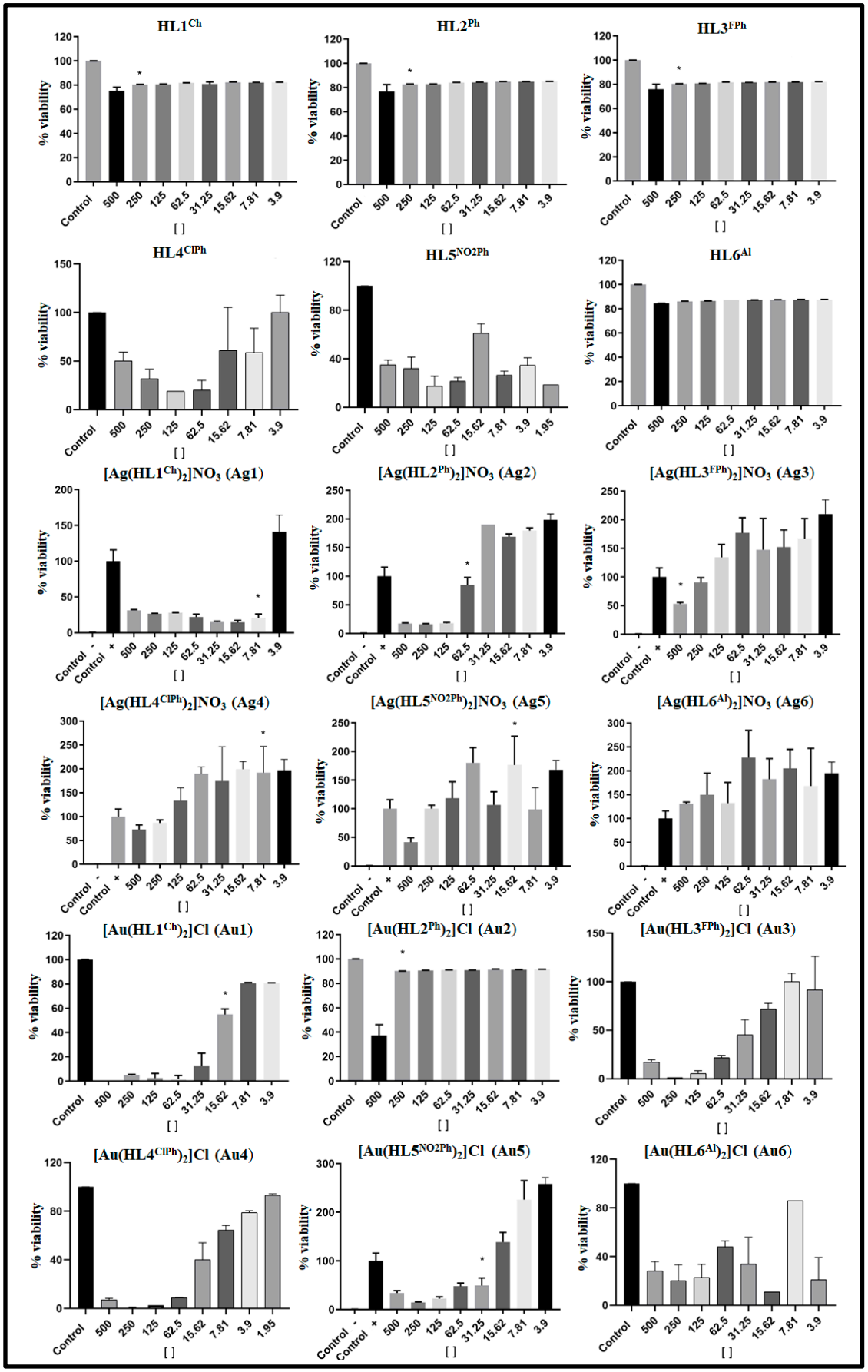

Figure S7.2 – Leishmanicidal activity against to the *Leishmania infantum* parasite by concentrations of the compound. Blue curve represents the reference leishmanicidal drug, Glucantime. Black curve represents each compound.

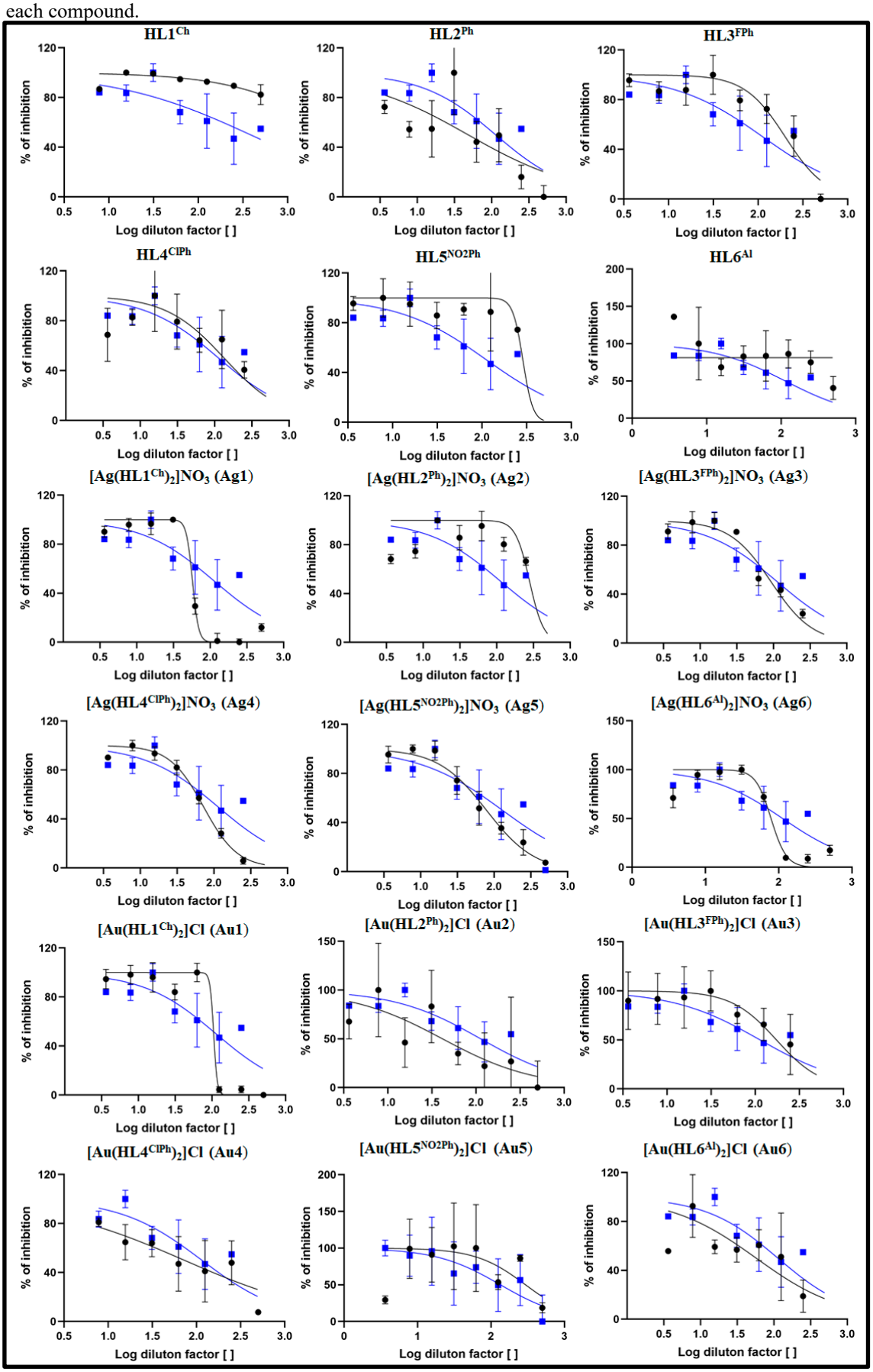

Figure S7.3 – Leishmanicidal activity against to the *Leishmania braziliensis* parasite by concentrations of the compound. Blue curve represents the reference leishmanicidal drug, Glucantime. Black curve represents each compound.

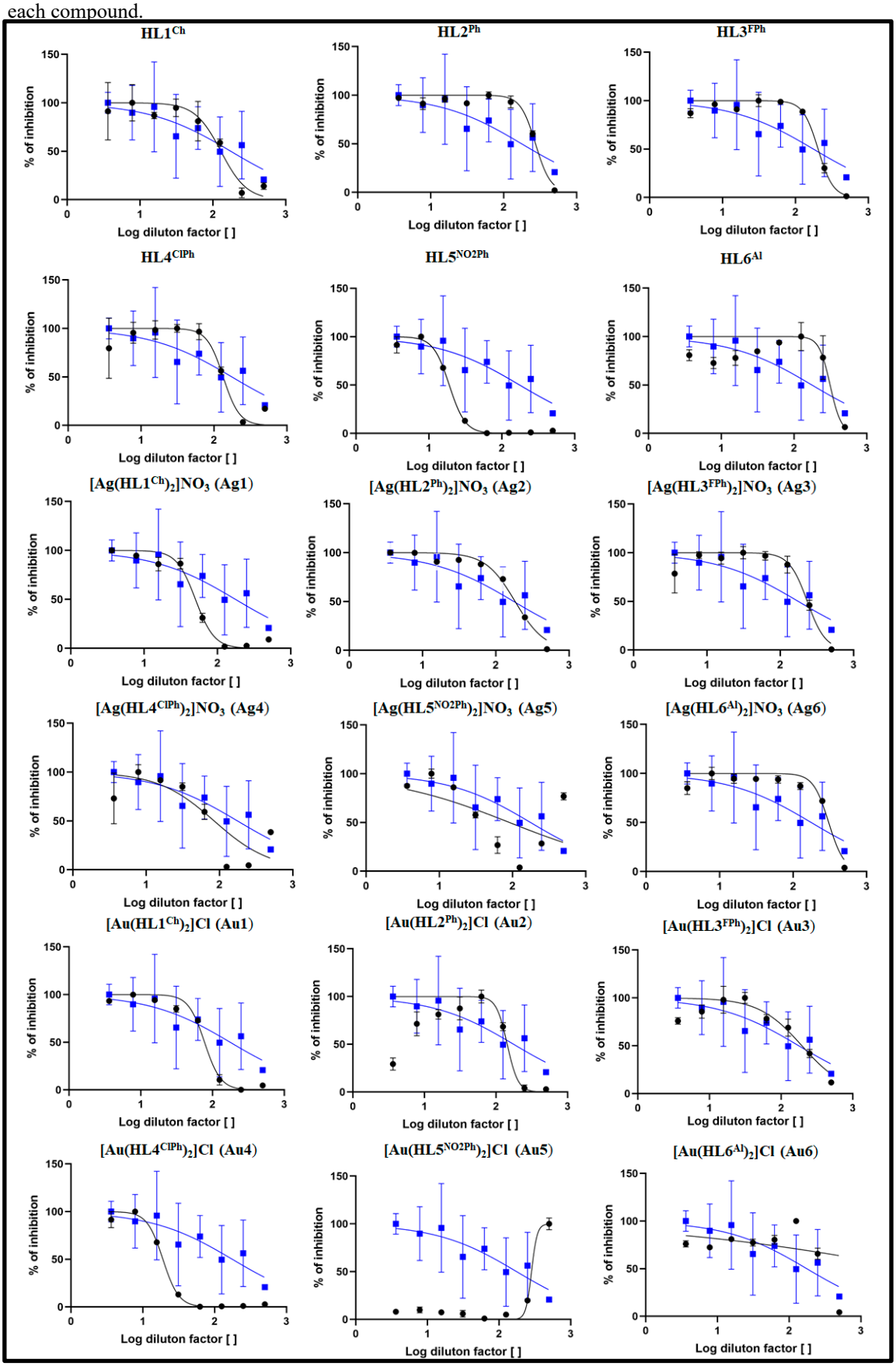

Figure S7.4 – (a) percentage of the number of infected in 200 macrophages by *Leishmania infantum*; (b) percentage of leishmaniasis that infect 100 cells/macrophages; (c) average percentage of leishmaniasis that infect 200 cells/macrophages; of the selected compounds.

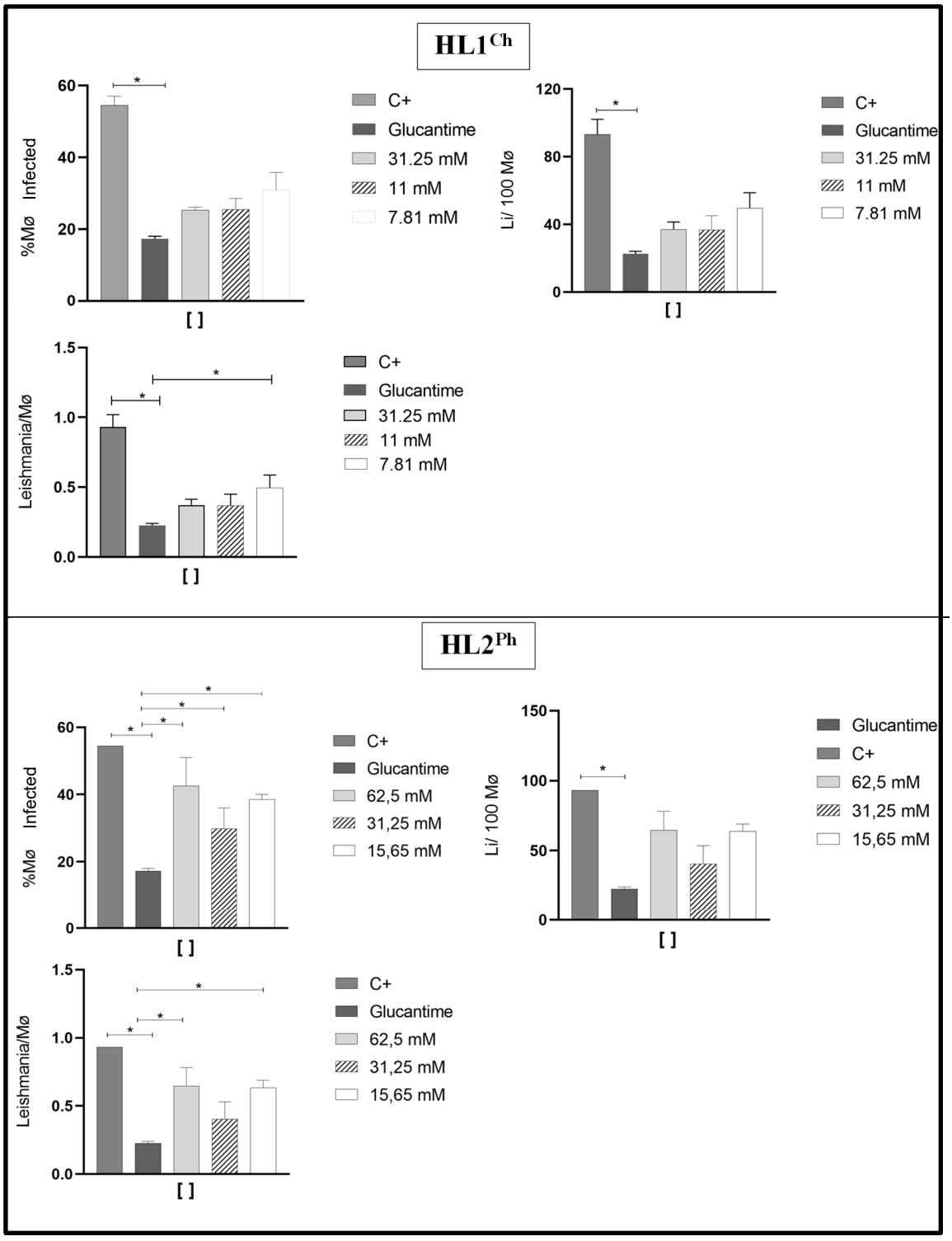

$[Ag(HL3^{FPh})_2]NO_3$ (Ag3)

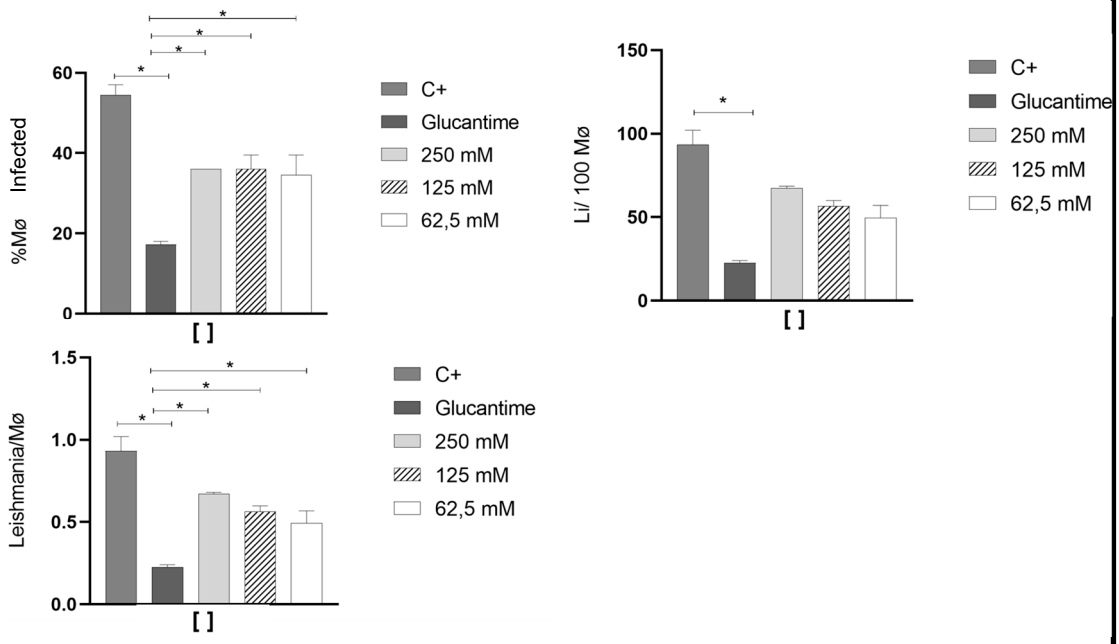

$[Ag(HL4^{ClPh})_2]NO_3$ (Ag4)

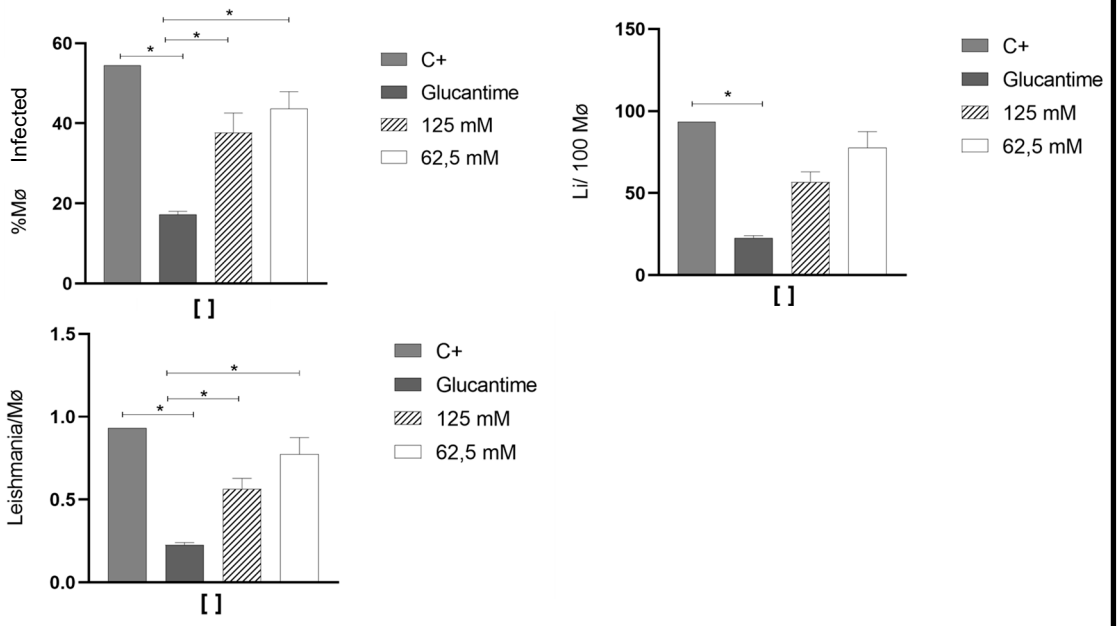

$[Ag(HL6^{Al})_2]NO_3$ (Ag6)

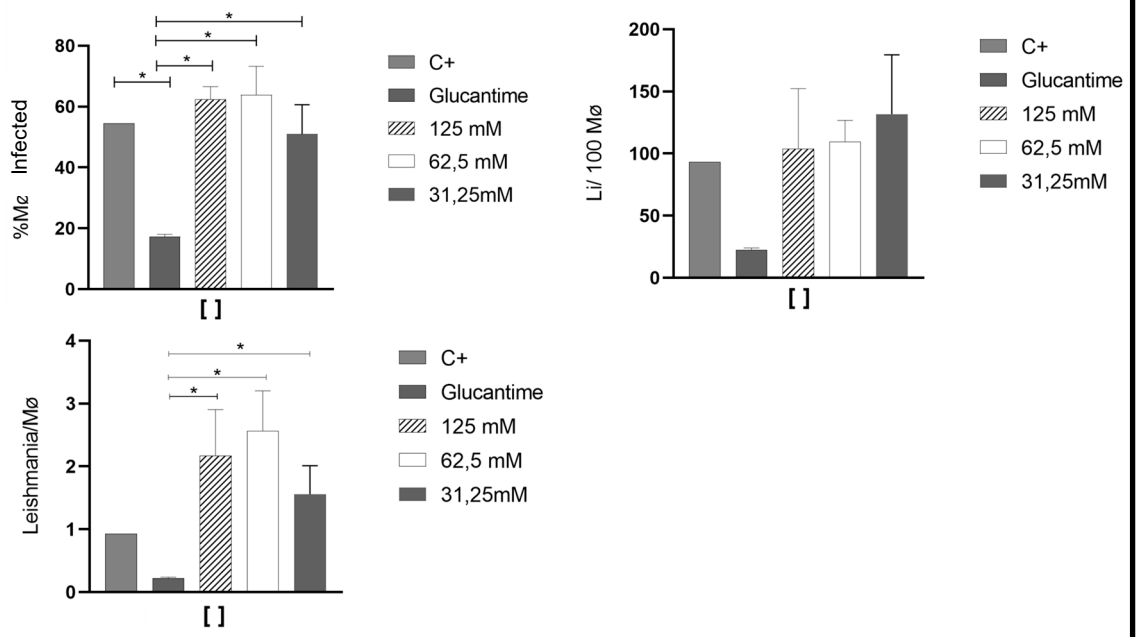

$[Au(HL2^{Ph})_2]NO_3$ (Au2)

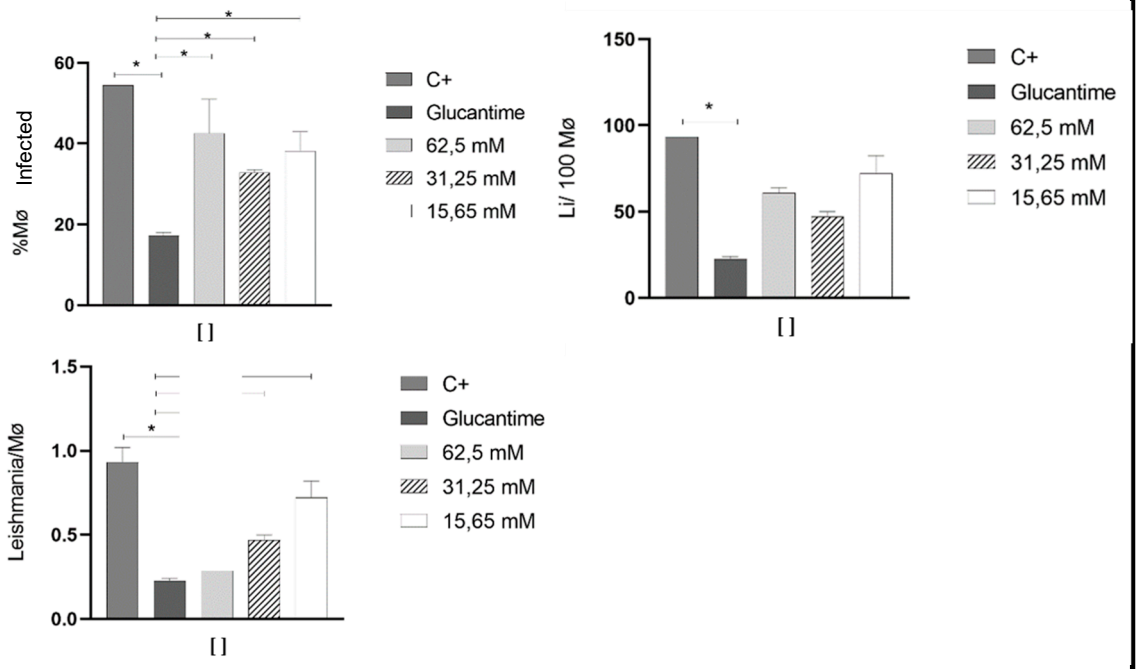

Figure S7.5 - Image captured under a fluorescence microscope (EVOS) of Raw macrophages infected by *Leishmania infantum* after treatment with a Glucantime (leishmanicidal drug) (A) and the selected compounds;

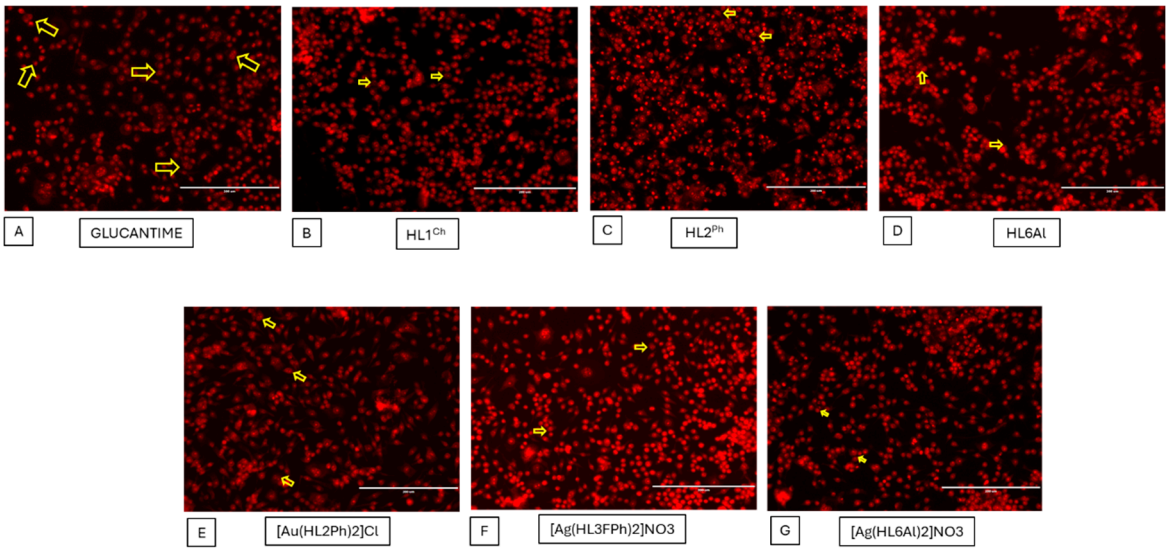

Figure S7.6 – (**A**) Fluorescence emission spectra (λ_{ex} = 295 nm) of LbOYE protein in the concentration of 1 µmol L^{-1} in the presence of increasing concentrations of the $HL5^{NO2Ph}$ compound. (**B**) Variation of maximum fluorescence intensities (λ_{max} = 333 nm) and non-linear fit to the Hill equation (Equation 1). (**C**) Logarithmic relationship to obtain the number of bonding sites according to Equation 2. (**D**) Comparison between the temperatures of 25 and 37 °C. The spectra were obtained in Tris-HCl buffer, pH 8.0; 100 mmol L^{-1} of NaCl and 2.5 % of DMSO.

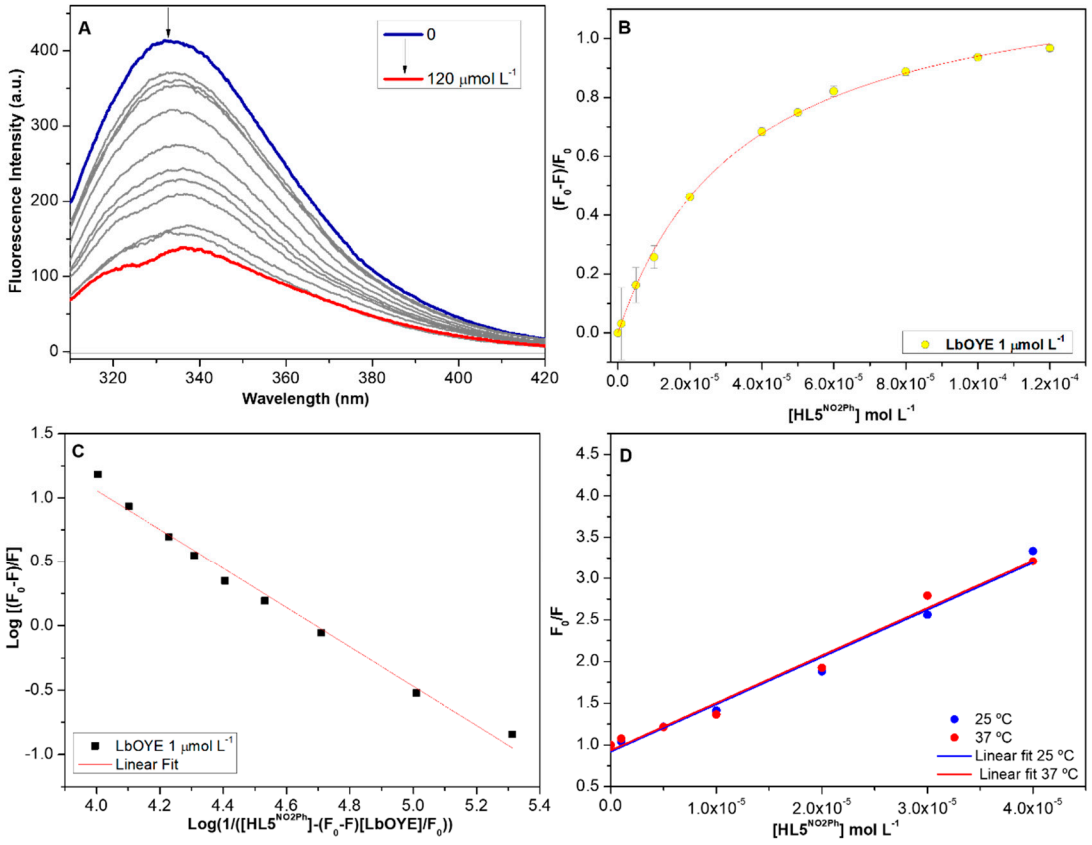

Figure S7.7 – Fluorescence emission spectra (λ_{ex} = 295 nm) of LbOYE protein in the concentration of 1 µmol L^{-1} in the presence of increasing concentrations of the **(A)** $HL1^{Ch}$ and **(B)** $HL3^{FPh}$. The spectra were obtained in Tris-HCl buffer, pH 8.0; 100 mmol L^{-1} of NaCl and 2.5% of DMSO and 25 °C .

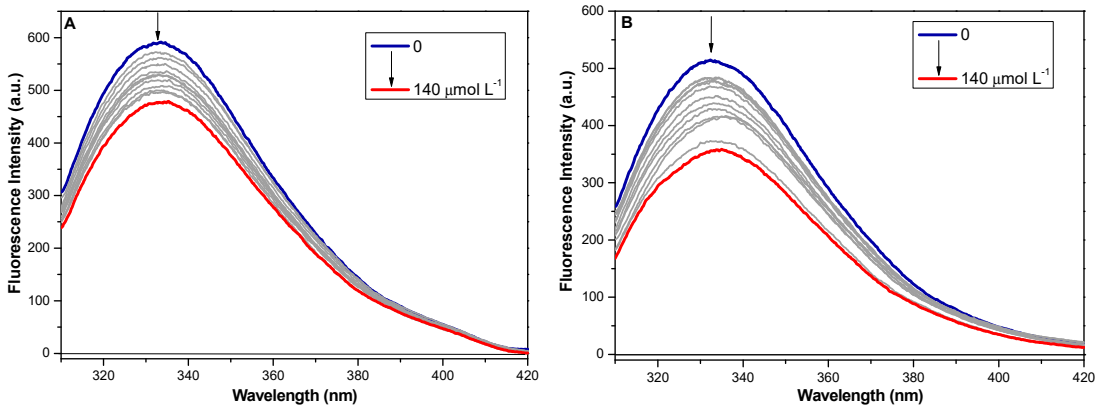

Figure S7.8. Fluorescence emission spectra (λ_{ex} = 295 nm) of LbOYE protein in the concentration of 1 μmol L^{-1} in the presence of increasing concentrations of the [Au(HL1^{Ch})$_2$]Cl (**Au1**) complex. (B) Variation of maximum fluorescence intensities (λ_{max} = 333 nm) and non-linear fit to the Hill equation (Equation 1). (C) Logarithmic relationship to obtain the number of bonding sites according to Equation 2. (D) Comparison between the temperatures of 25 °C and 37 °C. The spectra were obtained in Tris-HCl buffer, pH 8.0; 100 mmol L^{-1} of NaCl and 2.5 % of DMSO.

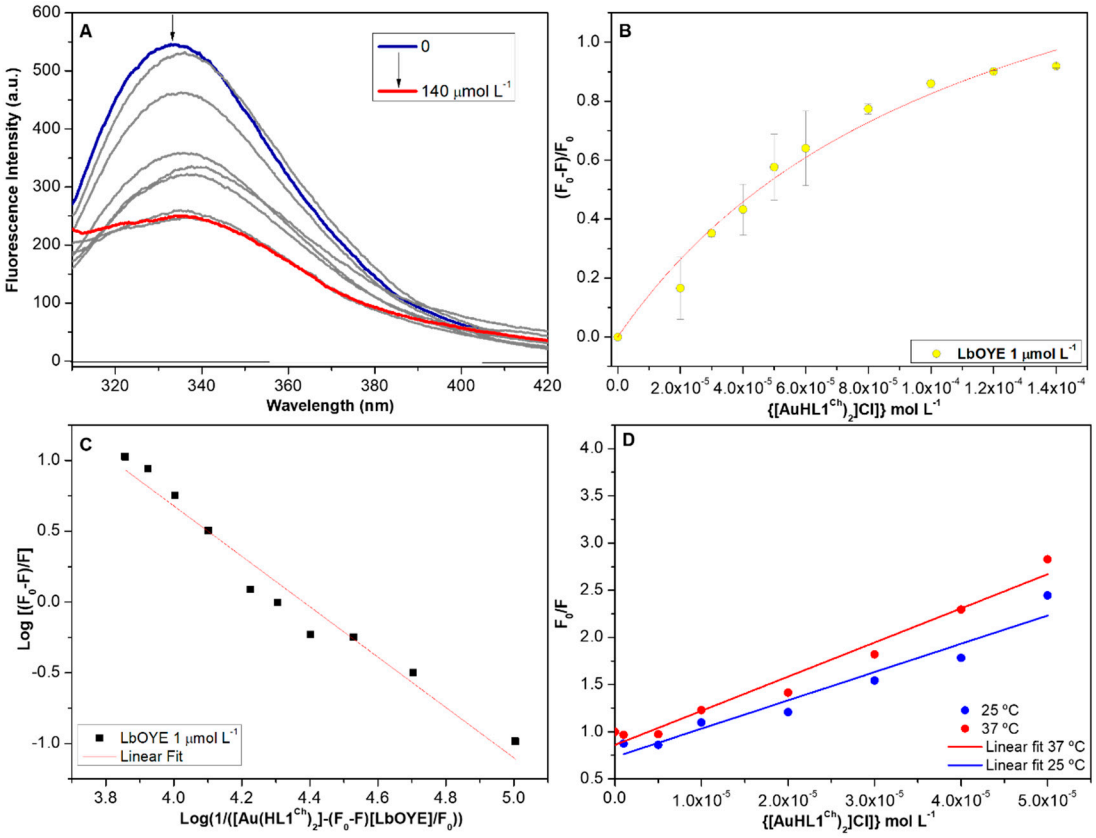

Figure S8.1 – Representative figure of the HL1^{Ch} ligand at the site of the OLD Yellow enzyme from *Leishmania braziliensis*.

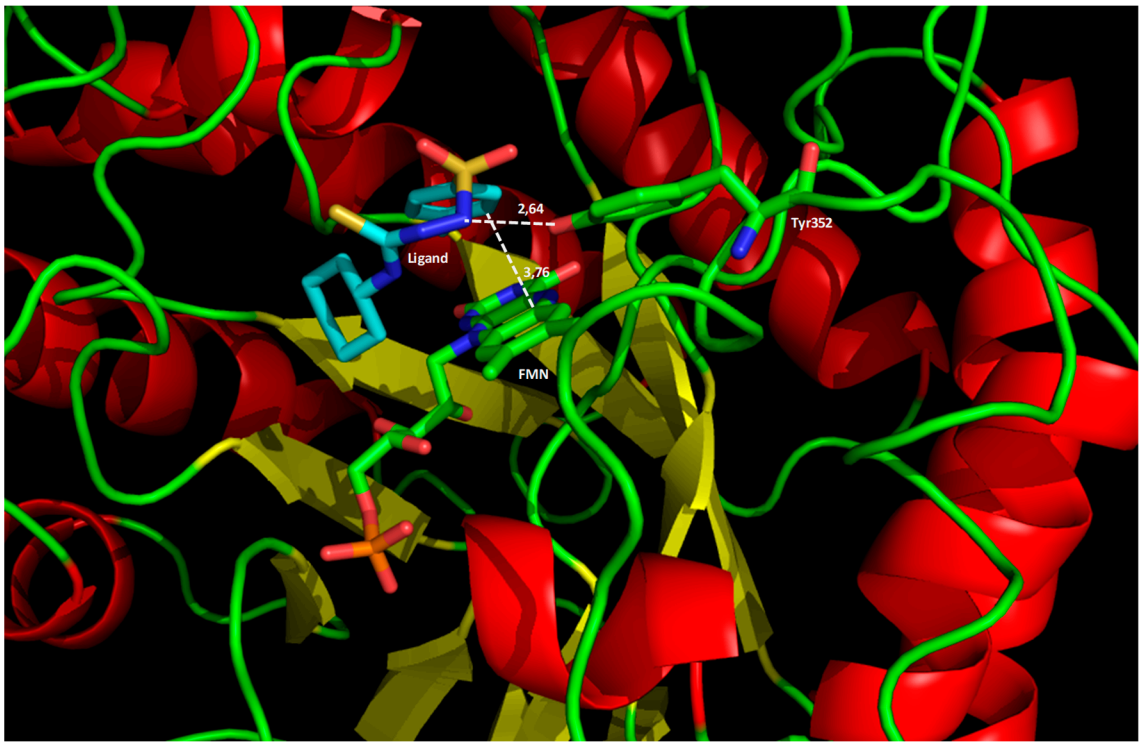

Figure S8.2 – Representative figure of the HL3^{FPh} ligand at the site of the OLD Yellow enzyme from *Leishmania braziliensis*.

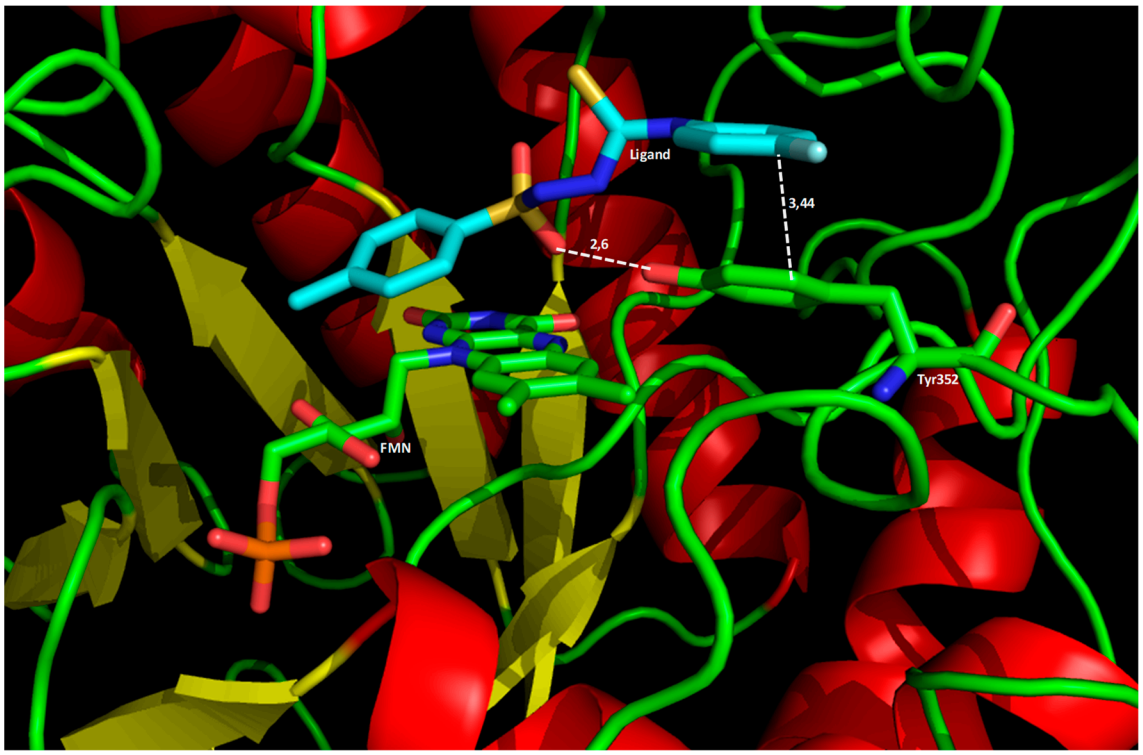

Figure S8.34 – Representative figure of the HL4^{ClPh} ligand at the site of the OLD Yellow enzyme from *Leishmania braziliensis*.

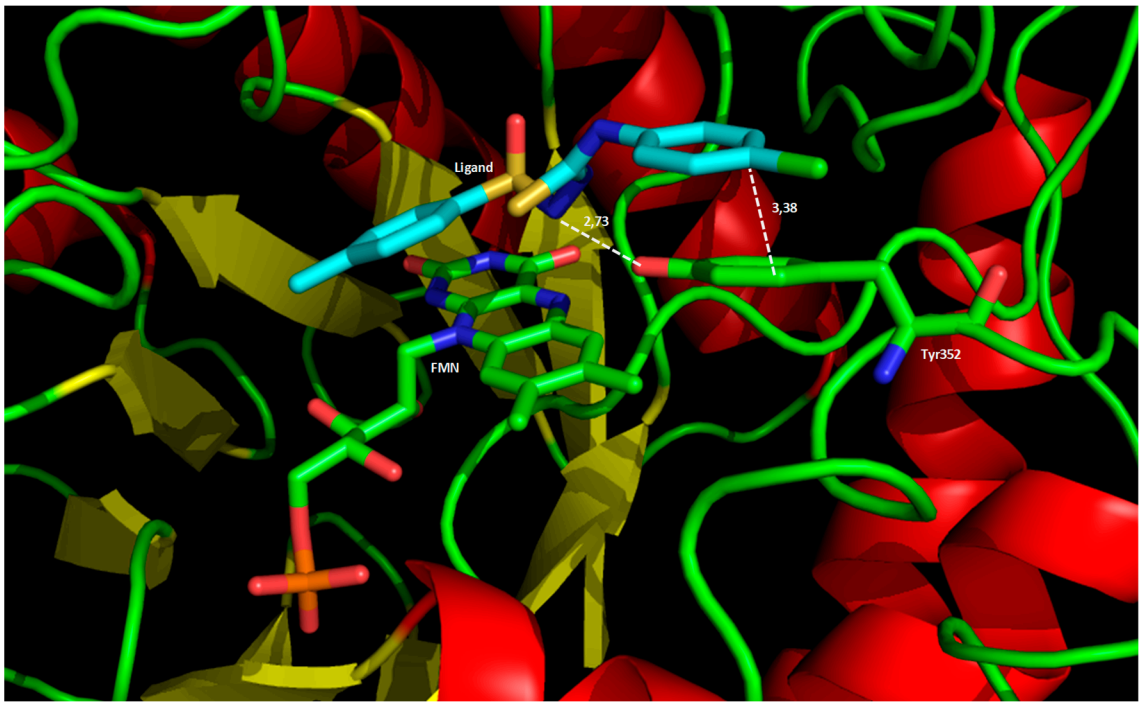

Figure S8.35 – Representative figure of the HL5^{NO2Ph} ligand at the site of the OLD Yellow enzyme from *Leishmania braziliensis*.

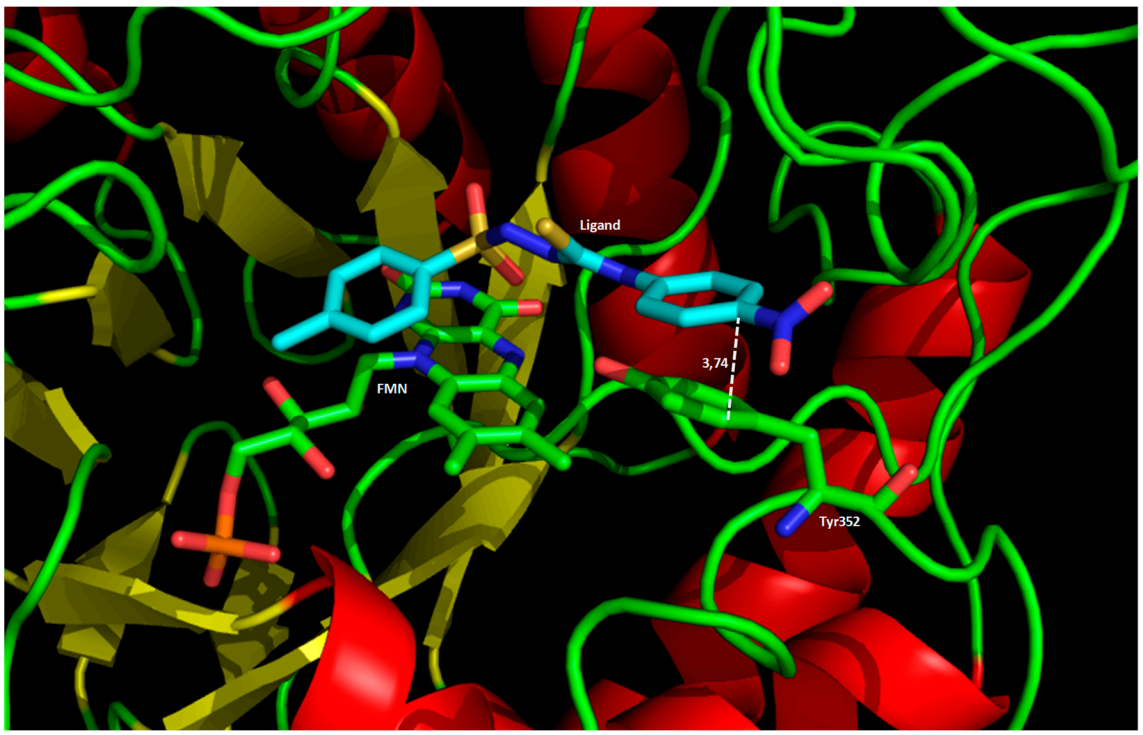

Figure S8.36 – – Representative figure of the $HL6^{Al}$ ligand at the site of the OLD Yellow enzyme from *Leishmania braziliensis*.

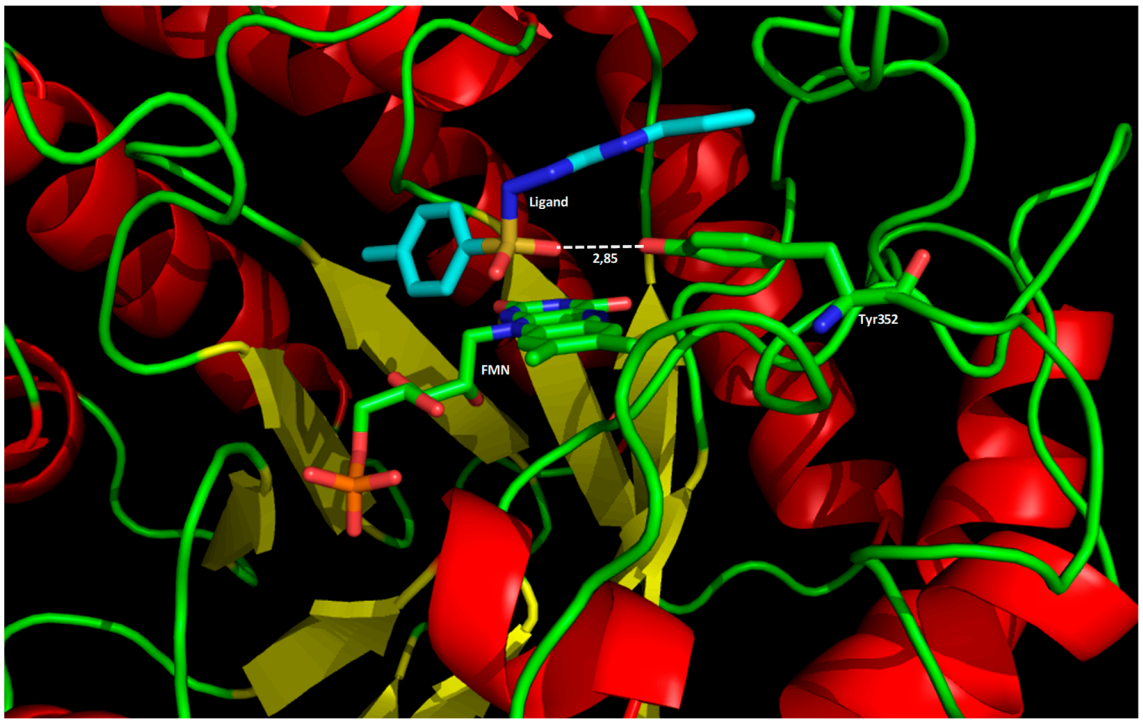

Figure S8.37 – Representative figure of the $[Ag(HL1^{Ch})_2]NO_3$ complex at the site of the OLD Yellow enzyme from *Leishmania braziliensis*.

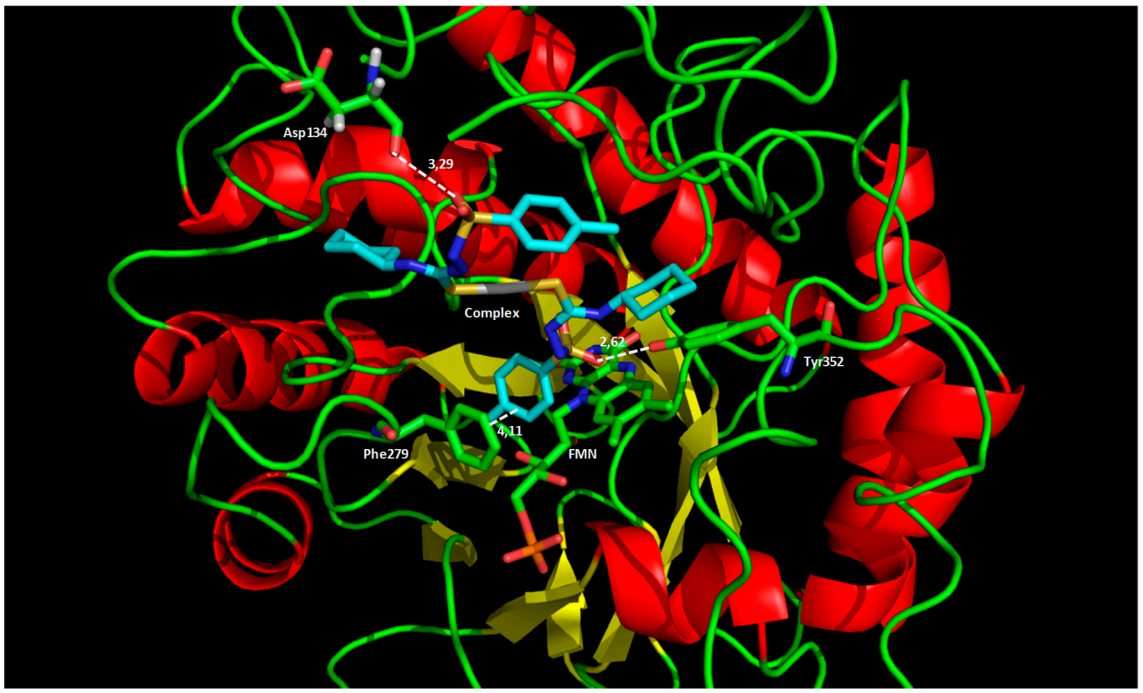

Figure S8.38 – Representative figure of the $[Ag(HL2^{Ph})_2]NO_3$ complex at the site of the OLD Yellow enzyme from *Leishmania braziliensis*.

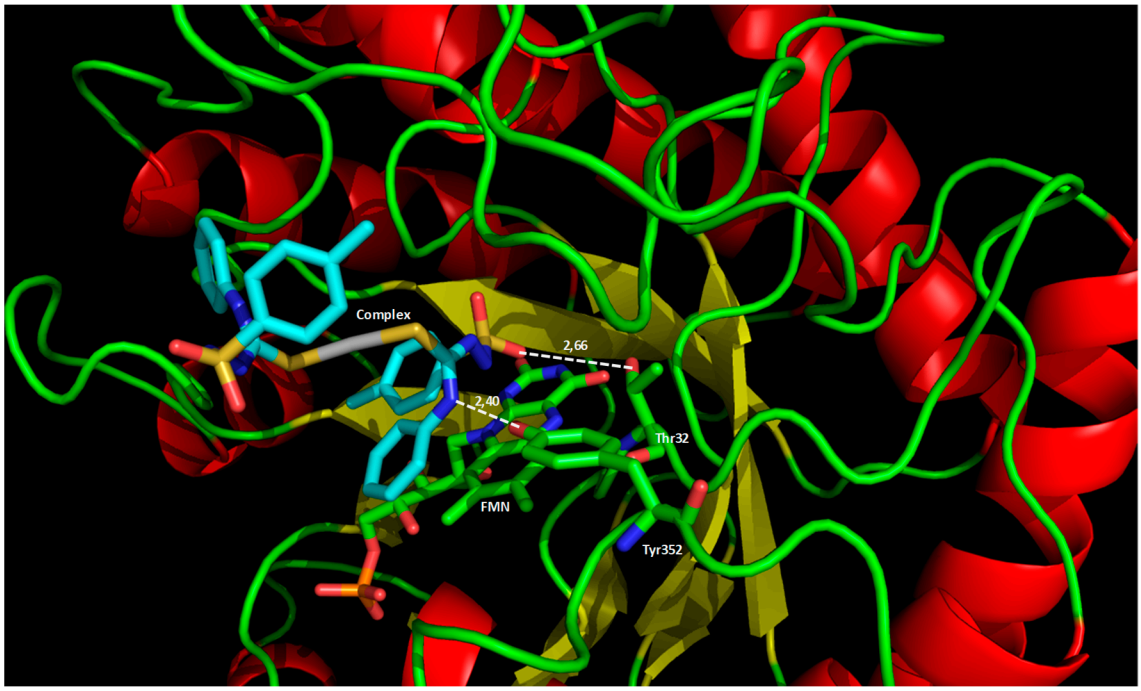

Figure S8.39 – Representative figure of the $[Ag(HL3^{FPh})_2]NO_3$ complex at the site of the OLD Yellow enzyme from *Leishmania braziliensis*.

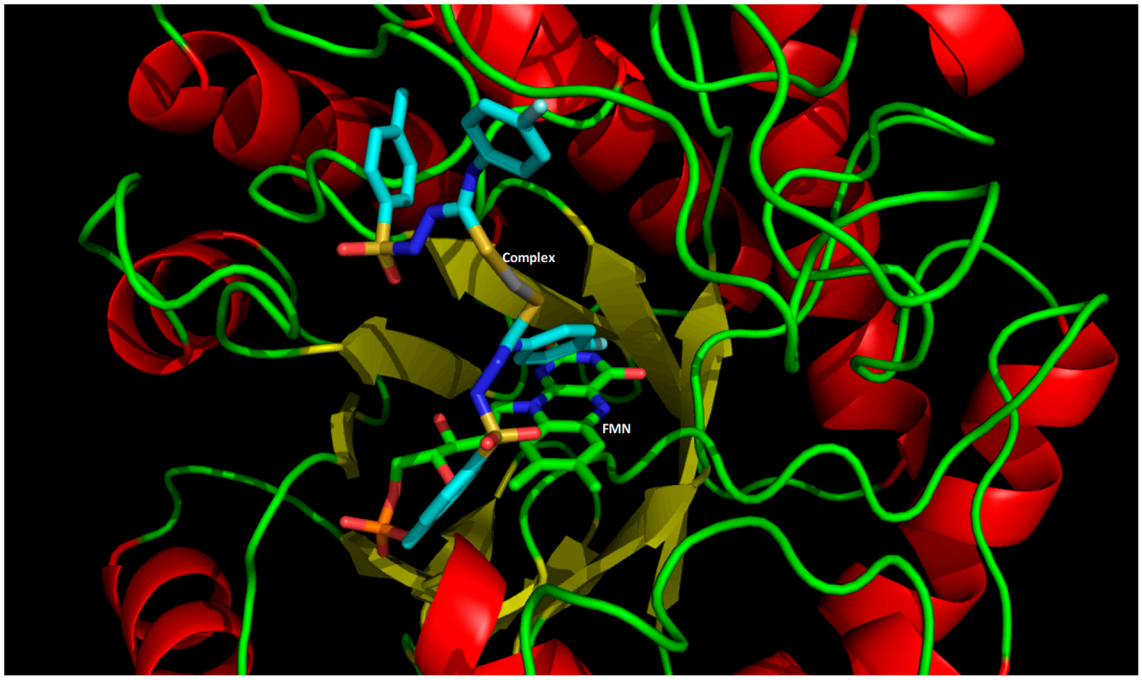

Figure S8.40 – Representative figure of the $[Ag(HL4^{ClPh})_2]NO_3$ complex at the site of the OLD Yellow enzyme from *Leishmania braziliensis*.

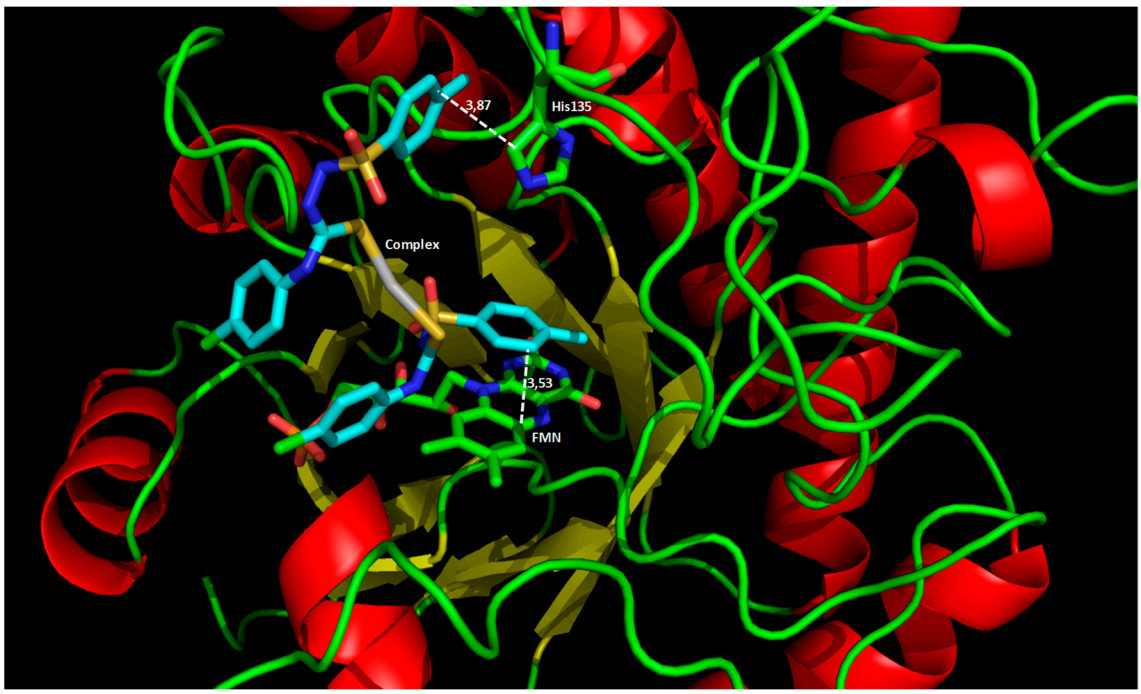

Figure S8.41 – Representative figure of the $[Ag(HL5^{NO2Ph})_2]NO_3$ complex at the site of the OLD Yellow enzyme from *Leishmania braziliensis*.

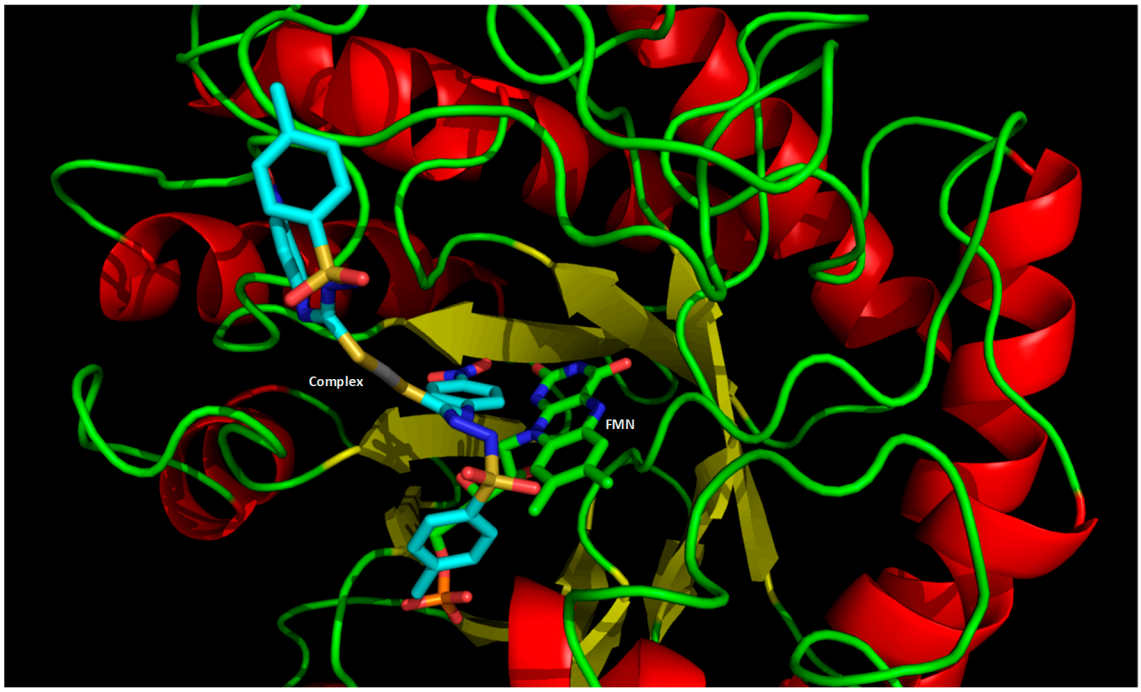

Figure S8.42 – Representative figure of the [Au(HL1^{Ch})$_2$]Cl complex at the site of the OLD Yellow enzyme from *Leishmania braziliensis*.

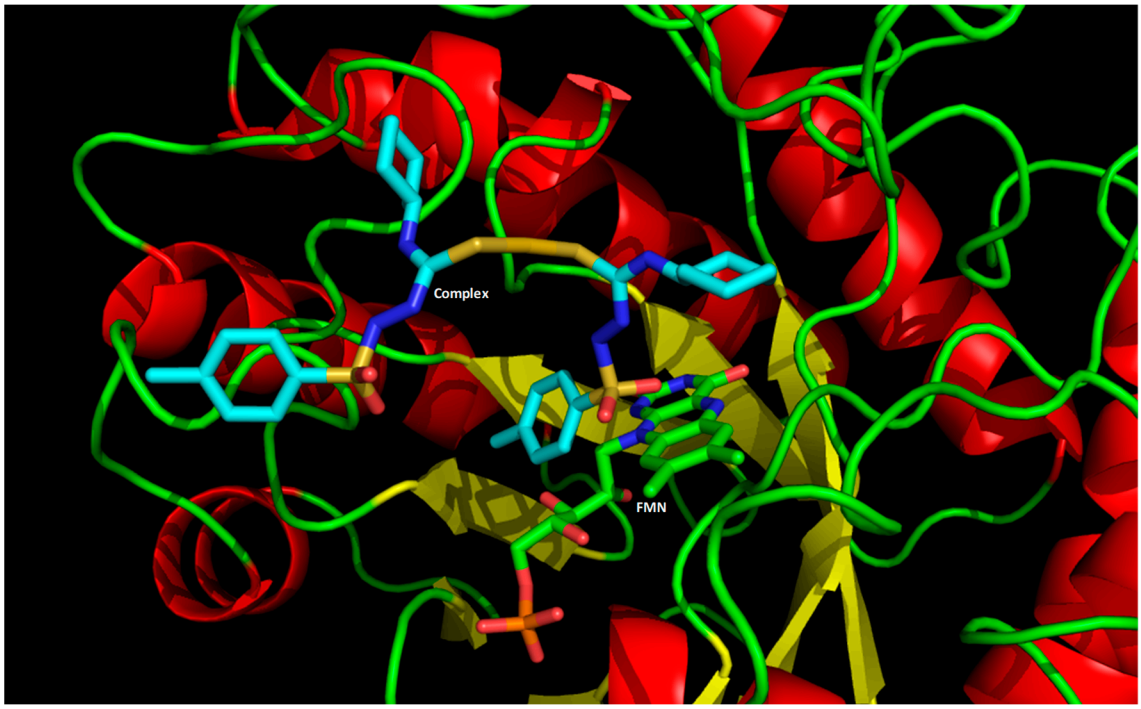

Figure S8.43 – Representative figure of the [Au(HL2^{Ph})$_2$]Cl complex at the site of the OLD Yellow enzyme from *Leishmania braziliensis*.

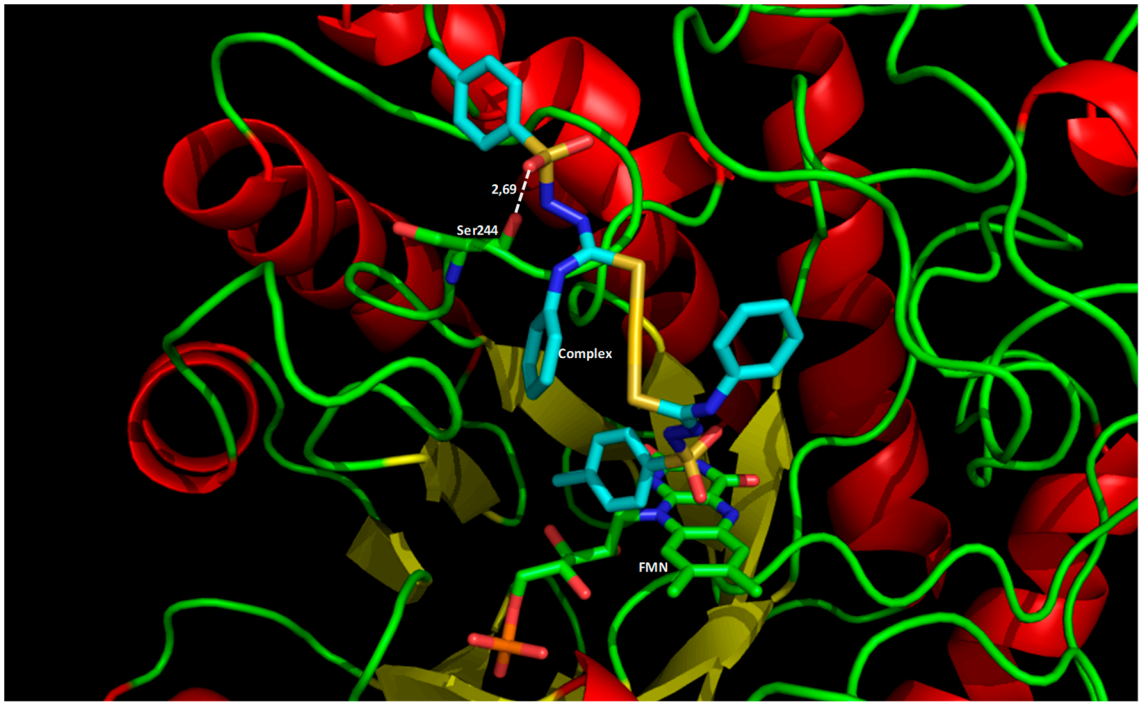

Figure S8.44 – Representative figure of the [Au(HL3^{FPh})$_2$]Cl complex at the site of the OLD Yellow enzyme from *Leishmania braziliensis*.

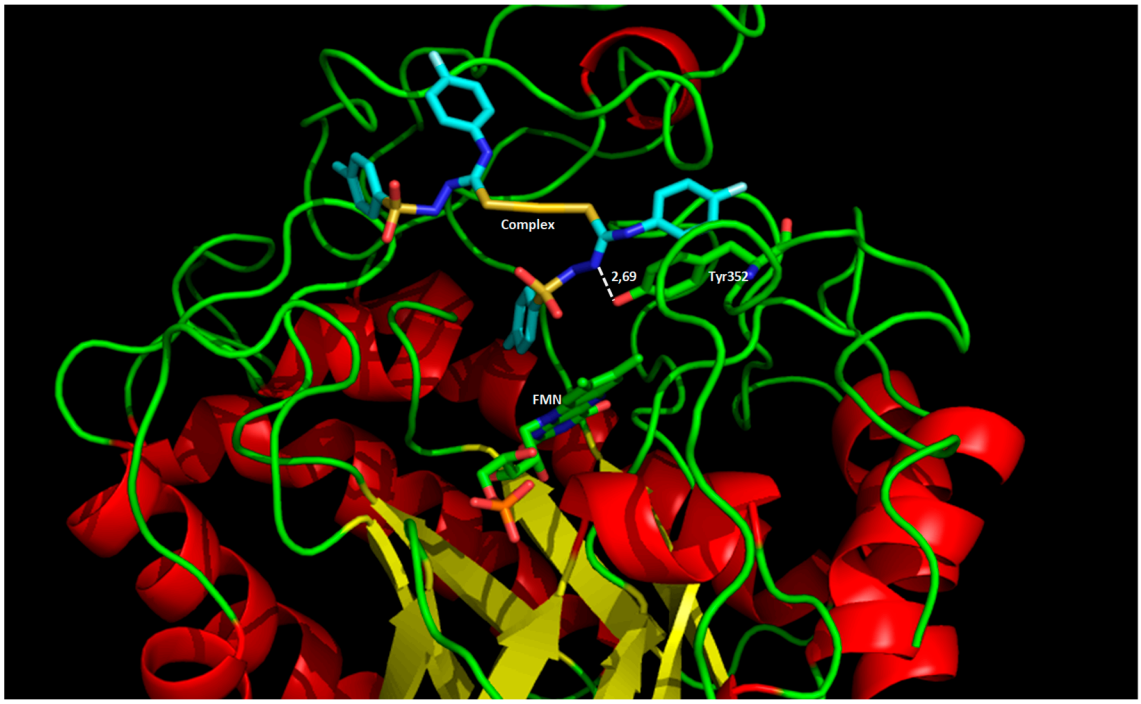

Figure S8.45 – Representative figure of the [Au(HL4^{ClPh})$_2$]Cl complex at the site of the OLD Yellow enzyme from *Leishmania braziliensis*.

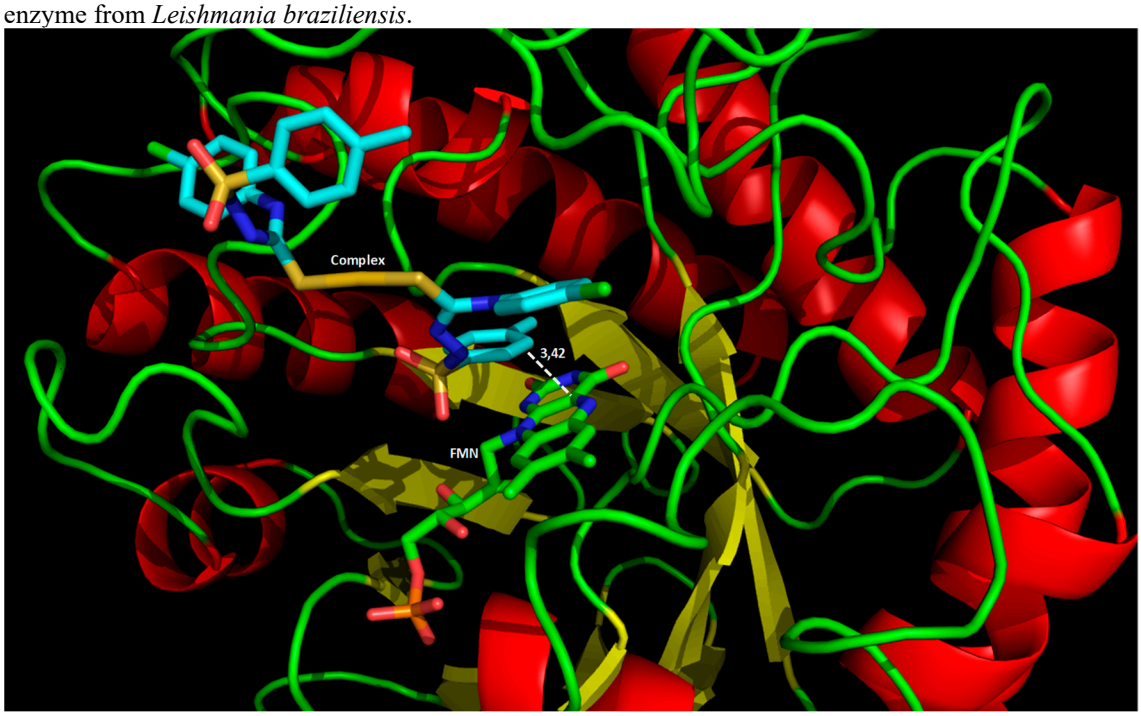

Figure S8.46 – Representative figure of the [Au(HL5^{NO2Ph})2]Cl complex at the site of the OLD Yellow enzyme from *Leishmania braziliensis*.